Doctoral Dissertation

Novel technology to control dimensional change of poly(lactic acid) through molecular orientation

Vo Dai Hoang Giang

Supervisor: Masayuki Yamaguchi

Graduate School of Advanced Science and Technology

Japan Advanced Institute of Science and Technology

Materials Science

December 2025

Abstract

Structural modification through crystallization improved the thermal and mechanical properties of semi-crystalline polymer. In actual processing, the applied flow-played a key role in the structural modification, which commonly promoted the crystallization, i.e., flow-induced crystallization. In this study, the post-process annealing was employed to improve the crystallization for a semi-crystalline polymer, e.g., poly(lactic acid) (PLA), having a low crystallization rate. Generally, the entropic elasticity is decreased by the orientation to the shear flow direction, leading to the increase entropic elasticity during post-process annealing. This phenomenon contributed to the orientation relaxation and isotropic crystallization, leading to shrinkage. This study provided a new phenomenon, that is, entropy reduction (orientation enhancement) during annealing. From this achievement, a fibrous nucleating agent was introduced to increase the orientation of PLA during annealing. As a result, the shrinkage was limited, compared to pure PLA sample. Moreover, a low-molecular-weight poly(vinyl alcohol) (PVA) was blended with PLA to fabricate an immiscible blend for injection-molding. During post-process annealing, the anomalous expansion to flow direction of the PLA/PVA injection-molded bar has been first investigated. The mechanism of an anomalous expansion was elucidated in the blend of PLA with a flexible poly(tetrafluoroethylene) (PTFE). This study opens the possibility to control the shrinkage of injection-molded products during annealing.

Keywords: Poly(lactic acid), Poly(vinyl alcohol), Poly(tetrafluoroethylene), Crystallization, Molecular orientation, Expansion, Shrinkage.

Acknowledgements

First and foremost, I am deeply grateful to my supervisor, Professor Yamaguchi Masayuki for his invaluable guidance, support, and great patience throughout my Ph.D. journey in Japan Advanced Institute of Science and Technology (JAIST). To be a member of Yamaguchi laboratory has been an invaluable opportunity for my academic path.

Secondly, I sincerely thank my committee members: Associate Professor Okeyoshi Kosuke, Professor Saito Takushi, Professor Matsumura Kazuaki, and Professor Murata Hideyuki. I am also grateful to my minor project advisor at National Cheng Kung University, Professor Ruan Jr-Jeng, and to Professor Matsumura Kazuaki at JAIST for their guidance. I deeply appreciate my former supervisor in Vietnam, Dr. Do Thi Vi Vi, for her support, encouragement, and invaluable advice.

Thirdly, I am also indebted to all of former and present members of Yamaguchi Laboratory for their kind assistance and collaboration at JAIST. I would like to offer special thanks to Mrs. Matsumoto Masami for her continuous support and dedication to the laboratory members.

Finally, I wish to express my heartfelt gratitude to my beloved family for their trust, understanding, and encouragement. Their support and love have been my greatest source of motivation throughout my academic journey and will continue to inspire my future endeavors.

Vo Dai Hoang Giang

September 2025

Ishikawa, Japan

Contents

Chapter 1. General introduction

1.1 Poly(lactic acid)

In the early 19th century, Pelouze synthesized a low-molecular-weight poly(lactic acid) (PLA) and lactide by condensing lactic acid through water distillation [1]. However, the PLA produced by this method had low purity and yield. Nearly 100 years later, Carothers discovered that PLA could be produced by heating lactide (a lactone cyclic ester) under vacuum [1]. Despite this discovery, the method was highly expensive for industrial synthesis because of the high cost of purification. In 1990, the Cargill Corporation successfully produced high molecular weight PLA on a commercial scale using lactide ring-opening polymerization. Later, Cargill partnered with Dow Chemical to establish the Cargill Dow company, commercially producing PLA under the trade name Ingeo™ since 1997 [2]. Currently, PLA research is increasing worldwide, as shown by the number of global publications in **Figure 1.1** [1].

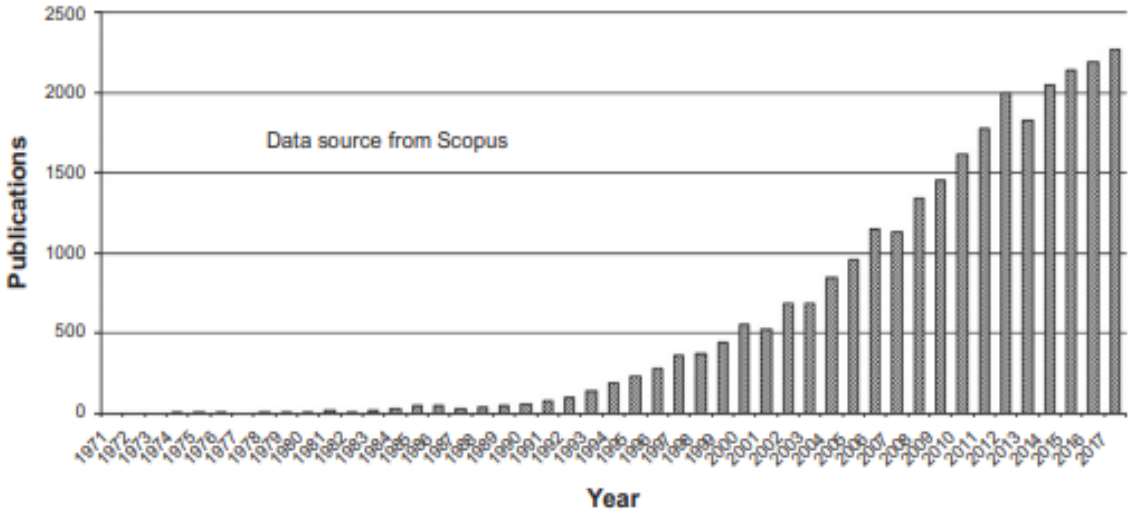

Figure 1.1. Recent studies about PLA from 1971 to 2017 (47 years) [3].

1.2 Structure and synthesis method

Lactic acid (LA) is a chiral molecule that exists as two enantiomers, L-lactic acid and D-lactic acid, as illustrated **in Figure 1.2**. Polymers made from pure L- or D-forms are called PLLA and PDLA, respectively. Most L-isomer lactic acid comes from biological sources, and therefore, PLA usually contains a higher amount of the L-isomer. PLA can be produced by different methods, including ring-opening polymerization of lactide, azeotropic dehydration polycondensation, and direct polycondensation [3]. Particularly, high molecular weight PLA used commercially is mainly produced through the ring-opening polymerization of lactide [3].

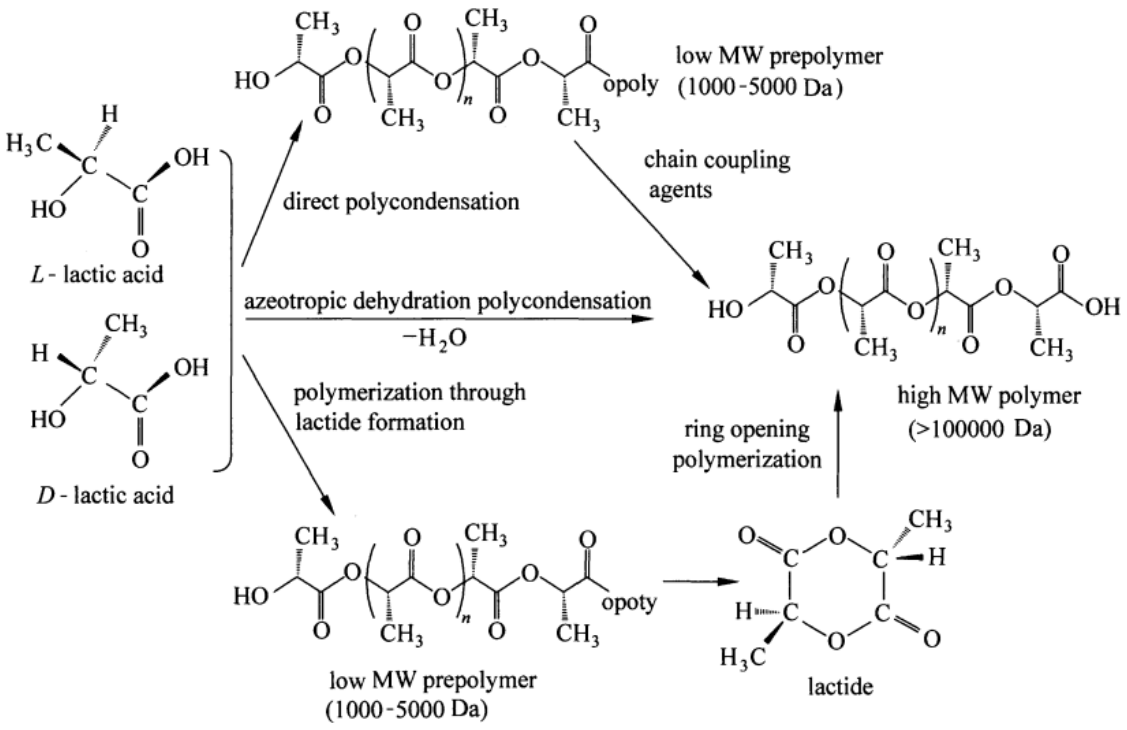

Figure 1.2. Chemical structure and synthesis route of PLA from L- and D-lactic acid [3].

Direct polymerization of lactic acid (LA) is a low-cost method to produce PLA, but lactide ring-opening polymerization (ROP) is the commercially used technique. Although ROP was first studied a long time ago, in 1932, it initially produced only low molecular weight polymers. In 1954, DuPont introduced a purification method for lactide, allowing the production of high-molecular-weight PLA. In addition, NatureWorks corporation developed a cost-effective and continuous bulk polymerization method to produce PLA from dextrose obtained from corn. This biopolymer has gained significant attention from manufacturers and researchers for many years, because it is considered as a promising replacement for petroleum-based plastics in the future.

1.3 Processing technology

Prior to processing, the compound was prepared in an extruder to fabricate the pellets. The formulation is variety, such as fillers, reinforcements, polymers, pigments, additives and/or processing aids, which are typically in pellets, powders, pastes or flakes. Various technologies were employed to manufacture the plastic products, such as injection-molding, blown-film, thermoforming, T-die extrusion, or blown-molding, from the prepared compound.

1.3.1 Injection-molding technique

Plastic injection molding is one of the most widely used manufacturing processes for producing plastic components due to its ability to create a precisely-complex shapes with high-quality surface finishes and efficiently [4–6]. Moreover, it supports the production of parts ranging from very small to very large, demonstrating versatility across various industries, including automotive, electronics, packaging, and medical fields [7,8]. Despite these advantages, careful control of processing parameters such as temperature, pressure, and cooling time is critical to ensure the quality and performance of the final molded product [8,9]. Most of the injection-molding machines require an extruder for melting the polymer solids and conveying the polymer melt into a mold, as shown **Figure 1.3** The nozzle is connected to a mold equipped with a sprue to deliver the melts. Once the

melt is injected, it flows in the runner and full-fills the mold under high pressure, followed by cooling/quenching and solidifying to form the final product.

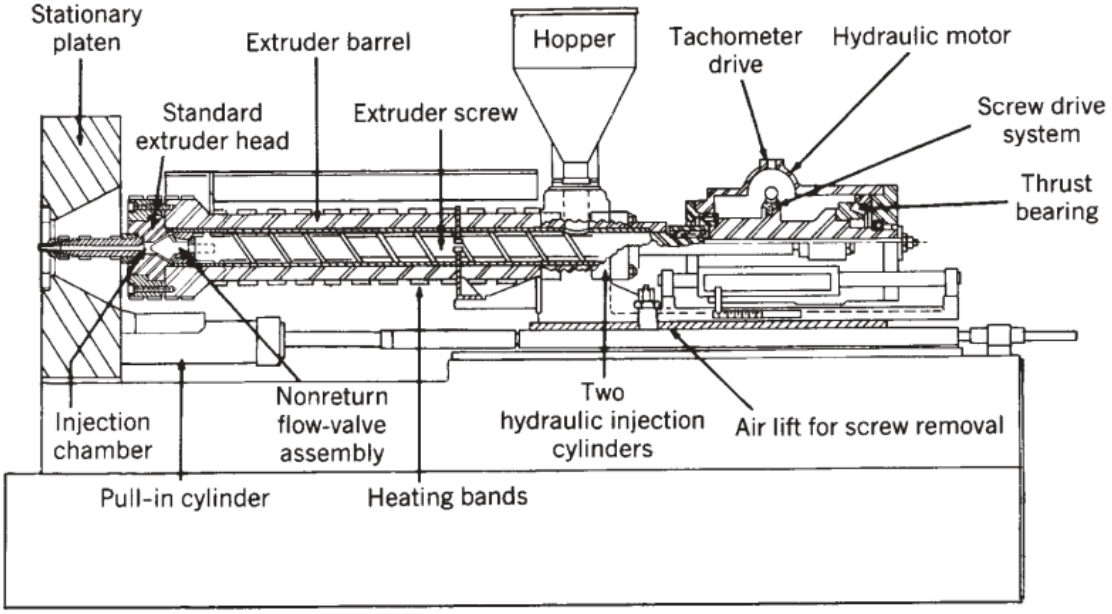

Figure 1.3. Schematic of an injection-molding machine [10].

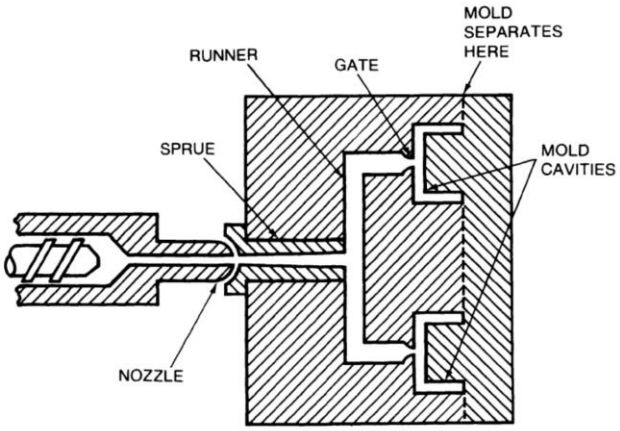

Figure 1.4. Schematic for the inside of a simple mold showing the nozzle, sprue, runners, gates, and mold cavities [4].

Figure 1.4 illustrates the key stages of melt flow in injection molding. Initially, the resin is melted in a reciprocating screw extruder. Once a sufficient volume of melt accumulates, it is pushed through a nozzle and sprue system into the runners, which distribute it to the mold cavities. Before entering each cavity, the melt passes through a gate. This narrow section facilitates detachment of solidified material and prevents backflow after pressure release. Upon contacting the cooled mold surfaces, the melt begins to solidify. Following cavity filling, an additional pressure is applied in the packing stage to compensate for volumetric shrinkage during cooling.

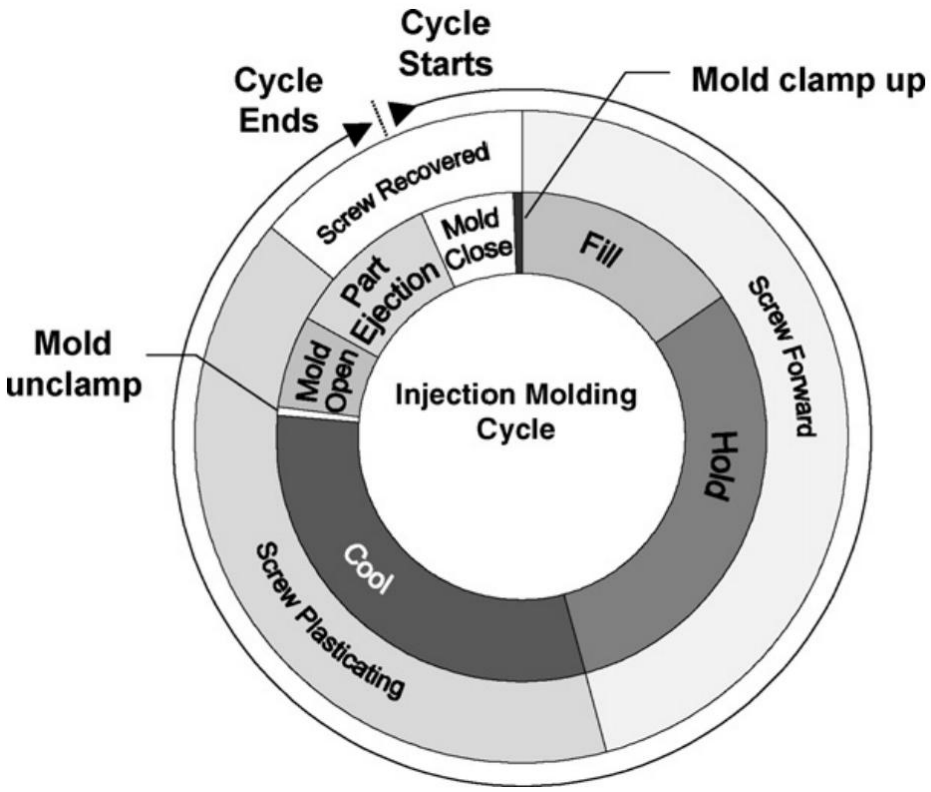

Figure 1.5. Common cycle for an injection-molding process [4,5]

The period distribution of the cooling stages is shown in **Figure 1.5**. During the injection molding process, cooling plays a critical role in determining the quality and dimensional accuracy of the final product. Firstly, the cycle starts with the closing mold, followed by the plastic filling by the injection-molding. After the mold cavity completely filled, the melt is held for several periods under a pressure to prevent the shrinkage. Secondly, the melt begins to solidify once contacting the cool-mold walls. This cooling phase continues until the molded part achieves sufficient rigidity to be ejected without deformation. Moreover, the cooling time depends on several factors, including the thermal conductivity of the materials, mold temperature, melting temperature, and the thickness of the products. The efficient cooling is vital to prevent shrinkage, warpage, sink marks, and residual stresses, i.e., orientation relaxation. Finally, once the adequate cooling is achieved, the mold opens, then the part is ejected. Notably, in the screw plastication phase, new material is melted and prepared for the next shot, often overlaps with the cooling phase to improve cycle efficiency. The cooling period, t_{cycle}, is the most time consumption in the entire cycle, as shown in the equation (1.1) [9].

$$t_{cycle} = t_{closing} + t_{cooling} + t_{ejection} \tag{1.1}$$

where $t_{closing}$, $t_{cooling}$, and $t_{ejection}$ are the period for closing and injecting into the mold, cooling, and product ejection, respectively. In actual processing, reducing $t_{cooling}$ is an appropriate method to increase the product capacity.

1.3.2 Shrinkage

When the barrel temperature is excessively high, the resin absorbs excessive thermal energy. This heat causes the resin to expand excessively, creating the number of voids between the molecules. After injection-molding, the outer (skin) layer of the molded product cools and solidifies first. As the remaining resin inside cools down, it shrinks and fills these molecular voids, pulling the solidified outer skin inward, leading to appearance of defects, as shown in **Figure 1.6**. Lowering the barrel temperature can help keep the resin melting without forming too many voids. As a result, shrinkage will return to normal. Typical shrinkage values are published for each material, although actual shrinkage can vary depending on flow direction. Material suppliers usually provide shrinkage ranges for different flow directions.

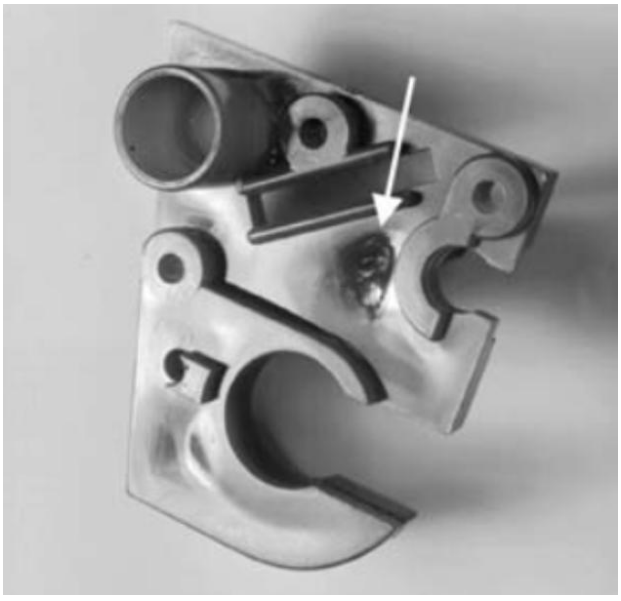

Figure 1.6. Excessive shrinkage of an injection-molded product [8].

1.3.3 Controlling shrinkage

Shrinkage represents the dimensional change between a plastic product in its freshly molded state and after it has cooled. Generally, every materials expands once heated and then shrinks when cooled. The shrinkage (rate) value is usually expressed as inches per inch (in the U.S. Customary System) or meters per meter (International System of Units, SI). For example, a plastic has a shrinkage of 0.050 cm per 1 cm, leading to the shrinkage of 1%. It means, therefore, the mold cavity must be oversized by that amount. To produce a final part length having exactly 10 cm, the mold cavity length should be around 10.10 cm. After cooling, the part will shrink to the desired dimension. Assuming that the shrinkage occurs equally in all directions, i.e., isotropic shrinkage, the additional adjustment, such as increasing 1% of the dimension, in the width or thickness should be considered.

It is important to comprehend how shrinkage varies between amorphous and crystalline polymers. The amorphous plastics generally exhibit a lower shrinkage than crystalline plastics. Moreover, the shrinkage in crystalline polymers is greater in the flow direction than the perpendicular direction, e.g., transversal direction (TD) and normal direction (ND). This is called the anisotropic shrinkage. Another factor that can be considered is volume reduction, induced by crystallization. The amorphous structure is a disordered and non-crystalline molecular structure. In contrast, the crystalline domain has a tighter chain-packing, resulting in a higher density than that for amorphous domain.

1.3.3.1 Effect of temperature adjustments

There is a method to control the shrinkage of a specific product by adjusting the plastic temperature during processing. Due to the thermal expansion of plastic, a lower processing temperature is also applied in actual processing to reduce the shrinkage. The temperature of the mold can be adjusted to control the shrinkage. As an example, a hot mold produces less shrinkage than a cold mold because rapid solidification of the surface layer occurs in the colder mold. As a result, the material tends to shrink before an applied pressure. In contrast, a hot mold enables the Therefore, this applied pressure compensates for volumetric shrinkage during solidification. However, the mold temperature is important, and depends on the glass-transition temperature, T_g, of the polymers. The crystallization may occur once the mold temperature is beyond T_g. This phenomenon may affect to the dimensions of plastics, as previously mentioned. In actual processing, post-process annealing is often used to enhance the crystallinity of polymers having low crystallization rate such as PLA, poly(3-hydroxybutyrate-co-3-hydroxyhexanoate) (PHBH) [11], or poly(ethylene terephthalate) (PET) [12]. Various factors, including the temperatures of the resin and mold, gate design, injection pressure and time, and holding pressure, play crucial roles in controlling shrinkage, as mentioned later. Moreover, post-process annealing affects the dimensions of injection-molded products, particularly those that undergo cold crystallization during post-processing annealing. During post-process annealing, crystal

growth generally leads to a reduction in product dimensions, which can pose significant issues.

1.3.3.2 Effect of pressure adjustments

Pressure in injection-molding affects directly shrinkage. Higher pressure means lower shrinkage because it packs the polymer chains more tightly and limits their mobility during cooling, leading to a lower shrinkage. To control shrinkage, therefore, the pressure is applied as long as the material is molten until it solidifies. In other word, once the applied pressure is released before solidification, the shrinkage will increase because of the relaxation.

1.3.3.3 Effect of residual stress

One of the most important causes of failures in injection-molded is residual stress, i.e., molded-in stress. In other word, the stress is the internal resistance to deformation or changing shape once applied to a force. The molded-in stress often happens during injection molding. Once the polymer is melted, a screw delivers and injects the molten plastic into the mold. This pushing action causes the polymer chains aligned, oriented and/or stretched to the flow direction. In molding, these oriented structure is solidified under a high pressure. For an example, a rubber band is stretched at room temperature,

followed by freezing (solidifying) at that stretching position. After thawing, the rubber band tends to go back to its original state due to relieving stress. This phenomenon is also similar to the injection-molding. The injection-molding part is allowed to relax after solidification at a temperature beyond its T_g. As a result, the shrinkage, warpage, cracking, twisting, crazing, and/or shatter may occur after heating, which may be serious problems in practical application.

1.3.3.4 Effect of fillers

An exception to the anisotropic shrinkage is found in reinforced composite materials, which shrink less to some extent along the flow direction and more in the transverse direction. This behavior is caused by the orientation of the reinforcement of fibers [8]. The common fillers are mica, glass beads, glass fiber, carbon black, talc, and rubber [13]. The coefficient of thermal expansion (CTE) and density of these materials, as provided in **Table 1.1.**

Table 1.1. Density and coefficient of thermal expansion of fillers [13]

Fillers	Density ($kg\ m^{-3}$)	Coefficient thermal expansion ($ppm\ K^{-1}$)	Significant anisotropy
Carbon black	2000	0.5	No
Glass bead	2600	3	No
Glass fiber	2600	3	Yes
Mica (silicate minerals)	2800	10	No
Rubber particles	1500	80	No

Except rubber particles (commonly used as an impact modifier), most fillers have a very low CTE ($5 \times 10^{-6}\ K^{-1}$), compared to polymer (around $100 \times 10^{-6}\ K^{-1}$). Because of this large difference, adding one or more fillers to a polymer can reduce the volumetric shrinkage. The change in shrinkage generally varies in proportion to the volume fraction of fillers.

1.4 Polymer crystallization

Nucleation in polymer crystallization occurs in two stages: the formation of an initial crystal seed, known as primary nucleation. In contrast, if the nucleation takes place at interfaces, such as on the surface of foreign particles or container walls, it is known as heterogeneous nucleation [14].

1.4.1 Homogeneous nucleation

Homogeneous nucleation occurs only when the system overcomes a free-energy barrier [15]. For example, crystal nuclei generated sporadically from a supersaturated solution which is energetically metastable and in which density fluctuations occur [16]. A similar mechanism also takes place during crystallization from the melt [14]. Following crystal nucleation theory, a small crystal from the melt having a size of $a \cdot b \cdot l$ is shown in **Figure 1.7**.

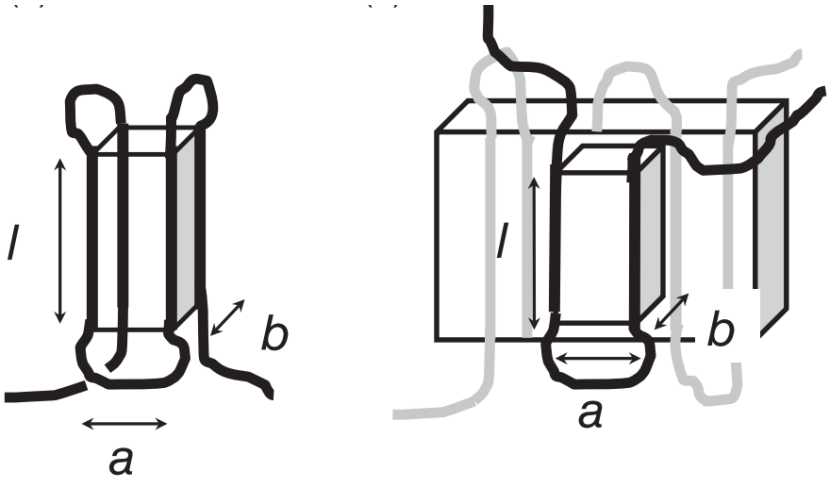

Figure 1.7. Schematic of the primary nucleus [14]

The formation of a stable nucleus is a prerequisite for initiating crystallization. The change in free energy for crystallization from the melt, i.e., Gibbs free energy, $\Delta G_{crystals}$, is:

$$\Delta G_{crystals} = \Delta G_{nucleus} - \Delta G_{melt} \quad (1.2)$$

where $\Delta G_{nucleus}$ is the surface free energy change and ΔG_{melt} is the volume free energy change. The equation (1.2) can be expressed further, as follows:

$$\Delta G_{crystals} = [2 \cdot a \cdot b \cdot \sigma_e + 4 \cdot a \cdot l \cdot \sigma_s] - [a \cdot b \cdot l \cdot \Delta F_{melt}] \quad (1.3)$$

$$= [2 \cdot a \cdot b \cdot \sigma_e + 4 \cdot a \cdot l \cdot \sigma_s] - [a \cdot b \cdot l \cdot (\Delta H_{\text{melt}} - T\Delta S_{melt}]$$

where σ_e and σ_s are the surface energy of the $a \cdot b$ and $a \cdot l$ plane, respectively. In some case, the $\Delta G_{nucleus}$ and ΔG_{melt} can be known as the surface (ΔG_s) and bulk free energy change (ΔG_b), respectively. Thus, $\Delta G_{crystals}$ can be referred to the following equation:

$$\Delta G_{crystals} = \Delta G_b + \Delta G_s = -\frac{4}{3}\pi r^3 \Delta F_{melt} + 4\pi r^2 \sigma \quad (1.4)$$

where r is the radius of the sphere. ΔG_b is typically negative, which promotes the crystallization, whereas ΔG_s is positive, acting as an energy barrier to nucleation. As the radius increases, $\Delta G_{crystals}$ gradually increases until r reaches $r^* = \frac{2\sigma}{\Delta F_{melt}}$ (the critical radius of the stable nuclei). The $\Delta G_{crystals}$ decreases and become negative once $r > r^*$, resulting the crystallization.

1.4.2 Heterogeneous nucleation

Heterogeneous nucleation is important for the crystallization behavior of polymers, particularly in industry. Unlike homogeneous nucleation, secondary nuclei with chain-folded structures are formed as polymer chains in the melt or solution move and adsorb onto pre-existing substrates such as impurities, fillers, mold surfaces, or nucleating agents. These surfaces lower the energetic barrier for nucleation by reducing the interfacial free

energy required to form a stable nucleus. The overall ΔG change associated with nucleation includes the negative ΔG_b and the positive ΔG_s. In heterogeneous nucleation, the presence of a solid surface significantly lowers ΔG_s, thereby facilitating the formation of stable nuclei at a higher temperature and faster rate than in homogeneous systems. This phenomenon is especially important in controlling the crystallization kinetics, morphology, and final properties of semi-crystalline polymers. For instance, various nucleating agents such as talc [17], silica [18], clay [18], or N,N′-ethylenebis(12-hydroxystearamide) (EBHS) [19,20] have been widely employed to improve the crystallization rate and degree of crystallinity in polymers like polypropylene or PLA. The effectiveness of such agents is influenced by surface chemistry, roughness, and crystallographic compatibility with the polymer chains, which together determine the extent of epitaxial crystal growth. Thus, heterogeneous nucleation not only improves processing efficiency but also enables better control over the final thermal and mechanical properties of polymeric materials [14].

1.4.3 Structural development of polymer crystals

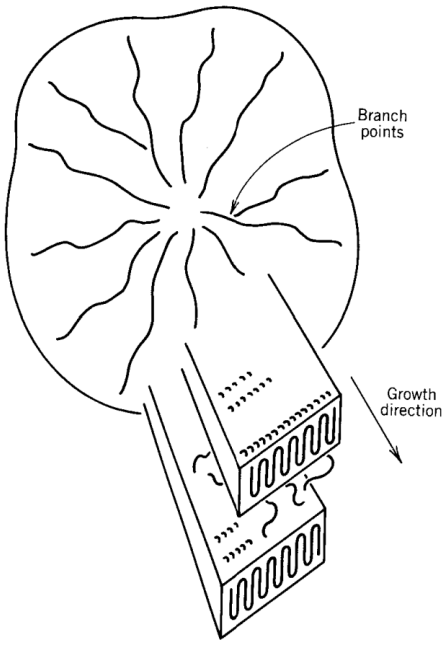

Figure 1.8. A model of a spherulite [21].

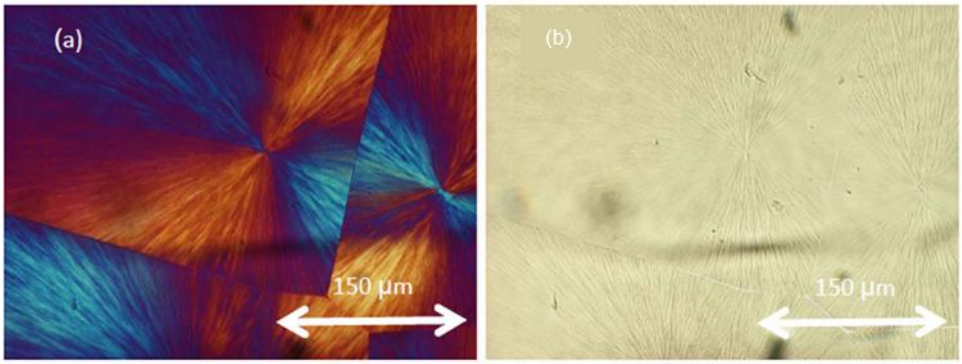

Figure 1.9: Polarized optical microscope images of poly(l-lactic acid) spherulites crystallized isothermal at 110 °C, obtained (a) with and (b) without cross polarizers and a full-wave plate [22].

Once the semi-crystalline polymers cool from the melt, they undergo the crystallization process. The crystallization temperature may be 10 or 20 °C lower than the melting temperature [21], called supercooling. Quenching the melt to a temperature below the T_g, produces a sample having amorphous structure, at which the random coils are aggregated. However, the amorphous phase is not always in a perfectly disordered state, but some degree of ordered structure may exist [21]. Slow cooling of the melt to room temperature promotes the development of various spherulitic structures. In other word, small nuclei start to appear randomly in the melt and polymer chains fold to form a lamellae. The fold-chain direction in the bulk lamellae is from the nuclei and perpendicular to the growth direction, as shown in **Figure 1.8.** The crystallization is usually observed in isotropic, leading to the formation of crystalline structure, called spherulites or bulk crystallization. **Figure 1.9** shows the spherulites texture of poly(l-lactic acid) using a polarized optical microscope under a crossed polarizers. Typically, spherulites initially develop in a spherical form during crystallization. Then, their subsequent growth leads to impingement with neighboring spherulites, resulting in the formation of boundaries.

1.5 Objective of the study

The main objective of this study is to improve the crystallization of polymer materials using heat-treatment, i.e., annealing, above the glass-transition temperature, T_g, and proposed a novel method to control the anisotropic shrinkage of polymer materials.

Firstly, the film having a shear history was prepared using a parallel plates rheometer. The film with or without shear history was annealed using the temperature controller. The structure and thermal properties were evaluated using two-dimensional wide-angle X-ray diffraction, differential scanning calorimetry, and dynamic mechanical analysis.

Secondly, the fibrous nucleating agent was introduced because the nucleating agent enhanced the crystallization rate of polymer materials, which has a low crystallization rate. Moreover, it has been known that the fibrous nucleating agent improved the orientation of the polymer during crystallization. The dimensional change after annealing was also observed.

Finally, the binary polymer blends were developed to control the shrinkage during post-process annealing. Moreover, the mechanism and elucidation of the anomalous dimensional change during annealing were reported.

References

[1] W. H. Carothers, G. L. Dorough, F. J. van Natta, Studies of polymerization and ring formation. X. The reversible polymerization of six-membered cyclic esters, *J. Am. Chem. Soc.,* 54, (1932), 761–772.

https://doi.org/10.1021/ja01341a046

[2] E. T. H. Vink, K .R. Rábago, D. A. Glassner, B. Springs, R. P. O'Connor, J. Kolstad, P. R. Gruber, The sustainability of naturework polylactide polymers and ingeo polylactide fibers: An update of the future, *Macromol. Biosci.*, 4, (2004), 551–564.

https://doi.org/10.1002/mabi.200400023

[3] L. T. Sin, B. S. Tueen, Polylactic Acid - A Practical Guide for the Processing, Manufacturing, and Applications of PLA – 2nd Edition, Elsevier, Netherland, 2019.

[4] J. M. Dealy, K. F. Wissbrun, Melt rheology and its role in plastics processing: theory and applications, Springer, Netherlands, 1999.

[5] Z. Tadmor, C. G. Gogos, Principles of Polymer Processing, 2nd Edition, Wiley, Hoboken, New Jersey, 2006.

[6] L. -T. Lim, R. Auras, M. Rubino, Processing technologies for poly(lactic acid), *Prog. Polym. Sci.*, 33, (2008), 820–852.

https://doi.org/10.1016/j.progpolymsci.2008.05.004

[7] D. O. Kazmer, Injection Mold Design Engineering, in: D. O. Kazmer (Ed.), Injection Mold Design Engineering (Second Edition), Hanser, 2016, I–XXIV.

[8] D. Bryce, Plastic Injection Molding: Manufacturing Process Fundamentals, SME, Southfield, MI, 2001.

[9] T. A. Osswald, J. P. Hernández-Ortiz, Polymer Processes, in: T. A. Osswald, J. P. Hernández-Ortiz (Ed.), Polymer Processing: Modeling and Simulation, Carl Hanser Verlag GmbH & Co. KG, München, Germany, 2006, 111–168.

[10] https://www.polyplastics.com/en/support/mold/outline/ani1.htm

[11] R. A. Rebia, K. Shizukuishi, T. Tanaka, Characteristic changes in PHBH isothermal crystallization monofilaments by the effect of heat treatment and dip-coating in various solvents, *Eur. Polym. J.*, 134, (2020), 109808.
https://doi.org/10.1016/j.eurpolymj.2020.109808

[12] Z. Chen, M. J. Jenkins, J. N. Hay, Annealing of poly (ethylene terephthalate), *Eur. Polym. J.*, 50, (2014), 235–242.
https://doi.org/10.1016/j.eurpolymj.2013.11.004

[13] D. O. Kazmer, Shrinkage and Warpage, in: D. O. Kazmer (2nd Ed.), Injection Mold Design Engineering, Hanser, 2016, 291–325.

[14] K. Tashiro, Growth of Polymer Crystals, in: E. Piorkowska, G. C. Rutledge (Ed.), Handbook of Polymer Crystallization, Wiley, Hoboken, New Jersey, 2013, 165–196.

[15] J. D. Hoffman, R. L. Miller, Kinetic of crystallization from the melt and chain folding in polyethylene fractions revisited: theory and experiment, *Polymer*, 38, (1997), 3151–3212.
https://doi.org/10.1016/S0032-3861(97)00071-2

[16] J. Yang, B. J. McCoy, G. Madras, Distribution kinetics of polymer crystallization and the Avrami equation, *J. Chem. Phys.*, 122, (2005), 064901.
https://doi.org/10.1063/1.1844373

[17] A. Shakoor, N. L. Thomas, Talc as a nucleating agent and reinforcing filler in poly(lactic acid) composites, *Polym. Eng. Sci.,* 54, (2014), 64–70.
https://doi.org/10.1002/pen.23543

[18] M. R. Rahman, Silica and Clay Dispersed Polymer Nanocomposites, Woodhead Publishing, Cambridge, UK, 2018.

[19] J. Y. Nam, M. Okamoto, H. Okamoto, M. Nakano, A. Usuki, M. Matsuda, Morphology and crystallization kinetics in a mixture of low-molecular weight aliphatic amide and polylactide, *Polymer*, 47, (2006), 1340–1347.
https://doi.org/10.1016/j.polymer.2005.12.066

[20] K. Saitou, M. Yamaguchi, Transparent poly(lactic acid) film crystallized by annealing beyond glass transition temperature, *J. Polym. Res.,* 27, (2020), 104.
https://doi.org/10.1007/s10965-020-02071-y

[21] L. H. Sperling, Introduction to Physical Polymer Science, Wiley, Hoboken, New Jersey, 2005.

[22] A. M. El-hadi, Increase the elongation at break of poly (lactic acid) composites for use in food packaging films, *Sci. Rep.* 7, (2017), 46767.
https://doi.org/10.1038/srep46767

Chapter 2. Effect of shear history on the structure development during annealing

2.1 Introduction

Poly(lactic acid) (PLA) is an eco-friendly biomass-based plastic that can potentially alternate traditional petroleum-based plastics because it is biodegradable and high rigidity [1–3]. Despite these advantages, PLA exhibits certain limitations, including brittleness, poor heat resistance and difficulties in processing (low melt strength), which must be improved. Increasing the crystallinity of PLA is particularly crucial for broadening its applications. Once PLA has a high crystallinity, its heat resistance properties, can be comparable to that of isotactic polypropylene and greater than that of poly(vinyl chloride), polystyrene, polyethylene, and poly(methyl methacrylate). Given that PLA also has higher rigidity compared to these conventional plastics, it is becoming increasingly attractive. As a result, the market for PLA has recently been growing significantly.

The relative glass transition temperature (T_g) of PLA was around 58 °C, which limits its heat resistance and thereby restricts broader applications [1–4]. From the processing perspective, controlling the cooling conditions is essential to promote crystallization. It has been reported that PLA exhibits its maximum lateral growth rate at a crystallization temperature of 130 °C, which corresponds to the average of its equilibrium melting point (T_m^0, 207 °C) [5] and T_g. However, the use of water as a cooling medium is limited at 130 °C

under atmospheric conditions, resulting in the disadvantage of cost performance. Introducing plasticizers effectively lowers the optimal crystallization temperature, promoting the crystallization rates using water cooling. This is because of the plasticization effect, leading to the enhancement of chain mobility [1,6–8]. To date, low-molecular-weight polyester compounds such as poly(ethylene glycol), oligomeric PLA, glycerol, cardanol and its derivatives, and citrate esters have been thoroughly studied and are commonly utilized as plasticizers in industry.

Another technique for enhancing the crystallization rate involves adding nucleating agents, such as carbon nanotubes [9], talc [9], calcium carbonate [9], boron nitride [9], orotic acid [9–11], zinc phenylphosphonate [11,12], hydrazide compounds [11,13], and various amide compounds [9,11,14,15]. This method can be also employed with plasticizers. However, under rapid cooling, i.e., quenching, the crystallinity achieved with nucleating agents and/or plasticizers is typically insufficient for effective heat resistance.

2.1.1 Flow-induced crystallization

The flow fields, from a thermodynamic perspective, effectively increase the Gibbs free energy of the melt (ΔF_{melt}). In other word, it decreases the bulk free energy, thereby lowering the barrier to nucleation and enhancing the crystal formation. Moreover, applying a shear flow not only accelerates crystallization kinetics but also significantly alters the crystallization morphology, such as shish-kebab structure instead of isotropic spherulites, as shown in **Figure 2.1** [16]. Polymer chains under flow conditions can align and form anisotropic structures such as shish-kebab structure, which consist of a central fibrillar "shish" with numerous lamellar "kebabs" structures that grew perpendicularly. This orientation is particularly important in enhancing mechanical and thermal properties of semicrystalline polymers under processing conditions such as extrusion or injection molding.

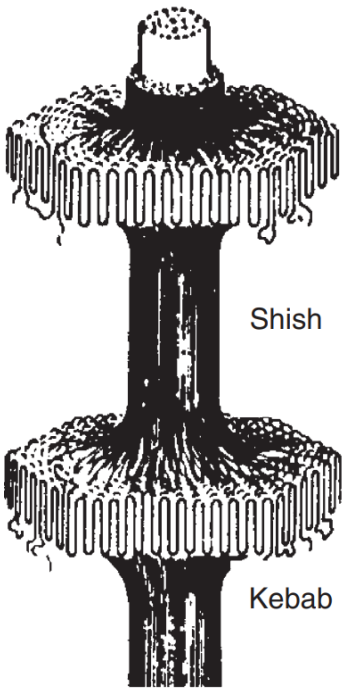

Figure 2.1. Scheme of shish-kebab structure [16].

In polymer processing, the flow-induced crystallization represents an effective approach to increasing crystallinity for PLA . It is generally believed that when polymer melt is applied by shear flow, they are stretched and/or aligned along the flow direction. As a result, the shish structure is formed. This situation is expressed by the Weissenberg number, *Wi*, as shown in the following equation:

$$Wi = \tau\dot{\gamma} \tag{2.1}$$

where τ is the characteristic time for a specific molecular relaxation mode and $\dot{\gamma}$ is the applied shear rate. When τ is the reptation time, τ_{rept}, *Wi* provides the information on the molecular orientation, which is denoted as Wi_{rept} in this thesis. Once τ is the Rouse

relaxation time, τ_R, W_i gives the information on the chain stretching, which is denoted as Wi_R. τ_R can be calculated based on the Doi and Edwards model:

$$\tau_R = \frac{\tau_{rept}}{3Z_e} \tag{2.2}$$

where Z_e is the average number of entanglements per a polymer chain ($Z_e = M/M_e$). Therefore, τ_R can be predicted from the molecular weight and τ_{rept}. According to Cooper-White et al., M_e of PLA is 8000 g mol^{-1} [17]. Previous studies on the flow induced crystallization were summarized as follows [18–21]:

- The first regime (Regime I) occurs when $Wi_R < 1$ and $Wi_{rept} < 1$, and shear flow is insufficient to affect the crystallization kinetic. Therefore, no apparent flow induced crystallization (FIC) effect will be observed.
- The second regime (Regime II) requires an increase in the shear rate, the molecular orientation occurs at $Wi_{rept} > 1$ and $Wi_R < 1$, which accelerated crystallization kinetics.
- The third regime (Regime III), chain stretching occurs at $Wi_R > 1$. This situation leads to the formation of extended chain crystals, i.e., shish.

However, there is an inconsistency relevant to Regime II. Rhoades and Pantani [20] supposed that 2 regimes would exist when $Wi_R < 1$ and $Wi_{rept} > 1$. One is the process of accelerating the crystallization kinetics and enhancing the formation of point-like nuclei. The other is the orientation of the "row" crystal nuclei.

2.1.2 Post-process annealing

As mentioned in Chapter 1, the significance of post-process annealing, known as heat-treatment, is inevitable in industry. From the viewpoint of manufacturer, post-process annealing is commonly utilized because it can save the cooling time by quench instead of cooling slowly in the mold. Generally, annealing at temperatures above T_g, at which the crystalline polymers undergo cold crystallization process once inadequately crystallization. Moreover, the degree of crystallinity is increased but reduces the molecular orientation. Therefore, shrinkage in the flow direction occurred, leading to the variety of dimension of a products [22–24]. In fact, PLA products exhibit shrinkage during post-processing annealing [25], posing a significant concern for composite systems incorporating metals and ceramics.

In this chapter, the thermal and rheological properties of PLA were investigated first. Then, the effect of the applied shear history on the structure development, such as crystallization and molecular orientation, during annealing was also studied. Furthermore, since similar phenomena occur in other crystalline polymers with slow crystallization rates, this research may provide new strategies for material design based on processing parameters.

2.2 Experimental procedure

2.2.1 Materials

A commercially available poly(lactic acid) (PLA) (Ingeo 4032D; NatureWork, Minnetonka, MN, USA) was used in this thesis. This PLA contained 1.5 % D-isomer with the average molecular weights of PLA in terms of number and weight were 1.0×10^5 and 1.8×10^5 Da, respectively. The PLA pellets were dried in a heater at 80 °C for 4 hours to remove the residual moisture.

2.2.2 Sample preparation

The procedure is shown in **Figure 2.2**. The 1.2 mm sheet was fabricated using a compression-molding machine at 200 °C for 2 min, followed by quench at 25 °C. Then, it was cut into square films with a length of 25 mm, and inserted into a parallel rheometer (MCR500, UBM, Mukō, Japan) at 180 °C. After reaching the designated temperature, the gap was set at 1 mm and kept for 5 min to remove the residual crystals. Once the temperature jumped to 160 °C, a shear flow with a shear rate at the edge of 30 s^{-1} was applied on the film for 2 min. After the cessation of shear flow, the film was quenched using water-spray and cut into two half-pieces. One piece was annealed in a heater at 80 °C for several periods. Another piece was used for further evaluation, as the film had a shear

history before annealing. In the case of the PLA film without shear history, a shear flow was not applied and kept for 2 min, followed by quench.

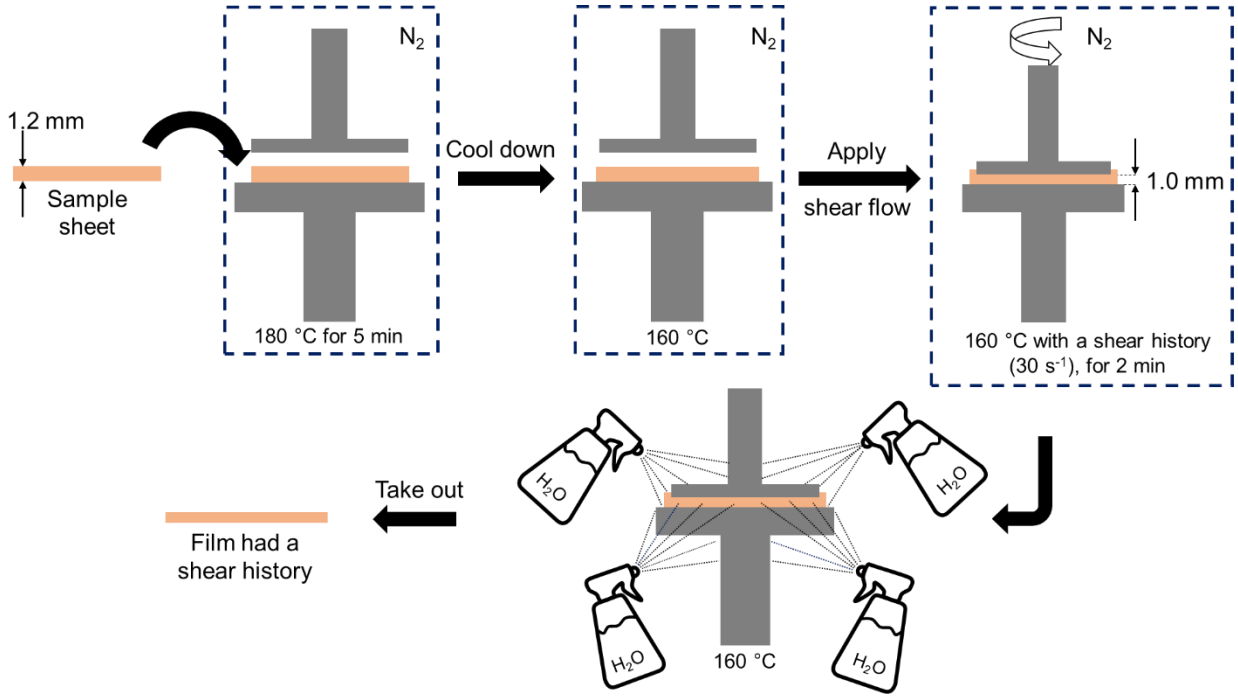

Figure 2.2. Sample preparation for the film with a shear history

2.3 Characterization

The compression-molded film was cut into rectangular samples (5 mm wide × 25 mm long × 0.9 mm thick) for DMA measurements (Rheogel E400, UBM, Kyoto, Japan). The measurements were conducted at 10 Hz in the temperature range from 30 to 200 °C at a heating rate of 2 °C min^{-1}.

The thermal properties of PLA were examined using a differential scanning calorimeter (DSC; DSC8500, PerkinElmer Inc, Shelton, CT, USA) under nitrogen flow.

The sample was heated from room temperature to 200 °C at a heating rate of 30 °C min^{-1} and kept at 200 °C for 2 min to remove the thermal history. Then, the cooling process was performed at various cooling rate, such as 30, 10, 3, and 1 °C min^{-1}. The heat of fusion Δh_f, enthalpy of cold crystallization Δh_{cc}, and enthalpy of crystallization Δh_c were collected from the program to calculate the degree of crystallinity (χ), as follows:

$$\chi_{DSC}\,(\%) = 100 \times \frac{\Delta h}{\Delta h_f^o} \tag{2.3}$$

where Δh_f^o is heat of fusion of perfect crystal, 93 J g^{-1} [26].

The frequency dependence of the oscillatory storage modulus G' and the loss modulus G'' was evaluated using a cone-and-plate rheometer (MCR301; Anton Paar, Graz Austria) at 160, 170, 180, 190, and 200 °C. The cone angle was 2°. The angular frequency was swept from 629.3 to 0.01 rad s^{-1}. All the measurements were conducted under a nitrogen gas.

The two-dimensional wide-angle X-ray diffraction (2D-WAXD) was employed to evaluate the crystallinity and orientation of the film before and after annealing using a X-ray diffractometer (SmartLab; Rigaku, Akishima, Japan). The CuKα radiation beam (45 kV and 200 mA) was directed in the normal direction to the film at a distance of 10 mm from the center of the pre-sheared films. The crystallinity was calculated using a fitting software “IgorPro”, applying the Gaussian method with a linear baseline.

2.4 Results and discussion

2.4.1 Thermal and rheological properties of PLA

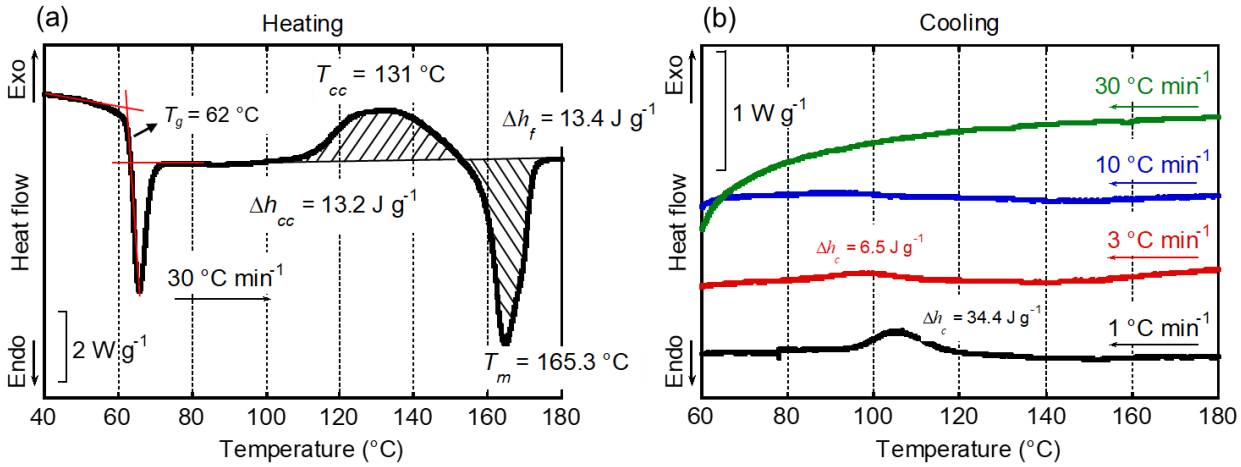

Figure 2.3. DSC curves of PLA during (a) heating at a heating rate of 10 °C min^{-1} and (b) cooling at various cooling rates.

Figure 2.3 shows the thermal properties of PLA. In the first heating, the step-wise change of heat flow was ascribed to the T_g of PLA, which was detected at 62 °C. An area of the endothermal peak after T_g, represented the enthalpy relaxation. Then, an exothermal peak at 131 °C and the endothermal peak at 165.3 °C were ascribed to the cold crystallization and the melting peak of PLA, respectively. The Δh_f and Δh_{cc} value was similar, indicating that the original film has no/few crystallinity. In the case of cooling process, the crystallization peak was clearly detected at 105 °C with a cooling rate of 1 °C

min^{-1}. The peak was shifted to a lower temperature with a small exothermal peak at the heating rate of 3 °C min^{-1}. Moreover, a clear crystallization peak cannot be detected at heating rate of 10 and 30 °C min^{-1}. These cooling rates were too fast for the sample to be crystallized. The crystallinity of PLA, calculated by equation (2.3) at various cooling rates of 30, 10, 3, and 1 °C min^{-1} were 0, 1, 9, and 37%, respectively.

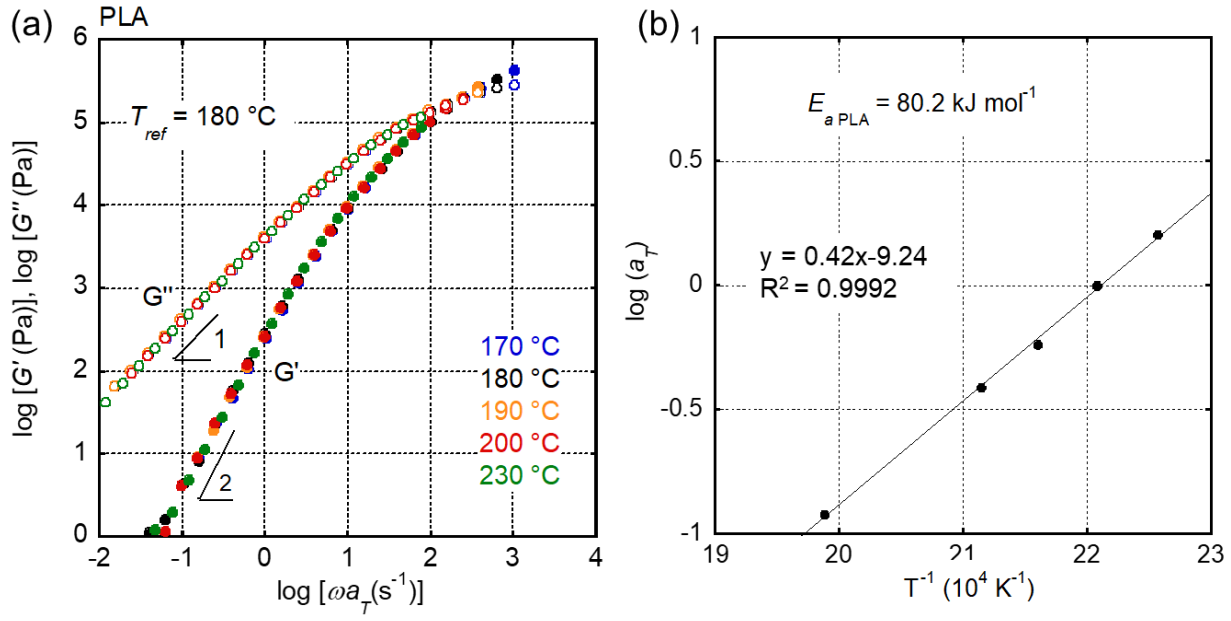

Figure 2.4. (a) Master curves of the angular frequency dependencies of the shear storage modulus G' and the loss modulus G'' of PLA and (b) horizontal shift factor a_T versus T^{-1} (10^4 K^{-1}) of PLA at the reference temperature T_{ref} of 180 °C.

Figure 2.4 shows the master-curves of PLA at the reference temperature of 180 °C. The G' and G'' of the PLA were proportional to ω^2 and ω, respectively [27,28]. This

behavior is similar to the viscoelastic behavior of the linear homopolymer in the molten state. The flow activation energy, E_a, was calculated from an Arrhenius-type equation, i.e., the Andrade equation, as follows:

$$a_T \propto Aexp\left(\frac{E_a}{RT}\right) \tag{2.4}$$

where a_T is the horizonal shift factor, R is the gas constant, T is the temperature, and A is the pre-exponential factor. The results of linear-fitting equation (1) are shown in **Figure 2.4b**, in which E_a values were calculated to be 80.2 kJ·mol^{-1}. This E_a value corresponded well with the data in the previous literatures [18,27,29]. From Figure 2.3, the zero-shear viscosity (η_0), steady-state shear compliance (J_e^0), and weight-average relaxation time (τ_w) were calculated, as follows:

$$\eta_0 = \lim_{\omega \to 0} \frac{G''}{\omega} \tag{2.5}$$

$$J_e^0 = \lim_{\omega \to 0} \frac{G'}{G''^2} \tag{2.6}$$

$$\tau_w = \frac{\int \tau^2 H(\tau)\, d\ln\tau}{\int \tau H(\tau)\, d\ln\tau} = \eta_0 J_e^0 \tag{2.7}$$

η_0 and J_e^0 of PLA at 180 °C were calculated to be around 4 × 10^3 Pa·s and 4.9 × 10^{-5} Pa^{-1}. Thus, the τ_w, given by equation 2.7, of PLA was 0.20 s. Using the Arrhenius-type equation (eq. 2.4), τ_w at various temperatures can be estimated as 0.41 s at 160 °C. It is well known that η_0 is proportional to $M_w^{3.4}$, where M_w is the weight-average molecular-weight. According to Dorgan [30], the following equation expresses the value of η_0 at 180 °C using the absolute value of M_w of PLA.

$$\log(\eta_0) = -14.26 + 3.4\log(M_w) \tag{2.8}$$

Thus, M_w was estimated to be 1.79×10^5 Da. This value is closely similar to the M_w obtained from gel permeation chromatography (GPC).

2.4.2 Effect of shear history on the structure growth of PLA during annealing

The small piece of a film had a shear history, i.e., a pre-sheared film, was cut at a radius of 10 mm from the center, where the shear history was calculated to be 24 s^{-1}. The DSC heating curves of the quenched film with/without a shear history is shown in **Figure 2.5**. For the quenched film without shear history, a broad exothermic peak at 135 °C and an endothermic peak at 166 °C correspond to the cold crystallization and melting of PLA, respectively. The melting peak was weak because the cold crystallization was insufficient. In contrast, the shear flow greatly enhanced the cold crystallization of the film. That is, a pronounced cold crystallization peak at a lower temperature was detected 124 °C. For both films, the Δh_f was almost the same as the Δh_{cc}. This result demonstrates that the quench method rapidly solidifies PLA films without crystallization, leading to an amorphous morphology. The enhanced cold crystallization observed in the pre-sheared film was likely due to the presence of tiny crystals, as discussed later.

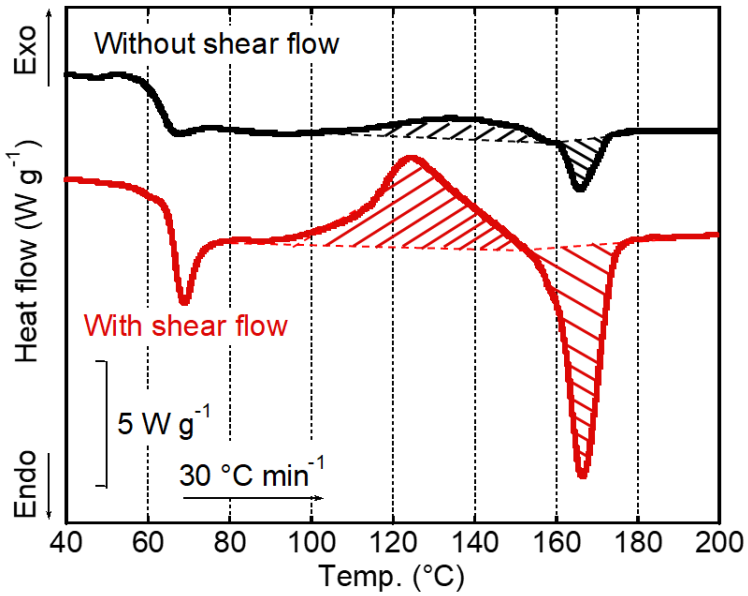

Figure 2.5. DSC heating curves of the films with (red) without shear history (black).

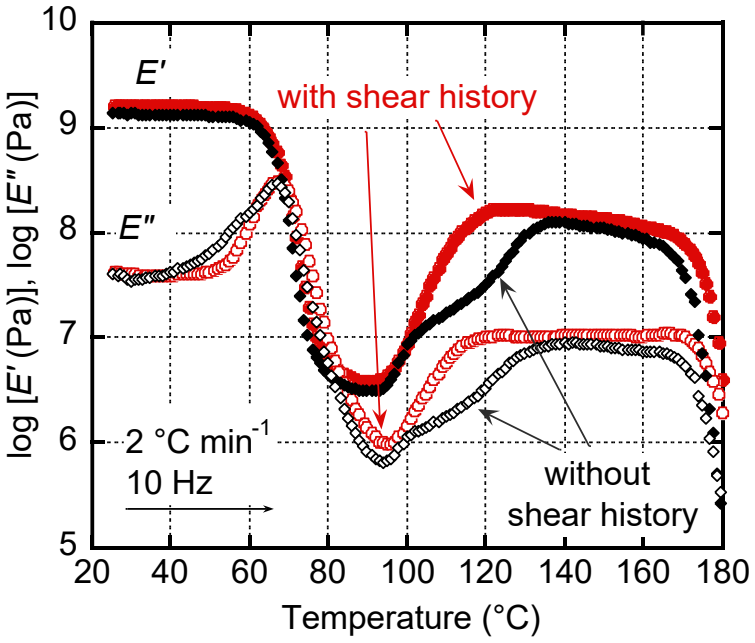

Figure 2.6. Temperature dependencies of tensile storage modulus (E') (filled symbols) and loss modulus (E'') (open symbols) at 10 Hz for the films with (red) and without shear history (black).

The temperature dependences of dynamic tensile moduli for the quenched films with/without shear history are shown in **Figure 2.6**. During heating, E' remarkably dropped between the temperature range of 60 and 80 °C, while a sharp peak of E'' at around 67 °C was assigned to the T_g. Subsequently, the E' increased with the temperature between 90 and 120 °C, corresponding to the cold crystallization. Notably, this increase in E' occurred earlier in the film with shear history, although the effect was less pronounced due to relatively slow heating rate (2 °C min^{-1}), compared to DSC measurement (30 °C min^{-1}). Above 165 °C, both moduli dropped significantly as a result of melting.

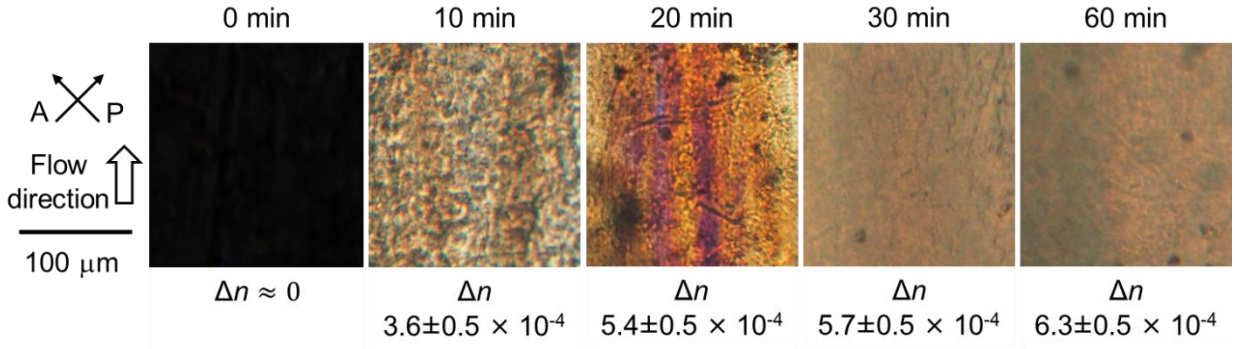

Figure 2.7. Polarized optical microscope images under cross-polarizers of the annealed film having a shear history at 80 °C.

Figure 2.7 shows the polarized optical microscope images of the pre-sheared film during annealing at 80 °C for various periods. Prior to annealing (0 min), there was a dark color, i.e., indicating the absence of light transmission and thus suggesting no molecular orientation. Optical retardation (Γ) was determined using a Berek compensator, and the birefringence (Δn) was subsequently calculated from the film thickness (d), measured with a micrometer, as follows:

$$\Delta n = \frac{\Gamma}{d} \tag{2.9}$$

Hermans orientation function was evaluated using the following equation:

$$F = \frac{\Delta n}{\Delta n^0} \tag{2.10}$$

where Δn_0 is the intrinsic birefringence, and the Δn^0 value was 0.30 for PLA [31]. From these calculation, the Δn increased with the annealing period, then reached the saturation state at a period of 60 min. This result indicates that molecular orientation was enhanced during annealing.

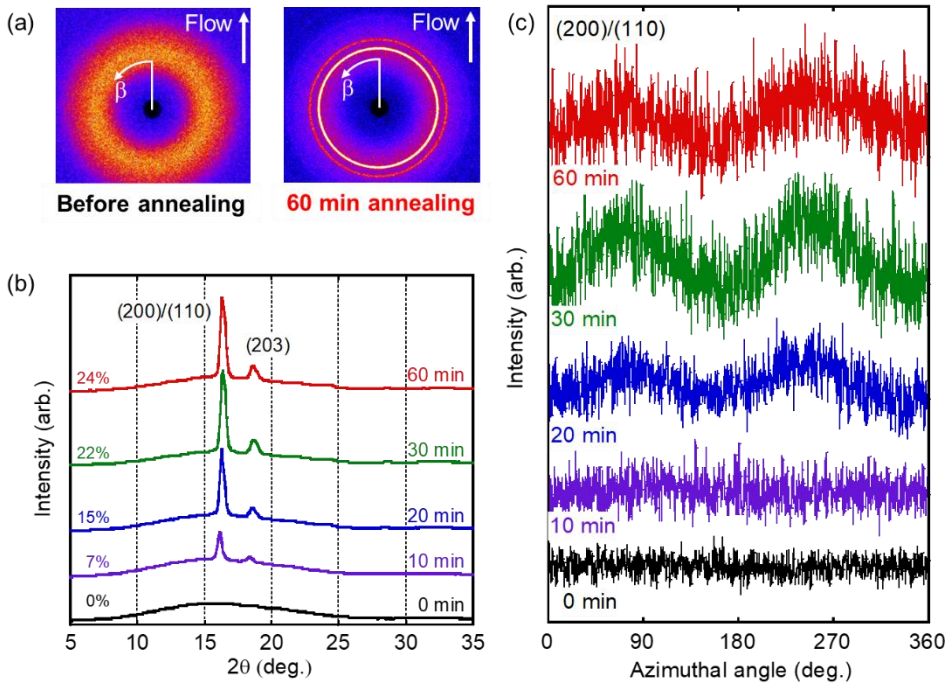

Figure 2.8. (a) 2D-WAXD images, (b) 2θ profile, and (c) azimuthal distribution at 2θ = 16° for the film had a shear history annealed at 80 °C for various periods.

The structure development of the films had a shear history annealed at 80 °C was evaluated using 2D-WAXD, as shown in **Figure 2.8**. Before annealing (0 min), 2θ profile

exhibited a broad peak, i.e., amorphous halo. In contrast, clear diffraction peaks appeared at 16° and 18° for the film annealed beyond 10 min, corresponding to the (200)/(110) and (203) planes of α-form crystals, respectively [3,32]. Although direct evaluation of orientation from the 2D-WAXD images was challenging, the azimuthal intensity distribution of the strongest reflection showed clear maxima at 90° and 270° (on the equator) after annealing. No peaks were observed in the film without annealing. This suggests that annealing promotes chain alignment along the flow direction, leading to molecular orientation. The molecular orientation increased as the annealing time increased but remained constant after 30 min. This finding matched the birefringence data in Figure 2.7. It should be noted that Wi_R associated with the Rouse relaxation at 160 °C should be larger than one at the shear rate of 24 s^{-1}, i.e., the applied shear rate before quench. Although the shear rate is a critical parameter governing the relaxation behavior of polymers, the shear strain also plays a role in describing the coil-stretch transition. The shear strain, however, is proportional to the shear time and shear rate, and the extended-chain crystals occur only once the shear rate exceeds the inverse of the Rouse relaxation time. In other words, the extended-chain crystals, i.e., shish, were promoted during applying shear flow (24 s^{-1} for 2 min) in the rheometer. Because of small amount of shish-structure, its crystallinity cannot be easily detected by WAXD and DSC measurements prior to annealing. For the same reason, orientation was also not observed by optical microscopy before annealing. However, these small crystals generated during shearing acted as effective nucleation sites during annealing, as shown by increased cold crystallization in the DSC heating curves. Additionally, the alignment of shish structures along the flow

direction induced the orientation of the crystalline chains grew during. In other words, the increase in molecular orientation during annealing resulted from the crystal growth from originating from the extended-chain crystals. This unusual growth of molecular orientation in PLA is important for controlling dimensions and mechanical properties, such as its anisotropy and modulus.

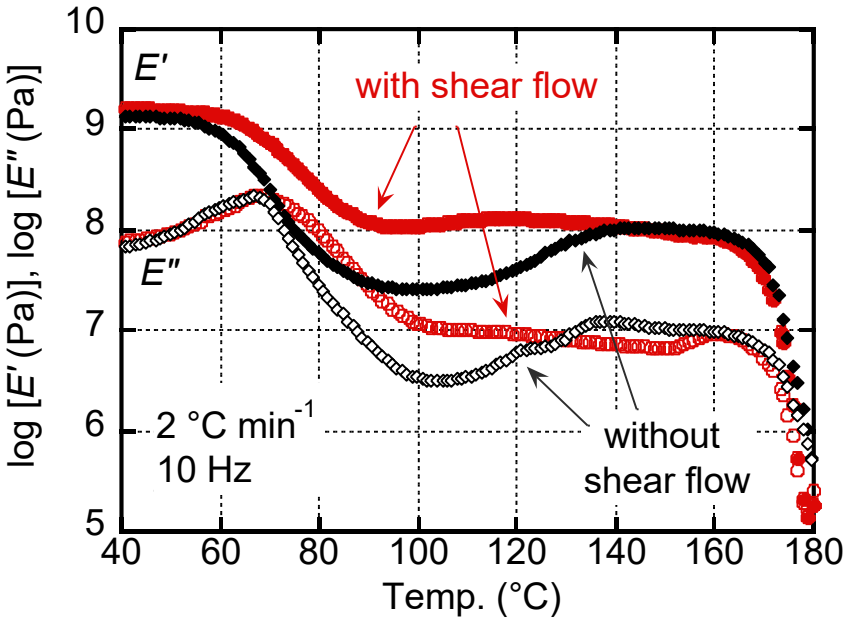

Figure 2.9. Temperature dependences of tensile storage modulus (E') and loss modulus (E'') at 10 Hz for the films with (red) and without shear history (black) after annealed at 80 °C for 60 min.

Figure 2.9 shows the solid-state viscoelastic properties of the films after annealing at 80 °C for 60 min, measure at a heating rate of 2 °C min^{-1}. One sample had a shear history, and the other did not. The film with a shear history exhibited a higher E' in the wide

temperature region, e.g., from 60 to 140 °C, reflecting its enhanced crystallinity and chain orientation. In contrast, the film without shear history showed a pronounced increase in modulus above Tg due to cold crystallization, even after annealing. These results indicate that applied shear flow plays a critical role in reducing the annealing time required to attain sufficient crystallinity.

2.5 Conclusion

The growth of polymer structure during annealing, an essential industrial technique for PLA, was examined using the quenched PLA films having a shear history. An applied shear rate of 24 s^{-1} for 2 min at 160 °C did not induce high chain orientation, despite the *Wi*, which governs molecular orientation via reptation, exceeding unity. It was attributed to the rapid orientation relaxation occurred before solidification (glassification). In addition, no significant crystallinity was detected after quenching. However, it was presumed that small quantities of extended-chain crystals remained oriented along the flow direction to some extent. During annealing above the T_g, those extended-chain crystals acted as nucleation sites, leading to accelerated cold crystallization. Moreover, analysis of the azimuthal distribution of the (200)/(100) crystalline diffraction peaks obtained by 2D-WAXD measurements clearly demonstrated the progressive chain orientation. These findings provide valuable insights for improving the dimensional stability, rigidity, and anisotropy, as well as heat resistance of PLA materials after annealing treatments. Exploiting this phenomenon, PLA can be effectively applied in diverse applications, such as injection-molded components used in automotive parts and electronic device housings. Enhancing rigidity with a thinner thickness, leading to weight reduction, has been demanded for lightweight automotive parts.

References

[1] M. Yamaguchi, Manufacturing of High performance biomass-based polyesters by rheological approach, in: V. K. Thakur, M.K. Thakur and M.R. Kessler (Ed.), Handbook of Composites from Renewable Materials, John Wiley & Sons, 2017, 25–47.

[2] L. T. Sin, B. S. Tueen, Polylactic Acid - A Practical Guide for the Processing, Manufacturing, and Applications of PLA – 2nd Edition, Elsevier, Netherland, 2019.

[3] R. A. Auras, L. -T. Lim, S. E. M. Selke, H. Tsuji, Poly(lactic acid): Synthesis, Structures, Properties, Processing, Applications, and End of Life, 2nd Edition, Wiley, Hoboken, New Jersey, 2022.

[4] K. Jamshidi, S. -H. Hyon, Y. Ikada, Thermal characterization of polylactides, *Polymer*, 29 (1988) 2229–2234. https://doi.org/10.1016/0032-3861(88)90116-4

[5] R. Vasanthakumari, A. J. Pennings, Crystallization kinetics of poly(l-lactic acid), *Polymer*, 24 (1983) 175–178.
https://doi.org/10.1016/0032-3861(83)90129-5

[6] K. Okamoto, T. Ichikawa, T. Yokohara, M. Yamaguchi, Miscibility, mechanical and thermal properties of poly(lactic acid)/polyester-diol blends, *Eur. Polym. J.*, 45, (2009) 2304–2312.
https://doi.org/10.1016/j.eurpolymj.2009.05.011

[7] M. Murariu, A. D. S. Ferreira, M. Alexandre, P. Dubois, Polylactide (PLA) designed with desired end-use properties: 1. PLA compositions with low molecular weight ester-like plasticizers and related performances, *Polym. Adv. Technol.* 19 (2008), 636-646.

[8] T. Huang, M. Miura, S. Nobukawa, M. Yamaguchi, Crystallization Behavior and Dynamic Mechanical Properties of Poly(l-Lactic Acid) with Poly(Ethylene Glycol) Terminated by Benzoate, *J. Polym. Environ.*, 22 (2014) 183–189. https://doi.org/10.1007/s10924-014-0638-y

[9] Y. Feng, P. Ma, P. Xu, R. Wang, W. Dong, M. Chen, C. Joziasse, The crystallization behavior of poly(lactic acid) with different types of nucleating agents, *Int. J. Biol. Macromol.*, 106, (2018), 955–962.
https://doi.org/10.1016/j.ijbiomac.2017.08.095

[10] Z. Qiu, Z. Li, Effect of orotic acid on the crystallization kinetics and morphology of biodegradable poly(l-lactide) as an efficient nucleating agent, *Ind. Eng. Chem. Res.*, 50, (2011), 12299–12303.
https://doi.org/10.1021/ie2019596

[11] T. Ageyeva, J. G. Kovács, T. Tábi, Comparison of the efficiency of the most effective heterogeneous nucleating agents for Poly(lactic acid), *J. Therm. Anal. Calorim.*, 147, (2022), 8199–8211.
https://doi.org/10.1007/s10973-021-11145-y

[12] Q. Han, Y. Wang, C. Shao, G. Zheng, Q. Li, C. Shen, Nonisothermal crystallization kinetics of biodegradable poly(lactic acid)/zinc phenylphosphonate composites, *J. Compos. Mater.,* 48, (2014), 2737–2746.
https://doi.org/10.1177/0021998313502064

[13] N. Kawamoto, A. Sakai, T. Horikoshi, T. Urushihara, E. Tobita, Nucleating agent for poly(L-lactic acid) - An optimization of chemical structure of hydrazide compound for advanced nucleation ability, *J. Appl. Polym. Sci.*, 103, (2007), 198–203. https://doi.org/10.1002/app.25109

[14] Q. Xing, X. Zhang, X. Dong, G. Liu, D. Wang, Low-molecular weight aliphatic amides as nucleating agents for poly (L-lactic acid): Conformation variation induced crystallization enhancement, *Polymer*, 53, (2012), 2306–2314. https://doi.org/10.1016/j.polymer.2012.03.034

[15] K. Saitou, M. Yamaguchi, Transparent poly(lactic acid) film crystallized by annealing beyond glass transition temperature, *J. Polym. Res.*, 27, (2020), 104. https://doi.org/10.1007/s10965-020-02071-y

[16] K. Tashiro, Growth of Polymer Crystals, in: E. Piorkowska, and G. C. Rutledge (Ed.), Handbook of Polymer Crystallization, Wiley, Hoboken, New Jersey, 2013, 165–196.

[17] J. J. Cooper-White, M. E. Mackay, Rheological properties of poly(lactides). Effect of molecular weight and temperature on the viscoelasticity of poly(l-lactic acid), *J. Polym. Sci. Part B: Polym. Phys*, 37, (1999), 1803-1814.

[18] Y. Zhong, H. Fang, Y. Zhang, Z. Wang, J. Yang, Z. Wang, Rheologically determined critical shear rates for shear-induced nucleation rate enhancements of poly(lactic acid), *ACS Sustainable Chem. Eng.*, 1, (2013), 663–672. https://doi.org/10.1021/sc400040b

[19] A. Jalali, S. Shahbikian, M. A. Huneault, S. Elkoun, Effect of molecular weight on the shear-induced crystallization of poly(lactic acid), *Polymer*, 112, (2017), 393–401.

https://doi.org/10.1016/j.polymer.2017.02.017

[20] A. Rhoades, R. Pantani, Poly(Lactic Acid): Flow-induced crystallization, in: M. L. Di lorenzo, R. Androsch (eds.), Thermal properties of bio-based polymers, Springer, Cham, Switzerland, 2019, 87–117

[21] Z. Zhang, S. G. Hatzikiriakos, Flow-induced crystallization of polylactides, *J. Rheo.*, 66, (2022), 257.

https://doi.org/10.1122/8.0000372

[22] K. M. B. Jansen, D. J. Van Dijk, M. H. Husselman, Effect of processing conditions on shrinkage in injection molding, *Polym. Eng. Sci.*, 38, (1998), 838–846.

https://doi.org/10.1002/pen.10249

[23] D. Annicchiarico, J. R. Alcock, Review of factors that affect shrinkage of molded part in injection molding, *Mater. Manuf. Process.*, 29, (2014), 662–682.

https://doi.org/10.1080/10426914.2014.880467

[24] N. Zhao, J. Lian, P. Wang, Z. Xu, Recent progress in minimizing the warpage and shrinkage deformations by the optimization of process parameters in plastic injection molding: a review, *Int. J. Adv. Manuf. Technol.*, 120, (2022), 85–101.

https://doi.org/10.1007/s00170-022-08859-0

[25] S. Singh, A. Rajeshkannan, S. Feroz, A. K. Jeevanantham, Effect of normalizing on the tensile strength, shrinkage and surface roughness of PLA plastic, *Mater. Today Proc.*, 24, (2020), 1174–1182.

https://doi.org/10.1016/j.matpr.2020.04.431

[26] E. W. Fischer, H. J. Sterzel, G. Wegner, Investigation of the structure of solution grown crystals of lactide copolymers by means of chemical reactions, *Kolloid Z. or Kolloid. Z.*, 251, (1973), 980-990.
https://doi.org/10.1007/BF01498927

[27] A. Jalali, M. A. Huneault, M. Nofar, P. C. Lee, C. B. Park, Effect of branching on flow-induced crystallization of poly (lactic acid), *Eur. Polym. J.*, 119, (2019), 410–420.
https://doi.org/10.1016/j.eurpolymj.2019.07.045

[28] A. Jalali, J. -H. Kim, A. M. Zolali, I. Soltani, M. Nofar, E. Behzadfar, C. B. Park, Peculiar crystallization and viscoelastic properties of polylactide/polytetrafluoroethylene composites induced by in-situ formed 3D nanofiber network, *Compos. B: Eng.*, 200, (2020), 108361.
https://doi.org/10.1016/j.compositesb.2020.108361

[29] Y. Zhong, H. Fang, Y. Zhang, Z. Wang, J. Yang, Z. Wang, Rheologically determined critical shear rates for shear-induced nucleation rate enhancements of poly(lactic acid), *ACS Sustainable Chem. Eng.*, 1, (2013), 663–672.
https://doi.org/10.1021/sc400040b

[30] D. Kugimoto, S. Kouda, M. Yamaguchi, Modification of poly(Lactic Acid) rheological properties using ethylene–vinyl acetate copolymer, *J. Polym. Environ.*, 29, (2021), 121–129.
https://doi.org/10.1007/s10924-020-01856-y

[31] J. R. Dorgan, J. S. Williams, D.N. Lewis, Melt rheology of poly(lactic acid): Entanglement and chain architecture effects, *J. Rheo.*, 43, (1999), 1141–1155.

https://doi.org/10.1122/1.551041

[32] Y. Furuhashi, Y. Kimura, H. Yamane, Higher order structural analysis of stereocomplex-type poly(lactic acid) melt-spun fibers, *J. Polym. Sci., Part B:Polym. Phys.*, 45, (2007), 218–228.

https://doi.org/10.1002/polb.21035

[33] Y. -T. Hsieh, S. Nozaki, M. Kido, K. Kamitani, K. Kojio, A. Takahara, Crystal polymorphism of polylactide and its composites by X-ray diffraction study, *Polym. J.*, 52, (2020), 755–763.

https://doi.org/10.1038/s41428-020-0343-8

Chapter 3. Structure development of polymer containing fibrous nucleating agent under post-process annealing

3.1 Introduction

In chapter 2, the overcoming limitations of PLA, such as poor heat resistance after annealing, were clarified. However, the requirement for annealing was long period to achieve the high crystallinity. Nucleating agents are commonly employed to accelerate crystallization and increase the crystallinity of polymers. A nucleating agent provides nuclei sites for the crystal development, accelerating the crystallization, and consequently improving mechanical strength, and thermal stability. As reported in Chapter 2, various nucleating agents can be used to enhance the crystallization rate of PLA. In industry, nucleating agents are sometimes used as a clarification agent for enhancing transparency with high crystallinity. One effective organic nucleating agent for PLA is N,N′-ethylenebis(12-hydroxystearamide) (EBHS) [1–5], as shown in **Figure 3.1**. Moreover, it significantly enhances PLA crystallization by promoting the formation of nuclei, thereby speeding up the crystallization rate. It has been known that EBHS was a fibrous nucleating agent because it segregated into fibril structures in the PLA matrix. The diameter of EBHS fibrils in PLA is known to be around 50 nm [3]. The addition of EBHS increases the degree of crystallinity and heat resistance of PLA products [1,3,6,7]. However, the crystallinity of PLA containing EBHS is still low when cooled rapidly at actual process, i.e., over 1000 °C

min^{-1} [8–11]. In fact, Saitou et al. revealed that quenched PLA films containing EBHS hardly showed crystallinity [3].

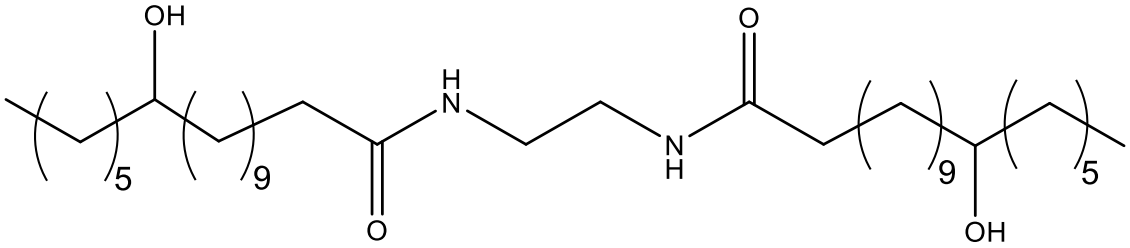

Figure 3.1 Structure of N,N′-ethylenebis(12-hydroxystearamide) (EBHS)

This chapter will focus on the effect of molecular orientation on controlling the natural shrinkage of extruded strands. The structural growth of the extruded strand of PLA and PLA/EBHS during annealing was studied. This study also elucidates the mechanism of anisotropic shrinkage after annealing.

3.2 Experimental procedure

3.2.1 Materials

The PLA pellets employed in this study were the same as those used in the previous chapter. EBHS powder (Itohwax J-550S; Itoh Oil Chemicals, Yokkaichi, Japan) was used as a nucleating agent. All materials were dried at 80 °C under vacuum.

3.2.2 Sample preparation

Figure 3.2 shows the process to prepare the sample. EBHS powder and PLA pellets were mixed in a 30cc internal mixer (Labo-plastomill, 10M-100, Toyo Seiki Seisakusyo, Tokyo, Japan) at 200 °C for 5 min. Rotation speed of the blade was set at 50 rpm. The EBHS content in the blend was decided to be 1 wt.%. For comparison, pure PLA without EBHS was prepared with the same processing history. Flat films (900 μm) were prepared by compression molding at 200 °C under 10 MPa for 2 min, followed by quenching at 25 °C for 5 min using a cooling system.

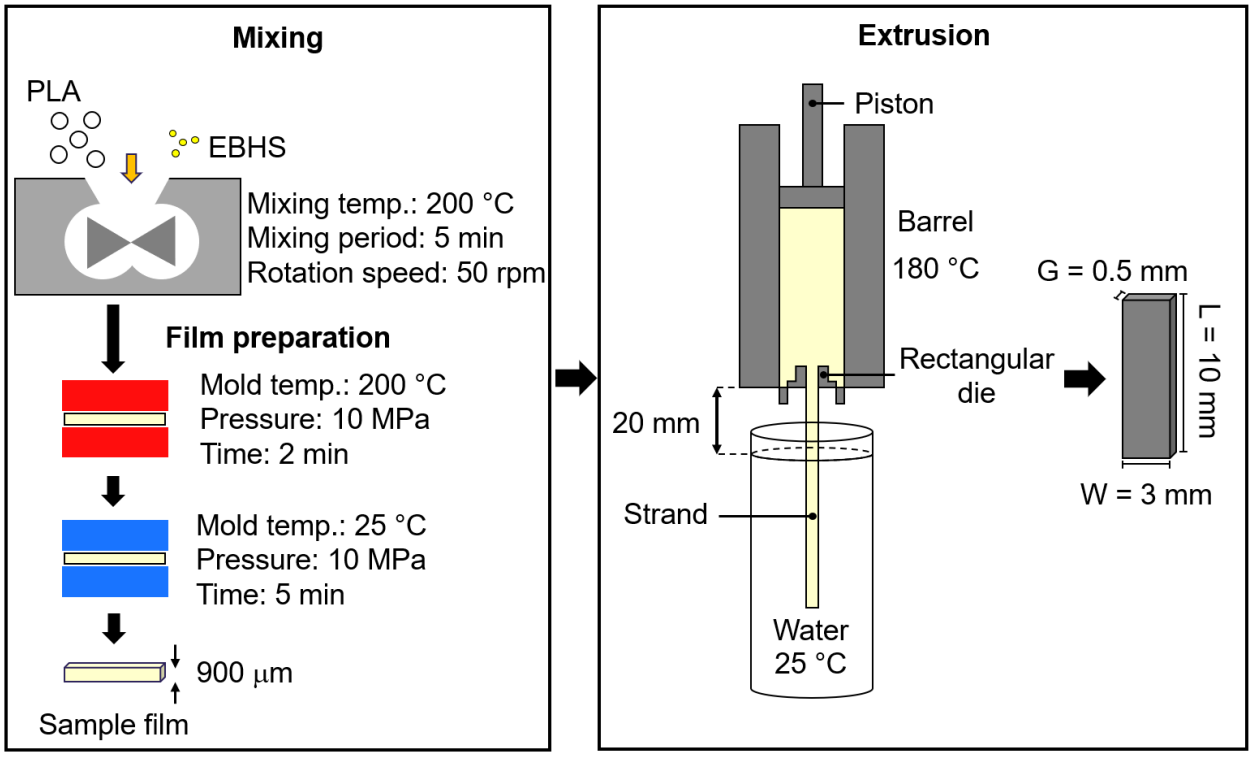

Figure 3.2. Scheme of sample preparation: (left) mixing and (right) strand extrusion

The films were cut into 3 mm-wide pieces and extruded using a capillary rheometer (140-SAS-2002; Yasuda Seiki Seisakusyo, Nishinomiya, Japan). The barrel and die temperature were set and controlled at 180 °C. A rectangular die measuring 3 mm wide (W), 0.5 mm gap (G), and 10 mm long (L) was used. The apparent shear viscosity (η) and shear rate at the wall were calculated using the Hagen–Poiseuille law, given by the following equations:

$$\eta = \frac{G^3 W \Delta P}{12QL}, \tag{3.1}$$

$$\dot{\gamma} = \frac{6Q}{G^2 W}, \tag{3.2}$$

where ΔP is the pressure drop across the die, and Q is the volumetric flow rate. The strands were extruded at a shear rate of 310 s^{-1}, a typical value for T-die extrusion. After extrusion, the strands were immediately quenched in a water at 25 °C. The distance between the exit of the die and water surface was 20 mm.

3.3 Characterization

The strand surface was observed using a scanning electron microscope (SEM; TM3030Plus; Hitachi, Tokyo, Japan) after platinum–palladium coating using an ion-sputtering machine.

Thermal properties were studied by differential scanning calorimetry (DSC; DSC8500; PerkinElmer, Shelton, CT, USA) under a purified nitrogen flow. The compression-molded PLA, EBHS, and PLA/EBHS films were heated to 180 °C and held

for 2 min to erase their thermal history, then cooled to 30 °C at 30 °C min^{-1} and then maintained at this temperature for 2 min. A second heating run was subsequently performed at 30 °C min^{-1}. Crsytallinity was calculated from the melting or crystallization peaks, assuming a heat of fusion of a pure PLA crystal is 93 J g^{-1} [12].

The angular frequency dependencies of the oscillatory shear storage modulus (G') and loss modulus (G'') were measured using a cone-and-plate rheometer (AR2000ex; TA Instruments, New Castle, MA, USA) with angular frequency swept from 100 to 0.06 rad s^{-1}.

The molecular orientation of the strands was observed using a polarized optical microscope (POM) (DMLP; Leica Microsystems, Wetzlar, Germany). The temperature-controller with a window (FP90/FP82HT; Mettler Toledo, Columbus, OH, USA) was placed in the POM. Each extruded strand was cut and inserted between cover glasses. The temperature profile used during annealing, as shown in **Figure 3.3**. A photodetector (PM16-121; Thorlabs, Newton, MA, USA) was inserted into one of the eyepieces of the POM to record the depolarized light intensity (DLI) through a bandpass color filter (633 nm). Moreover, a digital camera (E-PL10; Olympus, Tokyo, Japan) was set in the other eyepiece to capture morphological images. The optical retardation values were evaluated using a Berek compensator and measured five times. Then, the average value was calculated.

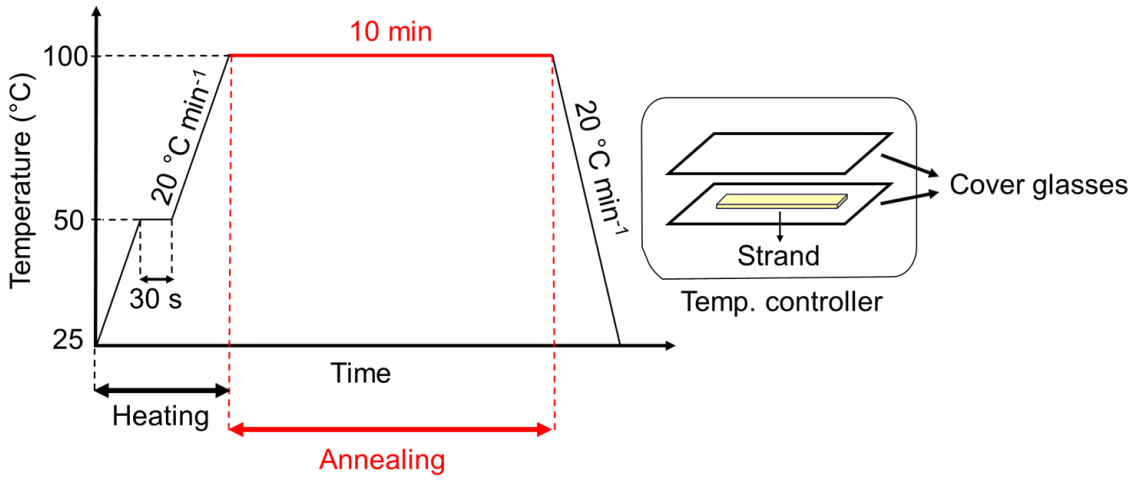

Figure 3.3. Temperature profile (left) and scheme of annealing protocol (right) of the sample setup during the annealing procedure.

The crystalline structure and molecular orientation of the extruded strand were evaluated using a 2D wide-angle X-ray diffraction (2D-WAXD) machine (SmartLab; Rigaku, Akishima, Japan). The degree of crystallinity (χ_{WAXD}) was calculated according to the following equation:

$$\chi_{WAXD} = \frac{\Sigma_i I_{Ac_i}}{\Sigma_i I_{Ac_i} + \Sigma_{Aa}}, \tag{3.3}$$

where I_{Aci} and I_{Aa} are the integrated areas of crystalline and amorphous peaks, respectively. Peak-fitting software (IgorPro) was used to calculated the integrated area of the fitting peaks with the Gaussian methodology and a linear baseline.

The temperature dependencies of the dynamic tensile moduli were evaluated using a dynamical mechanical analyzer (Rheogel E-4000; UBM, Muko, Japan) in tensile mode.

Measurements were performed at 10 Hz from 30 to 180 °C with a heating rate of 2 °C min^{-1}.

To evaluate the dimensional change caused by annealing, an extruded strand was cut into a length of 50 mm at 25 °C. This exact length of each sample at 25 °C was assumed as the strand before annealing. Then, it was annealed in hot water at 96 ± 1 °C for 10 min. After annealing, each sample was removed, dried and measured again at 25 °C. Three strands were tested for each sample type, e.g., PLA or PLA/EBHS. The average percentage of dimensional change and standard deviation were calculated.

3.4 Results and discussion

3.4.1 Thermal and rheological properties

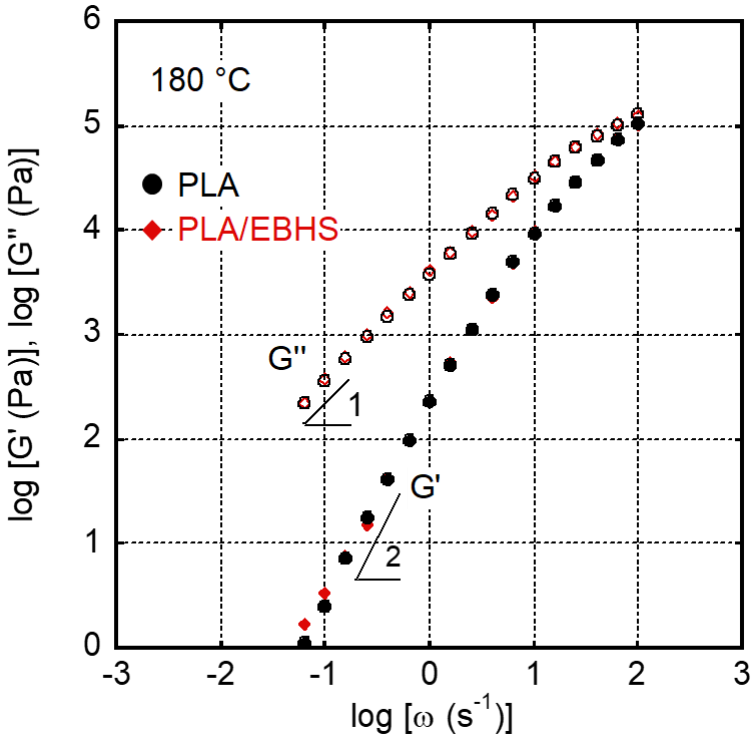

Figure 3.4. Angular frequency ω dependencies of shear storage modulus *G′* (filled symbols) and loss modulus *G″* (open symbols) at 180 °C for PLA (black circles) and PLA/EBHS (red diamonds).

The formation of an EBHS network structure in the PLA/EBHS blend was evaluated through viscoelastic measurements, as shown in **Figure 3.4**. It has been known that a plateau appears in the *G′* curve at low frequency when a network structure is present [13]. However, *G′* and *G″* for both samples at 180 °C were almost the same without a plateau. It

indicated that EBHS was not segregated into fibers but rather dissolved uniformly within PLA matrix at the molecular scale at this temperature. In other words, the segregation temperature of EBHS in PLA is lower than 180 °C, which will be discussed in detail later. Based on these measurements, rheological parameters, such as the zero-shear viscosity (η_0) and steady-state shear compliance (J_e^0) of PLA/EBHS, were similar to those of PLA at any temperatures. Thus, η_0 and J_e^0 of PLA/EBHS at 180 °C were calculated to be 4.0 × 10^3 Pa s and 4.9 × 10^{-5} Pa^{-1}, respectively. Thus, the weight-average relaxation time (τ_w), given by $\eta_0 J_e^0$, of PLA/EBHS was 0.20 s.

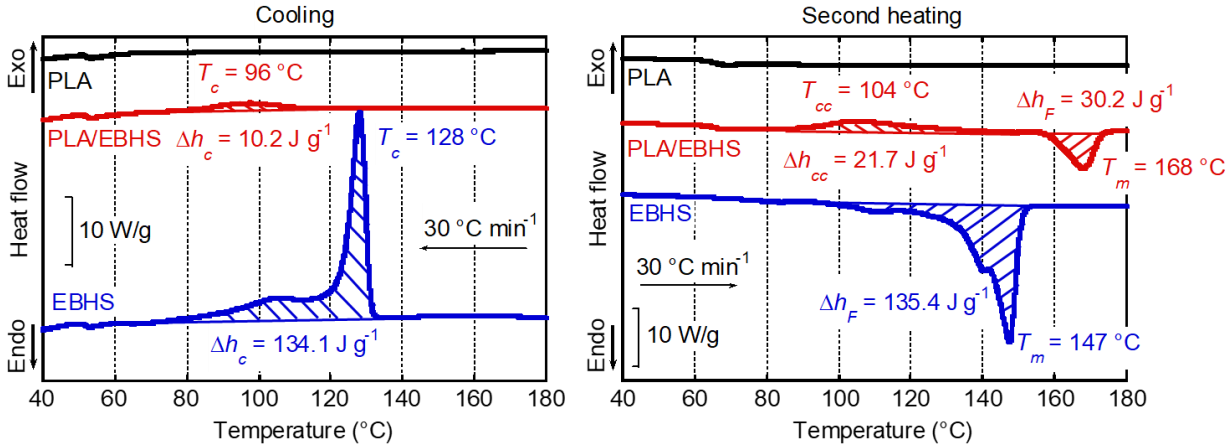

Figure 3.5. DSC (a) cooling and (b) second heating curves of PLA, EBHS, and PLA/EBHS

Figure 3.5 shows the thermal properties of PLA, EBHS, and PLA/EBHS. In the DSC cooling curves from 180 °C (Figure 3.5a), the crystallization peak of PLA was not detected during cooling at 30 °C min^{-1} due to low crystallization rate. In contrast, a sharp crystallization peak was found for pure EBHS at 128 °C. Therefore, it is reasonable that EBHS was dissolved in the molten PLA at 180 °C. PLA/EBHS showed a weak peak at around 96 °C, which was different from pure PLA. Considering that the EBHS content of

this blend was only 1 wt.%, this peak was attributed to PLA crystallization. The result confirmed that the role of EBHS acted as a nucleating agent, as mentioned in the introduction [1,3,14].

Figure 3.5b shows the second heating curves for PLA, EBHS, and PLA/EBHS. In the case of PLA/EBHS, a broad cold-crystallization peak temperature (T_{cc}) from 90 to 140 °C was detected at 104 °C. The peak area (Δh_{cc}) was estimated to be 21.7 J g^{-1}. For PLA/EBHS, a melting peak was at 168 °C with the heat of fusion (Δh_F) of 30.2 J g^{-1}, which was close to the sum of the crystallization peak area (Δh_c) for the melt (10.2 J g^{-1}) and Δh_{cc} (21.7 J g^{-1}). It can be concluded that the DSC heating curves of PLA and PLA/EBHS differ significantly. Because pure PLA did not show a melting peak under the same conditions, these crystals were developed from the EBHS fibers.

3.4.2 Structural of extruded strands

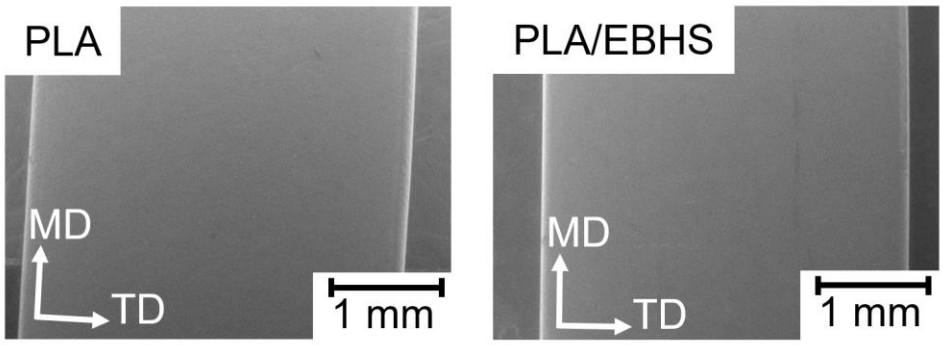

Figure 3.6. SEM images of the surface of PLA (left) and PLA/EBHS (right) strands. MD and TD are machine direction (MD) and transverse direction (TD), respectively.

The strands extruded from the rectangular die at an experimental shear rate of 310 s^{-1} showed a smooth surface without melt fracture. **Figure 3.6** shows SEM images of the surfaces of PLA and PLA/EBHS rectangular strands in the plane of the machine (MD) and transverse (TD) directions. The shear viscosity calculated using Equation 1 was 540 Pa s at 310 s^{-1} and 180 °C for both samples.

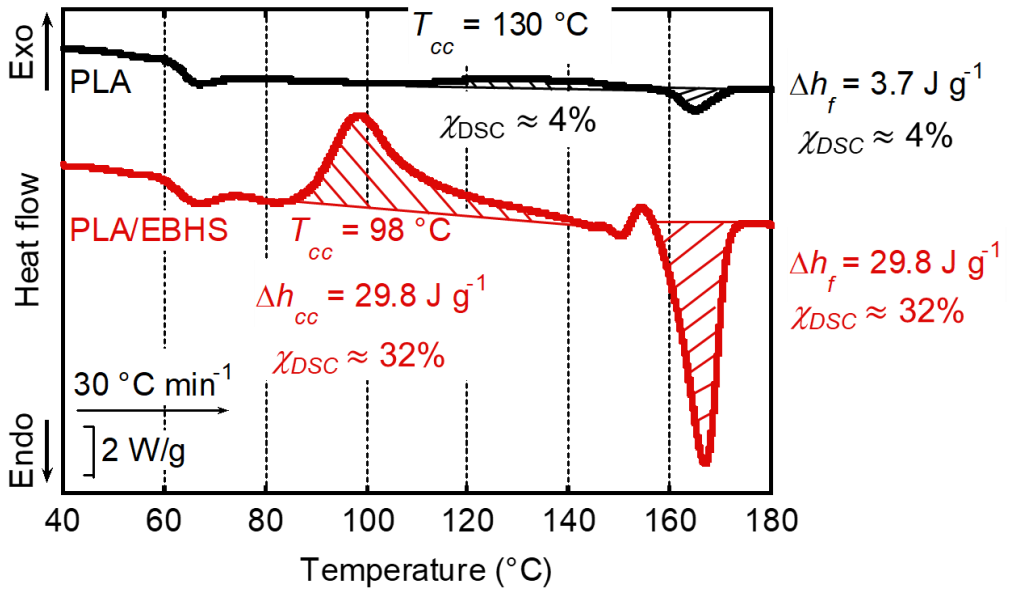

Figure 3.7. DSC heating curves of PLA (bottom) and PLA/EBHS (top) extruded strands. The heating rate was 30 °C min^{-1}.

After extrusion, the thermal behavior of the strands was evaluated by DSC, as shown in **Figure 3.7**. A cold-crystallization peak was clearly detected for PLA/EBHS as reported previously [3]. T_{cc}, which was located at 98 °C with Δh_{cc} of 29.8 J g^{-1}, corresponded to χ_{DSC} of 32 %. Moreover, the Δh_f was similar to Δh_{cc}, suggesting that there was no/little crystallization after extruded and quenched in water. In the case of PLA, a weak broad peak was detected from 110 to 150 °C, even though a cold-crystallization peak was not detected for PLA before extrusion (Figure 3.5b). The difference in the thermal properties of the PLA samples between before and after extrusion was attributed to crystal embryos, i.e., extended-chain crystals, which were provided by the applied flow during extrusion. In other words, extended-chain crystals must appear to some degree in the PLA extruded

strand. This result was similar to Chapter 2, that is, these extended-chain crystals acted as nuclei sites for PLA during heating.

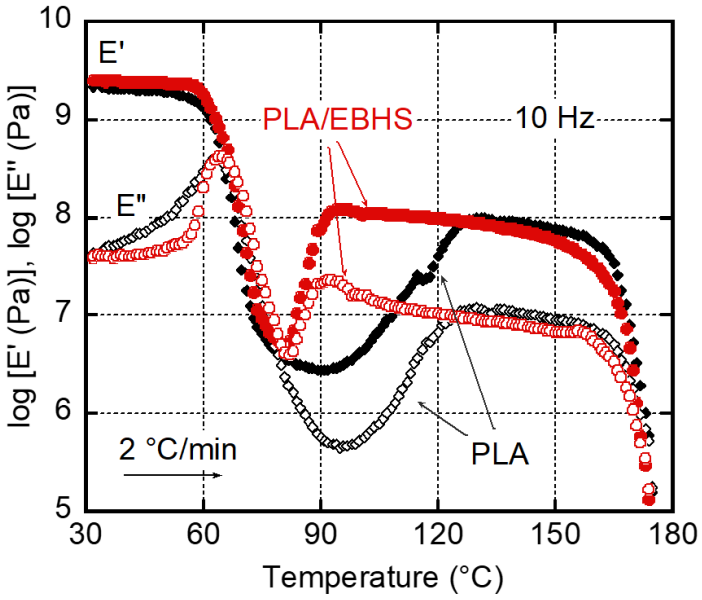

Figure 3.8. Temperature dependencies of tensile storage modulus (E') (filled symbols) and loss modulus (E'') (open symbols) at 10 Hz for extruded strands of PLA (diamonds) and PLA/EBHS (circles). The heating rate was 2 °C min^{-1}.

Figure 3.8 shows the viscoelastic properties in the solid state of the tensile storage modulus (E') and loss modulus (E'') for extruded strands of PLA and PLA/EBHS. E' decreased greatly above 60 °C, where E'' showed a maximum, which was ascribed to the T_g. Then, both strands showed an increase of E' caused by cold crystallization. PLA/EBHS showed a sharp increase of E' from a lower temperature (around 80 °C) than was the case for PLA, suggesting that EBHS acted as nucleating agent during heating. After cold

crystallization, E' of both samples was around 100 MPa. Above 160 °C, both moduli decreased because of melting.

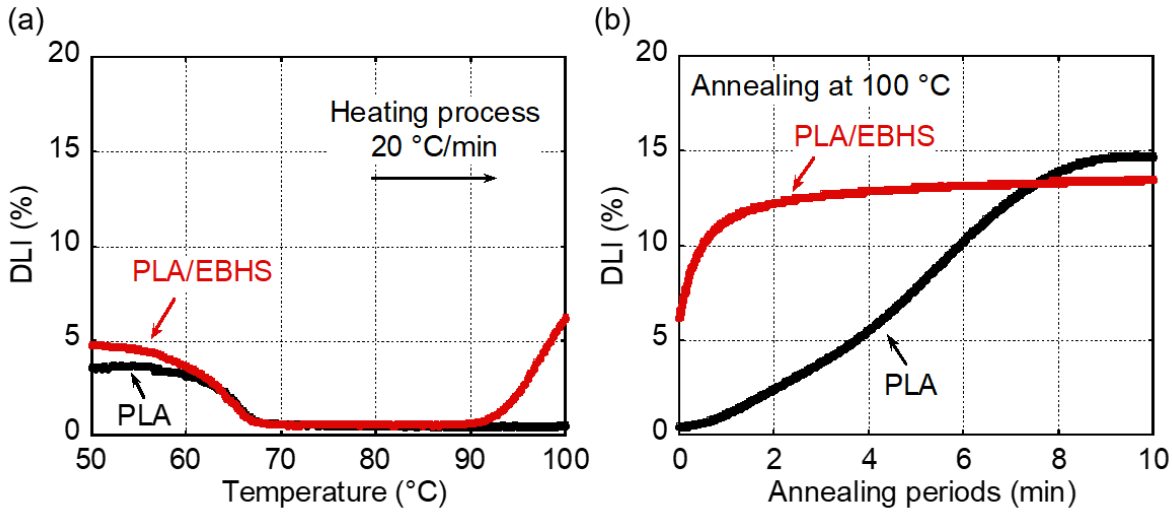

Figure 3.9. Depolarized light intensity (DLI) during (a) heating to 100 °C and (b) annealing at 100 °C for extruded strands of PLA and PLA/EBHS.

The strands were heated from 50 to 100 °C at 20 °C min^{-1} and kept at 100 °C for 10 min, as shown in Figure 3.3. During these processes, the light intensity under crossed polars, known as depolarized light intensity (DLI), was measured by a photo-detector. The angle between the MD and each polarizer was 45°. As indicated in **Figure 3.9**, DLI was ca. 4 – 5 % at 50 °C for both PLA and PLA/EBHS extruded strands. During the heating process (Figure 3.9a), DLI decreased to 0 % at around T_g. This result demonstrated that most of the transmitted light before heating was attributed to the oriented amorphous chains. Both samples showed low DLI from 66 to 90 °C, followed by an increase of DLI at 90 °C for the PLA/EBHS strand. This increase was related to the crystallization induced by the

nucleating agent and/or extended-chain crystals. The following step was annealing at 100 °C for 10 min, the DLI results of which are shown in Figure 3.9b. The sharp increase of DLI of PLA/EBHS during annealing indicated that crystallization occurred rapidly, whereas PLA required a longer period to reach an equilibrium DLI. Although such results have not been reported before, it can be predicted considering that the cold crystallization of PLA was greatly promoted with the addition of EBHS.

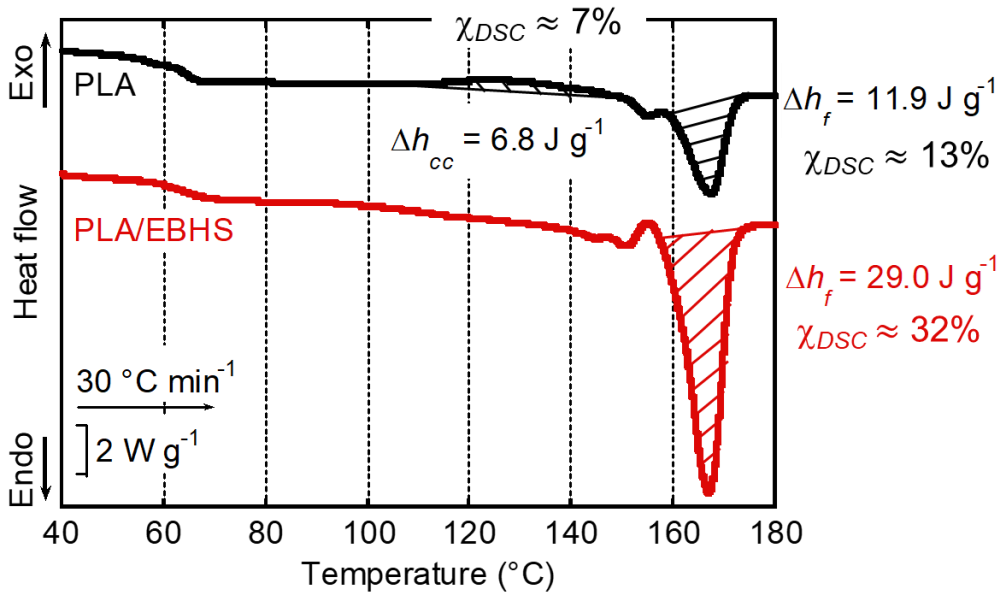

Figure 3.10. DSC heating curves of PLA (bottom) and PLA/EBHS (top) extruded strands after annealing at 100 °C for 10 min. The heating rate was 30 °C min^{-1}.

Figure 3.10 shows the thermal properties of the strands after annealing at 100 °C for 10 min. There was no exothermic peak for the PLA/EBHS strand during heating, suggesting that annealing at 100 °C for 10 min was sufficient to achieve the high

crystallinity. It was found that found that α′-crystal appears when PLA is crystallized below 100 °C. This crystalline form is similar to that of the α-crystal. However, the arrangement of chain packing in α′-crystal structure was not as compact as that in α-crystal. Moreover, in the temperature range from 100 °C to 120 °C, both α- and α′-crystal can co-exist [15,16]. The exothermic peak observed for PLA/EBHS before the melting peak (167 °C) was associated with the transformation of from disordered α′-crystals to the ordered α-crystals [15–17]. Contrary to PLA/EBHS, the annealed PLA strand before the DSC measurement still had low crystallinity, even though its DLI seemed to be saturated after 10 min at 100 °C. The difference between Δh_f and Δh_{cc} for PLA was about 5.1 J g^{-1}, which corresponded to the crystallinity was around 6 %.

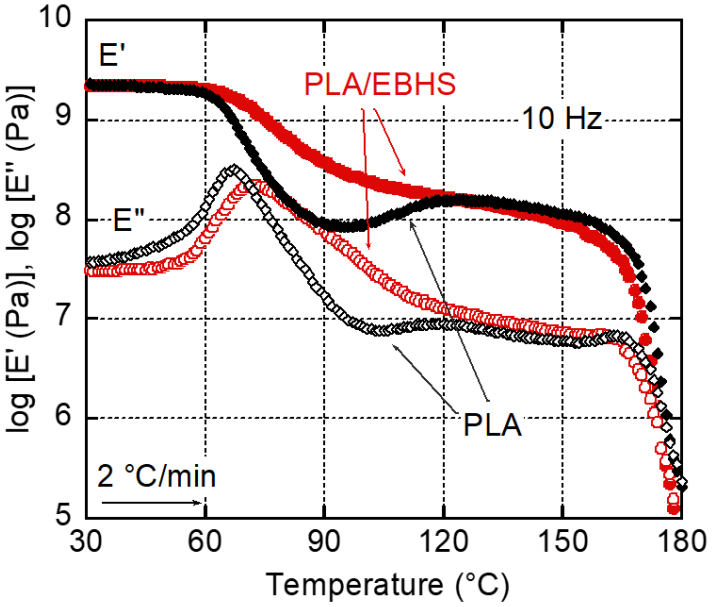

Figure 3.11. Temperature dependencies of E' (filled symbols) and E'' (open symbols) at 10 Hz for extruded strands of PLA (black diamonds) and PLA/EBHS (red circles) after annealing at 100 °C for 10 min. The heating rate was 2 °C min^{-1}.

Figure 3.11 shows the viscoelastic properties in the solid state of the annealed strands of PLA and PLA/EBHS. It should be noted that the E'' peaks (T_g) of PLA/EBHS located at a higher temperature than that before annealing (Figure 3.7), resulting in a better heat resistance. Moreover, the cold crystallization did not occur in that sample due to sufficient crystallization. In contrast, the crystallinity of the PLA strand was significantly low (approximately 6 %), although the heat treatment was applied. These results implied that both the nucleating agent addition and annealing improved the heat resistance of PLA after quench.

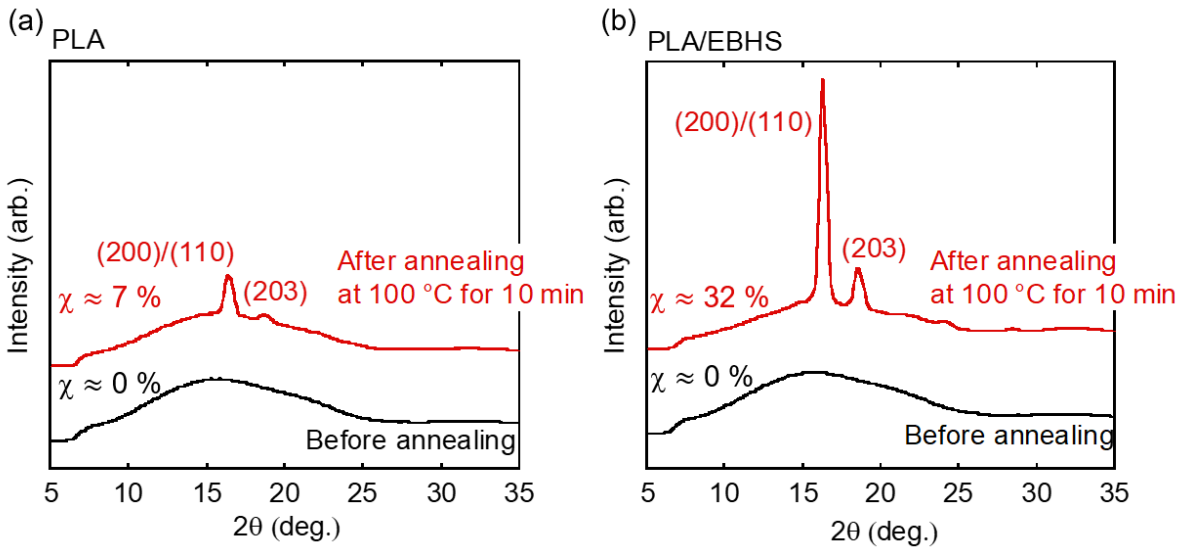

Figure 3.12. 2θ-WAXD profiles of (a) PLA and (b) PLA/EBHS strands before and after annealing at 100 °C for 10 min.

Figure 3.12 shows the 2θ-WAXD profiles of the PLA and PLA/EBHS extruded strands before and after annealing. Prior to annealing, only an amorphous halo was observed in PLA and PLA/EBHS strands, suggesting no crystalline structure. This result agreed with the DSC curves in Figure 3.7. Following annealing, clear diffraction peaks appeared at 16° and 18°, corresponding to the (200)/(110) and (203) planes, respectively. The analysis of the 2θ-WAXD profiles indicated that the crystallinity of the PLA and PLA/EBHS strands after the annealing treatment were 7 % and 32 %, respectively, consistent with the DSC measurements in Figure 3.10.

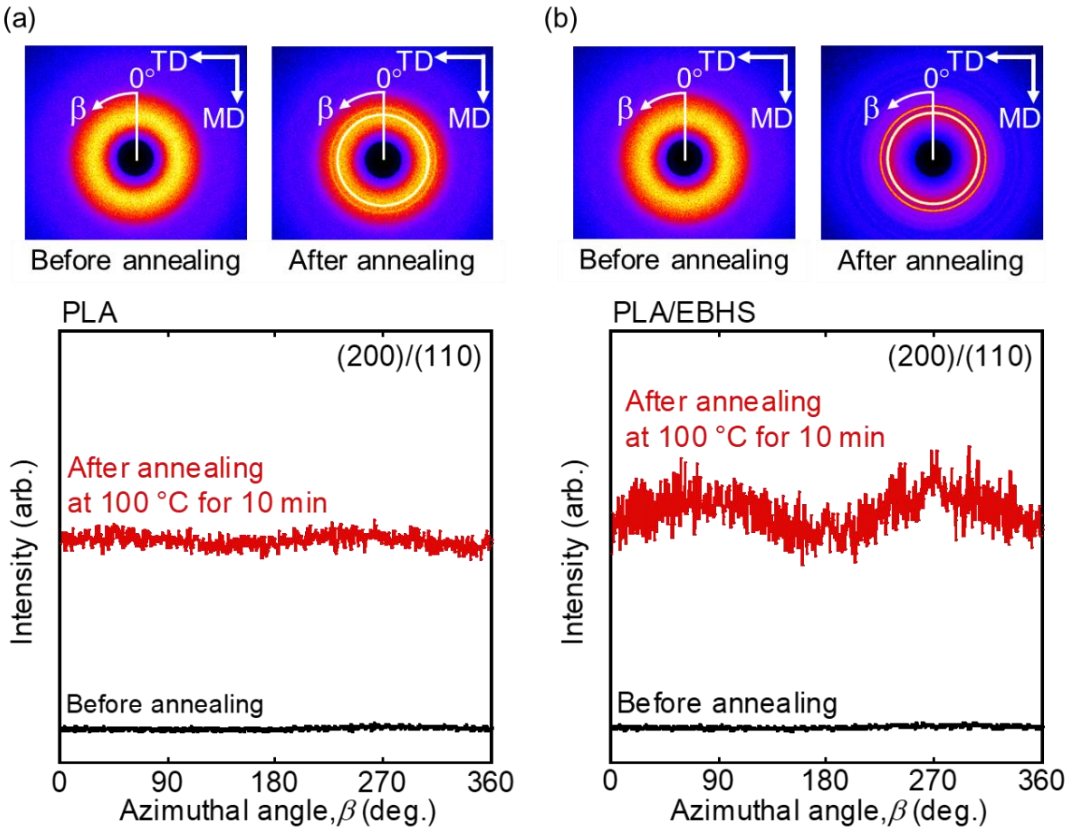

Figure 3.13. 2D-WAXD images (top) and azimuthal angle distribution at 2θ = 16° (bottom) for extruded strands of (a) PLA and (b) PLA/EBHS before and after annealing at 100 °C for 10 min.

Figure 3.13 presents the azimuthal angle distributions of the (200)/(110) plane for the PLA and PLA/EBHS strands before and after annealing, as obtained from the 2D-WAXD images. Only an amorphous halo was detected for both PLA and PLA/EBHS strands before annealing. In contrast, the annealed PLA/EBHS strand exhibited distinct azimuthal peaks at 90° and 270° (on the equator), indicating that the crystalline chains were oriented in the flow direction.

The growth of the molecular orientation during heating (Figure 3.9) was further evaluated by a POM under crossed polarizers with a Berek compensator. The Hermans orientation function (F) was evaluated using the following equation:

$$F = \frac{\Gamma}{d\Delta n^0}, \tag{3.4}$$

where Γ, d, and Δn^0 are the optical retardation, strand thickness, and intrinsic birefringence, which is known to be 0.03 [18], respectively. For the PLA/EBHS extruded strands, F values were calculated to be 1.8×10^{-3} and 6.0×10^{-3} before and after annealing, respectively.

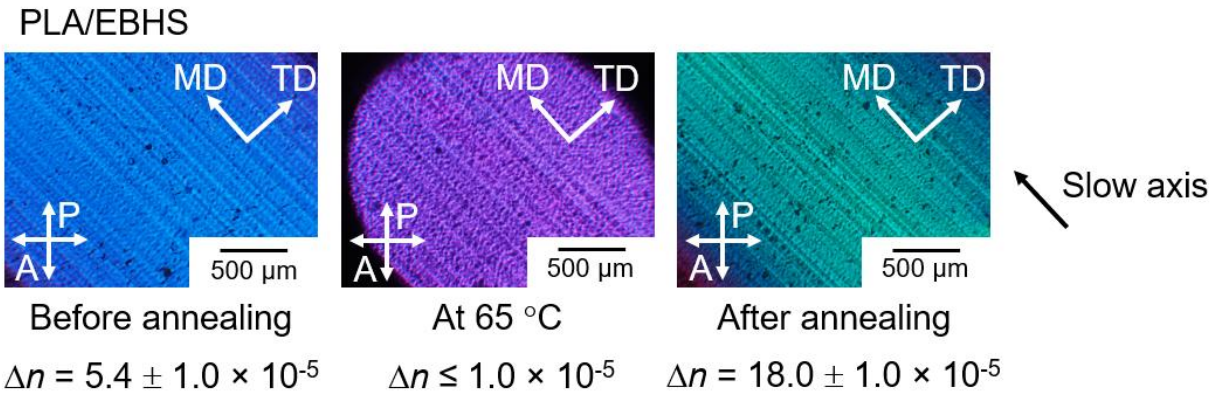

Figure 3.14. POM images under crossed polarizers with a full-wave plate for PLA/EBHS extruded strands (left) before annealing, at 65 °C (center) during heating, and (right) after annealing at 100 °C for 10 min. Birefringence Δn is denoted at the bottom of each image.

To confirm the molecular orientation in the PLA/EBHS strands, a full-wave plate introducing a 530 nm to the optical path-length was inserted into the POM, as shown in

Figure 3.14. The POM images revealed that the color of the strand before annealing was blue. According to the WAXD profiles, the observed color reflects the weak orientation of amorphous PLA chains along the flow direction. Upon heating and subsequent annealing, the optical retardation was significantly changed. At 65 °C, the retardation was around zero; i.e., the color became red-purple. Then, the observed color transitioned to green-blue, indicating the alignment of crystalline PLA chains in the flow direction after annealing at 100 °C for 10 min. This phenomenon was explained by the transcrystallization of PLA driven by the EBHS fibers, at which chain axis of PLA was oriented along the flow direction, presumably owing to the epitaxial growth of PLA crystals from the EBHS surface. A similar phenomenon was reported in polypropylene containing fibrous nucleating agents [19]. In the present study, the EBHS fibers were oriented in the MD by the applied shear flow and acted as a "pseudo-shish" structures. The transcrystallization behavior of PLA has also been reported in other tube- [20] or fiber-[21] reinforced composite materials.

In this study, we also evaluated the dimensional change of the extruded strands during annealing. Three specimens of equal initial length were cut from each of the PLA and PLA/EBHS strands and dipped in a hot-water bath at 96 ± 1 °C for 10 min. Post-annealing, the lengths were re-measured at 25 °C to determine shrinkage. The PLA strands demonstrated a shrinkage of 2.04 % ± 0.27 %, whereas the PLA/EBHS strands exhibited a reduced shrinkage of 0.80 % ± 0.19 %. These results clearly indicated that the molecular alignment of PLA chains in the flow direction effectively mitigated the shrinkage of PLA in MD during annealing.

3.5 Conclusion

In this chapter, the crystallization behavior and dimensional changes of PLA containing EBHS as a fibrous nucleating agent during annealing were investigated. It was confirmed that EBHS was uniformly dissolved in molten PLA at 180 °C without any phase separation. The strand extruded at a shear rate of 310 s^{-1} and subsequently quenched in a water bath exhibited no/less crystallinity with a slight molecular orientation of amorphous PLA chains. It suggested that the addition EBHS did not act as nuclei sites for enhancing PLA crystallinity under rapid cooling conditions. In contrast, EBHS acted as an efficient nucleating agent during the post-process annealing, promoting significantly the cold crystallization of PLA. In the case of the annealed PLA strand, the orientation of amorphous PLA chains rapidly relaxed upon heating and crystallization occurred, leading to shrinkage. In contrast, the crystalline chains formed during annealing to the flow direction were attributed to transcrystallization from the oriented EBHS fibers. As a result, the shrinkage of the annealed PLA/EBHS strand was minimized, compared to annealed PLA strand. This unique structural development enables precise control of dimensional changes in PLA products caused by annealing. Consequently, this processing technique holds significant promise for extending the applicability of PLA to high-precision industrial components, including those used in automotive, aerospace, and consumer electronics sectors.

Reference

[1] J. Y. Nam, M. Okamoto, H. Okamoto, M. Nakano, A. Usuki, M. Matsuda, Morphology and crystallization kinetics in a mixture of low-molecular weight aliphatic amide and polylactide, *Polymer*, 47, (2006), 1340–1347.
https://doi.org/10.1016/j.polymer.2005.12.066

[2] Z. Tang, C. Zhang, X. Liu, J. Zhu, The crystallization behavior and mechanical properties of polylactic acid in the presence of a crystal nucleating agent, *J. Appl. Polym. Sci.*, 125, (2012), 1108–1115.
https://doi.org/10.1002/app.34799

[3] K. Saitou, M. Yamaguchi, Transparent poly(lactic acid) film crystallized by annealing beyond glass transition temperature, *J. Polym. Res.*, 27, (2020), 104.
https://doi.org/10.1007/s10965-020-02071-y

[4] X. Chen, J. Yao, J. Yu, M. Mi, Y. Xu, H. Bai, Toward heat-resistant and transparent poly(l-lactide) by tailoring crystallization with an aliphatic amide as a nucleating agent, *Ind. Eng. Chem. Res.,* 61, (2022), 13921–13928.
https://doi.org/10.1021/acs.iecr.2c02811

[5] X. Zhao, J. Liu, J. Li, X. Liang, W. Zhou, S. Peng, Strategies and techniques for improving heat resistance and mechanical performances of poly(lactic acid) (PLA) biodegradable materials, *Int. J. Biol. Macromol.*, 218, (2022), 115–134.
https://doi.org/10.1016/j.ijbiomac.2022.07.091

[6] N. Kawamoto, A. Sakai, T. Horikoshi, T. Urushihara, E. Tobita, Nucleating agent for poly(L-lactic acid) - An optimization of chemical structure of hydrazide compound for advanced nucleation ability, *J. Appl. Polym. Sci.*103 (2007) 198–203. https://doi.org/10.1002/app.25109

[7] S. Saeidlou, M. A. Huneault, H. Li, C. B. Park, Poly(lactic acid) crystallization, *Prog. Polym. Sci.*, 37, (2012), 1657–1677. https://doi.org/10.1016/j.progpolymsci.2012.07.005

[8] A. Ram, Compounding and Processing of Plastics, in: A. Ram (Ed.), Fundamentals of Polymer Engineering, Springer US, Boston, MA, 1997,103–147.

[9] J. Seemork, M. Siriprumpoonthum, Y. Lee, S. Nobukawa, M. Yamaguchi, Effect of Die Geometry on drawdown force of polypropylene at capillary extrusion, *Adv. Polym. Tech.,* 34, (2015), 21477. https://doi.org/10.1002/adv.21477

[10] R. Nishikawa, M. Yamaguchi, Effect of carbon nanotube addition on structure and properties for extrudates of high-density polyethylene, *Appl. Polym. Sci.*, 136, (2019), 48010. https://doi.org/10.1002/app.48010

[11] D. Bryce, Plastic injection molding: Manufacturing process fundamentals, SME, Southfield, MI, 2001.

[12] E. W. Fischer, H. J. Sterzel, G. Wegner, Investigation of the structure of solution grown crystals of lactide copolymers by means of chemical reactions, *Kolloid Z. or Kolloid. Z.*, 251, (1973), 980-990.

[13] S. Iwasaki, M. Inoue, Y. Takei, R. Nishikawa, M. Yamaguchi, Modulus enhancement of polypropylene by sorbitol nucleating agent in flow field, *Polym. Cryst.*, 4, (2021), e10170.

https://doi.org/10.1002/pcr2.10170

[14] Q. Xing, X. Zhang, X. Dong, G. Liu, D. Wang, Low-molecular weight aliphatic amides as nucleating agents for poly (L-lactic acid): Conformation variation induced crystallization enhancement, *Polymer,* 53, (2012), 2306–2314.

https://doi.org/10.1016/j.polymer.2012.03.034

[15] J. Zhang, K. Tashiro, H. Tsuji, A. J. Domb, Disorder-to-order phase transition and multiple melting behavior of poly(l-lactide) investigated by simultaneous measurements of WAXD and DSC, *Macromolecules*, 41, (2008), 1352–1357.

https://doi.org/10.1021/ma0706071

[16] M. L. D. Lorenzo, R. Androsch, Influence of α′-/α-crystal polymorphism on properties of poly(l-lactic acid) - Di Lorenzo - 2019 - *Polym. Int.*, 68, (2019), 320-334.

https://doi.org/10.1002/pi.5707

[17] T. Kawai, N. Rahman, G. Matsuba, K. Nishida, T. Kanaya, M. Nakano, H. Okamoto, J. Kawada, A. Usuki, N. Honma, K. Nakajima, M. Matsuda, Crystallization and melting behavior of poly (l-lactic acid), *Macromolecules,* 40, (2007), 9463–9469.

https://doi.org/10.1021/ma070082c

[18] Y. Furuhashi, Y. Kimura, H. Yamane, Higher order structural analysis of stereocomplex-type poly(lactic acid) melt-spun fibers, *J. Polym. Sci., Part B:Polym. Phys.*, 45, (2007), 218–228.

https://doi.org/10.1002/polb.21035

[19] K. Janchai, T. Kida, T. Inoue, S. Iwasaki, M. Yamaguchi, Crystallization behavior of isotactic polypropylene containing a fibrous nucleating agent in a flow field, *Polym. J.*, 54, (2022), 367–375.

https://doi.org/10.1038/s41428-021-00596-7

[20] H. Tang, J. -B. Chen, Y. Wang, J. -Z. Xu, B. S. Hsiao, G. -J. Zhong, Z. -M. Li, Shear flow and carbon nanotubes synergistically induced nonisothermal crystallization of poly(lactic acid) and its application in injection molding, *Biomacromolecules,* 13, (2012), 3858–3867.

https://doi.org/10.1021/bm3013617

[21] Y. Li, S. Yang, Y. -K. Li, J. -Z. Xu, H. -W. Ni, Z. -H. Su, Z. -M. Li, Robust interfacial cylindrites of polylactic acid modulated by an intense shear flow field, *ACS Sustainable Chem. Eng.,* 4, (2016), 3558–3566.

https://doi.org/10.1021/acssuschemeng.6b00668

Chapter 4. Anomalous dimensional change under post-process annealing of immiscible blend

4.1 Introduction

With the increasing global emphasis on environmental preservation, the demand for sustainable or "green" plastics has grown significantly, such as polyhydroxyalkanoates [1], poly(butylene succinate) [2], poly(butylene adipate-co-terephthalate) [3], or poly(ε-caprolactone) [4]. Among them, poly(lactic acid) (PLA) has become particularly attractive due to its mechanical properties and heat resistance once crystallized sufficiently, comparable to those of isotactic polypropylene. However, the main drawback of PLA is slow crystallization rates [5–7]. To solve this problem, N,N′-ethylenebis(12-hydroxystearamide) [8] was introduced to enhance the crystallization rate of PLA, as reported in Chapter 3. Moreover, plasticizers has been also employed [9–12] simultaneously to improve the mobility of PLA, as well as lowering the T_g of PLA. Post-process annealing was reported to be effective and applicable in industry. For example, however, injection-molded products typically shrink and warp post-processing due to the reduction in specific volume from the molten state to solidification upon cooling [13–17]. This phenomenon is especially pronounced in crystalline polymers, which inherently possess lower specific volumes in their crystalline state. Thus, understanding and controlling the crystallinity and molecular orientation is essential to manage anisotropic

shrinkage and thermal expansion, particularly in large-scale plastic components combined with metals and ceramics. Processing parameters, such as resin temperature, mold temperature, gate design, injection pressure and duration, and hold pressure, significantly influence to shrinkage [13,14,18]. In addition, post-process annealing affects the final dimensions of injection-molded components, especially in materials that experience considerable crystallization during post-processing annealing. Polymers with slow crystallization rates during cooling, like PLA, often undergo significant dimensional change, e.g., shrinkage, upon annealing due to crystal growth, posing severe issues in practical applications.

The primary aim of this study is to examine the anomalous dimensional change, particularly the expansion in the flow direction during post-processing annealing of PLA-based binary blends containing low-molecular-weight PVA as the dispersed phase. To our best knowledge, this expansion behavior has not been reported previously. Hence, herein, the findings presented a novel technology in polymer processing to control the anisotropic shrinkage during annealing in plastic products. Moreover, from the materials perspective, both PLA and PVA are the biodegradable polymers, at which PVA can be dissolved in water/seawater. Recent studies indicate that PVA also accelerates the hydrolysis of PLA, thereby further enhancing its biodegradability [19]. Therefore, PLA/PVA blends have promising applications in disposable product markets.

4.2 Materials and sample preparation

The PLA pellets and PVA powder (G-polymer AZF8035Q; Mitsubishi Chemical, Tokyo, Japan) were dried at 80 °C for 4 h under vacuum. Then, they were blended in the molten-state using a co-rotating twin-screw extruder (TEM26SS; Shibaura Machine, Tokyo, Japan) at 190 °C. A strand cutter was employed to cut the blend strand into pellets. The output rate was 10 kg h^{-1}. The L/D, i.e., ratio of length/diameter of the screw, was 48. The PVA contents in the blend were 0, 5, and 10 wt.%, noted as PLA, PLA/PVA (95/5), and PLA/PVA (90/10), respectively.

After drying, the obtained pellets were processed using an injection-molding machine (JDAD-H; The Japan Steel Works, Tokyo, Japan) with a barrel temperature of 200 °C and a mold temperature of 20 °C. The cooling time was 60 s. Injection was performed at 90 MPa and 90 mm s^{-1}, followed by a holding pressure of 100 MPa. Dumbbell-shaped test specimens (4 mm thick and 192 mm long) were produced. The design of the mold, including the runner and gate positions, is shown in **Figure 4.1**. Post-injection, samples were annealed in an electric oven at various temperatures for 3 h, then cooled and maintained at room temperature (23 °C) for 1 day prior to dimensional measurements.

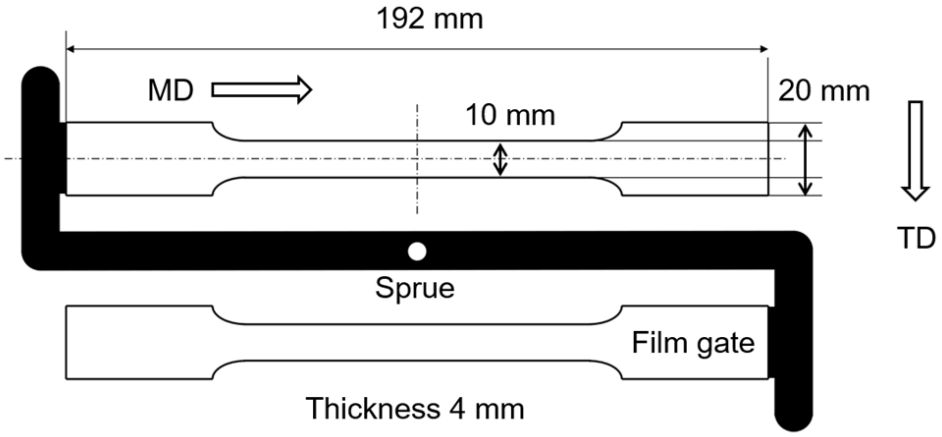

Figure 4.1. Dimension of the mold

The thin films were elaborated with the thickness of 300 μm using a compression-molding machine at 200 °C for 1 min. Then, they were consequently quenched for at 20 °C for 5 min using a circulating temperature-controller.

4.3 Characterization

The morphology of the compression-molded blend films was examined using a scanning electron microscope (SEM; TM3030Plus, Hitachi, Tokyo, Japan). The films were fractured in liquid nitrogen and then immersed in hot water at 80 °C to dissolve the PVA phase. After drying under vacuum at room temperature for 24 h, the platinum–palladium coating was applied on the fractured surfaces prior to SEM observation.

The angular frequency dependence of oscillatory shear modulus was investigated using a cone-and-plate rheometer (AR2000ex, TA Instruments, New Castle, DE, USA).

The cone angle was 4°. The experiments were conducted from 100 to 0.1 rad s^{-1} at 200 °C under a nitrogen environment.

Steady-state shear viscosities were evaluated using a pressure-driven capillary rheometer (140 SAS-2002, Yasuda Seiki Seisakusho, Nishinomiya, Japan) at various shear rate. Compression-molded PLA and PLA/PVA (90/10) films were cut into small pieces and inserted into the capillary rheometer at 200 °C. A flat circular die (length/diameter = 10/1) was utilized.

Temperature dependence of dynamic tensile moduli was measured from 40 to 180 °C at a heating rate of 2 °C min^{-1} using a dynamic mechanical analyzer (Rheogel-E4000, UBM, Mukō, Japan). The frequency was 10 Hz.

Thermal properties of PLA and PLA/PVA (90/10) films were evaluated using a differential scanning calorimetry (DSC; DSC8500, PerkinElmer, Waltham, MA). In the first heating, it run from 25 to 180 °C at a heating rate of 10 °C min^{-1}. Then, the sample was kept at 180 °C for 1 min, followed by cooling to 30 °C with various cooling rates to determine crystallization temperatures.

Polarized optical microscopy (POM) images were carried out using a POM (DMLP, Leica Microsystems, Wetzlar, Germany) under a full-wave plate and crossed polarizers. To form thin films (approximately 25 μm), PLA and PVA were melted between glass slides at 200 °C for 1 min and subsequently quenched in an ice-water bath. Then, the films were cut with a razor blade and combined, as shown in **Figure 4.2**. The joined-film was placed between cover glasses and heated to 110 °C at 20 °C min^{-1} in a temperature controller

(Mettler FP90, Mettler Toledo, Columbus, OH), and held at 100 °C for 10 min. Then, it was cooled to room temperature and then observed the crystallization.

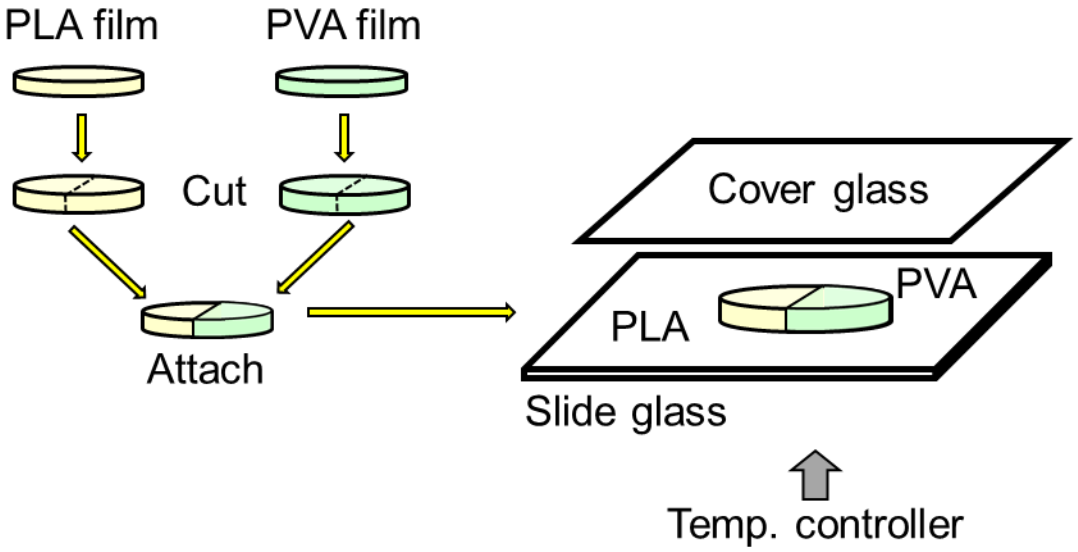

Figure 4.2. Experimental illustration to observe the crystallization growth of PLA from the surface of PVA

Two-dimensional wide-angle X-ray diffraction (2D-WAXD) patterns were examined for surface (skin) and inner (core) regions of injection-molded specimens using an X-ray diffractometer (SmartLab, Rigaku, Akishima, Japan). Graphite-monochromatized CuKα radiation beams (45 kV and 200 mA) were used for the measurements. The central section of each injection-molded bar was sliced to isolate the skin and core using a diamond cutter, then the cut surfaces were trimmed with an ultramicrotome (RX-860, Yamato Kohki Industrial, Osaka, Japan) to remove any thermally affected areas from cutting.

Polarized measurements were conducted to determine dichroic ratios of the injection-molded samples (before and after annealing) using the Fourier-transform infrared spectrometer (FTIR; FT-IR500, JASCO, Hachioji, Japan).

Three-point bending tests, i.e., flexural test, were evaluated using a universal testing machine (Autograph AG-X, Shimadzu, Kyoto, Japan) at 23 °C under the JIS K7171 (ISO 178) standard. Each test was repeated three times.

The morphology of injection-molded PLA/PVA (90/10) samples was examined with a digital microscope (VHX-2000, Keyence, Osaka, Japan). Prior to observation, specimens were sectioned using an ultramicrotome (HM-325, Carl Zeiss, Oberkochen, Germany), and the dispersed PVA phase was selectively removed by immersing the samples in hot water at 80 °C.

4.4 Results and discussion

4.4.1 Morphology, thermal and rheological properties

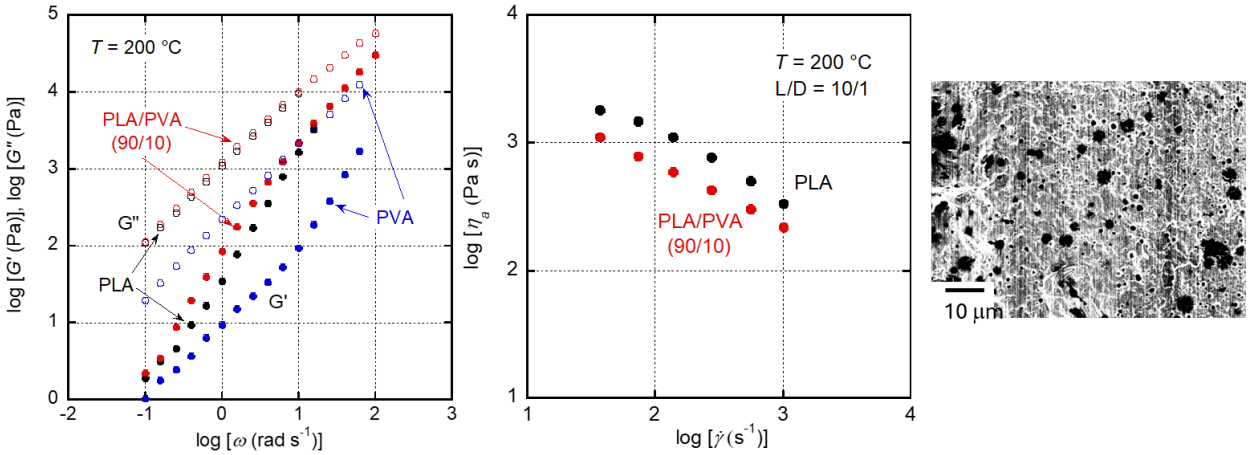

Figure 4.3. (left) Angular frequency dependence of shear storage modulus G' (open symbols) and (closed symbols) loss modulus G'' at 200 °C for PLA (black), PVA (blue), and PLA/PVA (90/10) (red). (middle) Apparent steady-shear viscosity η_a as a function of shear rate $\dot{\gamma}$ of the PLA (black), and PLA/PVA (red) at 200 °C. (right) SEM image of the cryofracture surface of a PLA/PVA (90/10) compression-molded film after PVA removal.

Rheological properties in the molten-state of PLA, PVA, and PLA/PVA were investigated at 200 °C, as shown in **Figure 4.3**. Due to having a low-molecular-weight, G' and G'' of PVA showed lower than those of PLA. The slope of G' was decreased at the low frequencies due to intermolecular hydrogen bonding [20,21]. In the case of PLA/PVA blend, the G' was higher than that for PLA, suggesting the long-time relaxation. The miscibility

between PLA and PVA was observed using SEM (right figure). Because PVA was soluble with water, the PVA droplets were easily removed from the blend after immersing in water. The sea-island structures, i.e., phase-separated structures, were observed and the diameter of PVA droplets was around 0.5 to 5 μm, indicating that PLA was immiscible with PLA. Therefore, the apparent viscosity of PLA/PVA was significantly decreased, compared to PLA. This phenomenon was attributed to the interfacial slippage (poor adhesion) at the enlarged interfacial area [22–24].

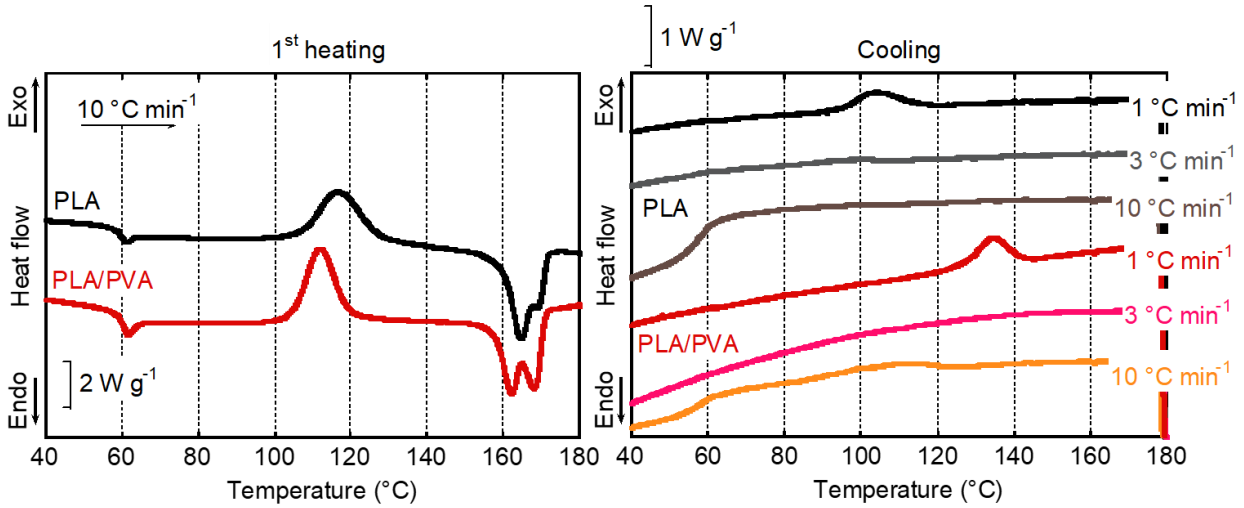

Figure 4.4. DSC curves of PLA and PLA/PVA (90/10) under heating at 10 °C min^{-1} and cooling from 180 °C at 10, 3, and 1 °C min^{-1}.

The thermal properties of PLA and PLA/PVA (90/10) are shown in **Figure 4.4**. The increase in heat flow at around 60 °C was attributed to the T_g of PLA. The exothermic peaks at 112 and 117 °C were ascribed to the cold crystallization of PLA/PVA (90/10) and PLA, respectively. It suggests that the PVA promoted the cold crystallization of PLA during

heating. In cooling process, PLA did not crystallize at a cooling rate of 3 °C min^{-1} due to slow crystallization rate. However, the crystallization peaks were detected at 1 °C min^{-1} for both PLA and PLA/PVA (90/10) samples. Moreover, the PLA/PVA (90/10) exhibited a crystallization peak at a higher temperature in cooling. Therefore, it suggested that PVA acted as a nuclei for PLA crystallization.

The solid-state viscoelastic was investigated using a dynamical tensile machine, as shown in **Figure 4.5**. As previously reported in chapter 2 and 3, T_g of PLA obtained from the dynamical tensile modulus was around 66 °C. The increase in E' was attributed to the cold crystallization, and the addition of PVA promoted the cold crystallization for PLA. This result is similar to the heating process in Figure 4.3.

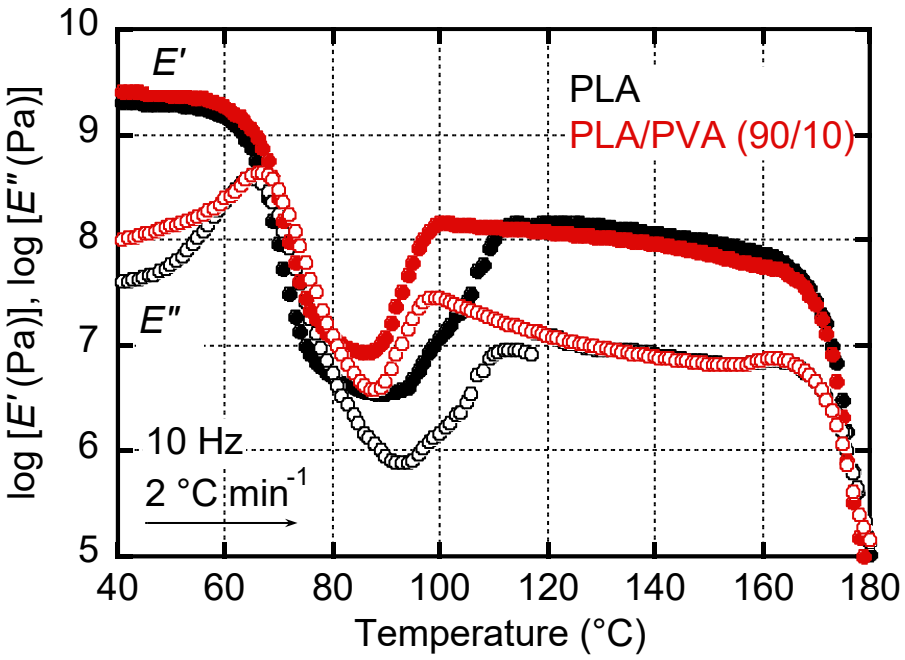

Figure 4.5. Dynamic tensile modulus of the compression-molded PLA and PLA/PVA at 10 Hz with a heating rate of 2 °C min^{-1}.

4.4.2 Shrinkage and anomalous expansion of the injection-molded bar during post-process annealing

After injection-molding, the sample was annealed in a temperature controller. **Figure 4.6** shows the injection-molded bars before and after annealing at 100 °C for 3 h. Due to rapid quench, the injection-molded PLA bar was transparent without crystallinity. After annealing, it was opaque because of crystallization. In the case of the blend, the blend bar showed an opaque because of immiscibility of PLA and PVA. Moreover, the length of the blend bar gradually increased to machine direction (MD), whereas the that of PLA bar experienced a shrinkage after annealing. Generally, the sample dimension in MD decreased during post-process annealing. However, the anomalous expansion to MD has not been previously reported.

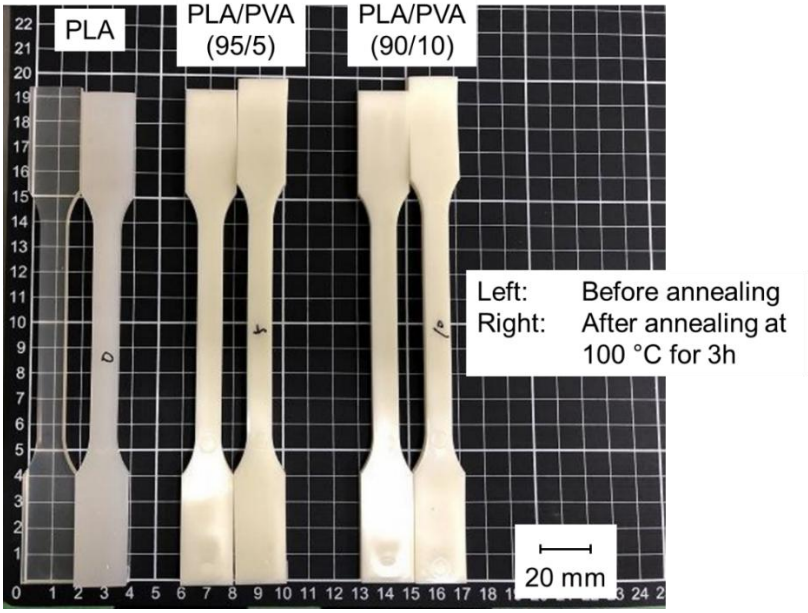

Figure 4.6. Injection-molded bars of PLA, PLA/PVA (95/5) and PLA/PVA (90/10) (left) before and (right) after annealing at 100 °C for 3h.

Table 4.1 summarizes the dimensional changes of PLA and PLA/PVA injection-molded bar before and after annealed at 100 °C for 3h. The width and thickness were measured at the center of each specimen. After annealing, the length of the PLA bar decreased from 192.0 to 188.5 mm (approximately 1.8%), while that of the PLA/PVA bar increased from 192.0 to 197.5 mm (about 2.9%). This considerable expansion to the machine direction (MD) caused slight warpage. In contrast to PLA, the PLA/PVA blend exhibited reductions in both width (transverse direction, TD) and thickness (normal direction, ND).

Table 4.1. Dimensions of injection-molded sample before and after annealing

		Length (mm)	Width (mm)	Thickness (mm)
PLA	Before annealing	192.0 ± 0.5	10.04 ± 0.03	4.06 ± 0.01
	After annealing	188.5 ± 0.5	10.07 ± 0.06	4.16 ± 0.03
PLA/PVA	Before annealing	192.0 ± 0.5	10.06 ± 0.02	4.06 ± 0.02
(95/5)	After annealing	195.5 ± 0.5	9.83 ± 0.03	4.06 ± 0.02
PLA/PVA	Before annealing	192.0 ± 0.5	10.03 ± 0.02	4.07 ± 0.01
(90/10)	After annealing	197.5 ± 0.5	9.80 ± 0.01	4.01 ± 0.03

Figure 4.7 shows the injection-molded test pieces annealed at different temperatures for 3 h, with images captured after cooling at 23 °C for one day. It was expected that annealing below T_g did not show a difference, compared to the blend bar before annealing. However, the shrinkage occurred once annealed around T_g, which is similar to the injection-molded PLA bar annealed at 100 °C. This is because the mobility was increased, leading to the relaxation during annealing. Moreover, it expanded in MD once annealed beyond 80 °C.

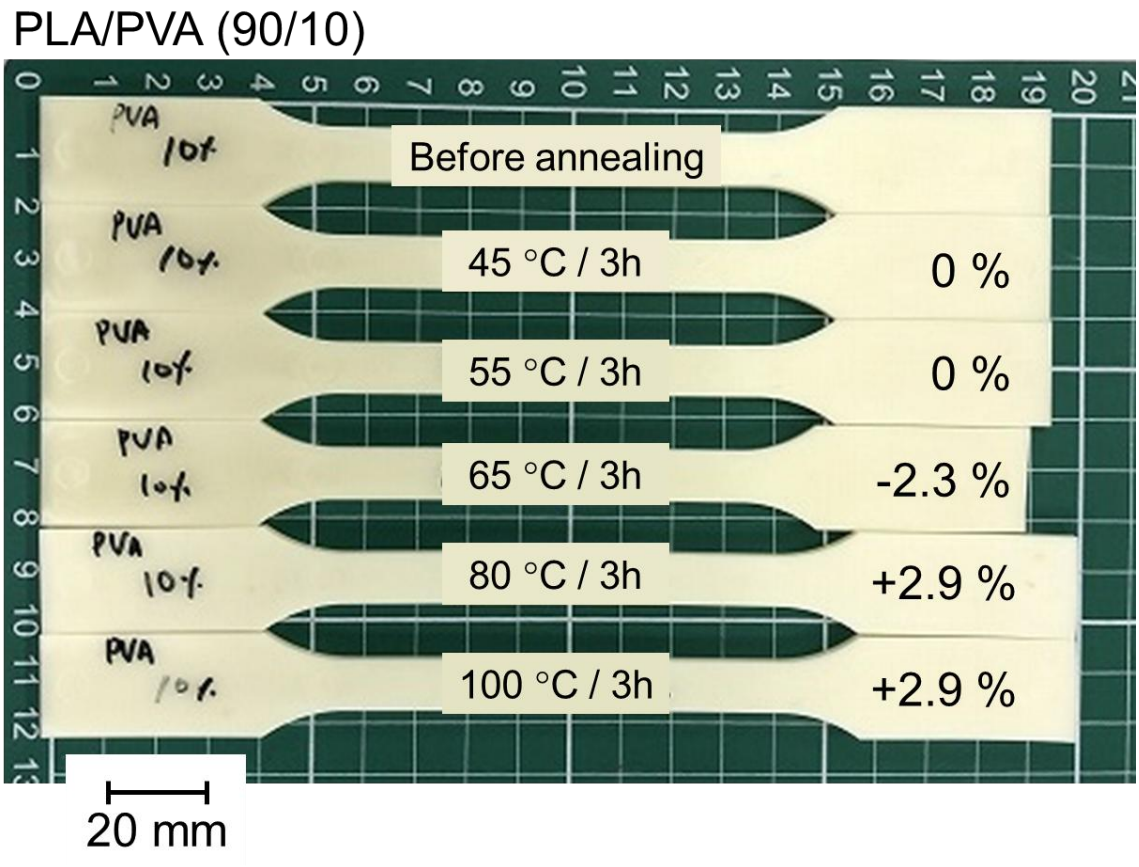

Figure 4.7. The effect of annealing temperature on the dimensional change of injection-molded PLA/PVA (90/10) bars.

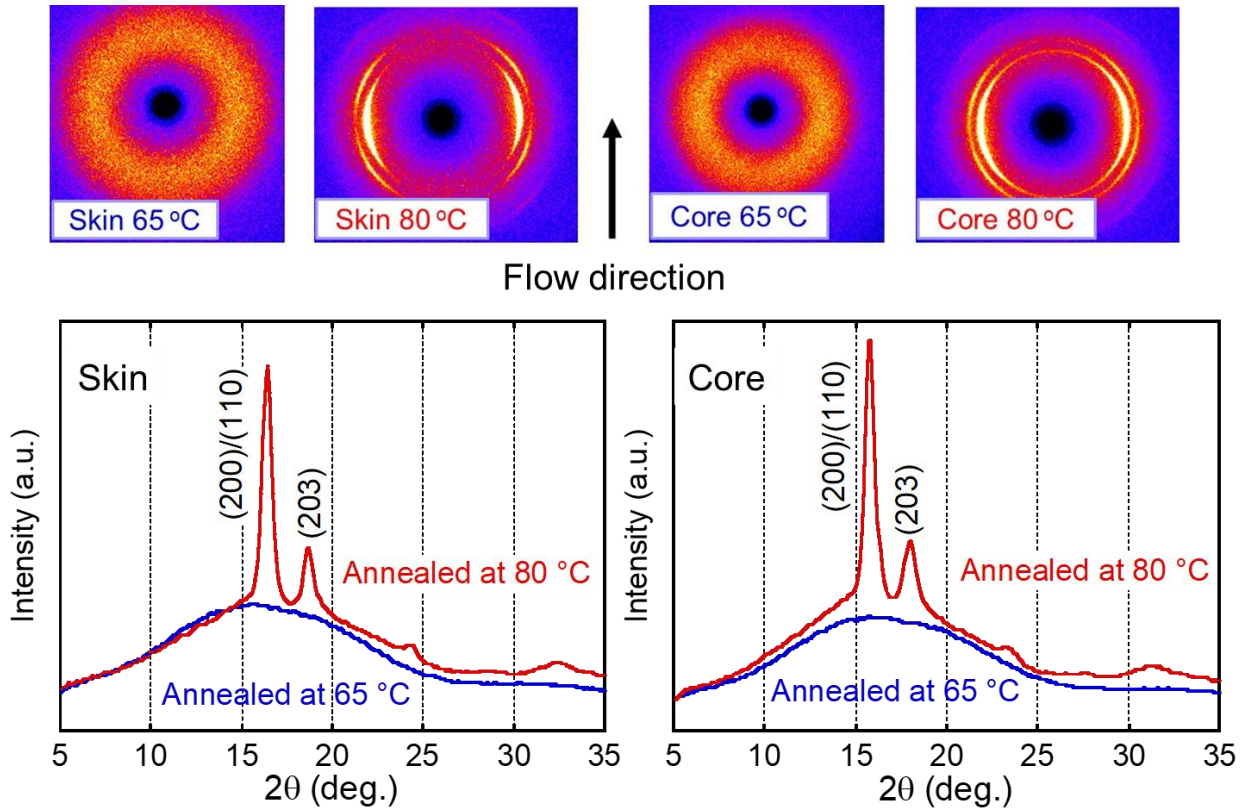

Figure 4.8. 2D-WAXD images with the 2θ profile of the skin and core layers for PLA/PVA (90/10) injection-molded bar after annealing at 65 and 80 °C for 3h.

Figure 4.8 shows the 2D-WAXD images and pattern of the skin and core regions of the PLA/PVA injection-molded bar. It was clear that both the skin and the core regions did not exhibit crystallinity after annealing at 65 °C, suggesting that an amorphous halo without any distinct peak in the azimuthal angle was detected. Thus, the shrinkage at this temperature was primarily attributed to isotropic contraction of the amorphous domains. In contrast, annealing at 80 °C led to pronounced crystallization. A clear diffraction peak near 16.3°, which assigned to the (200/110) planes, appeared along the equator. It indicated that

the PLA chains were oriented in the machine direction (MD). Notably, molecular orientation was evident even in the core region.

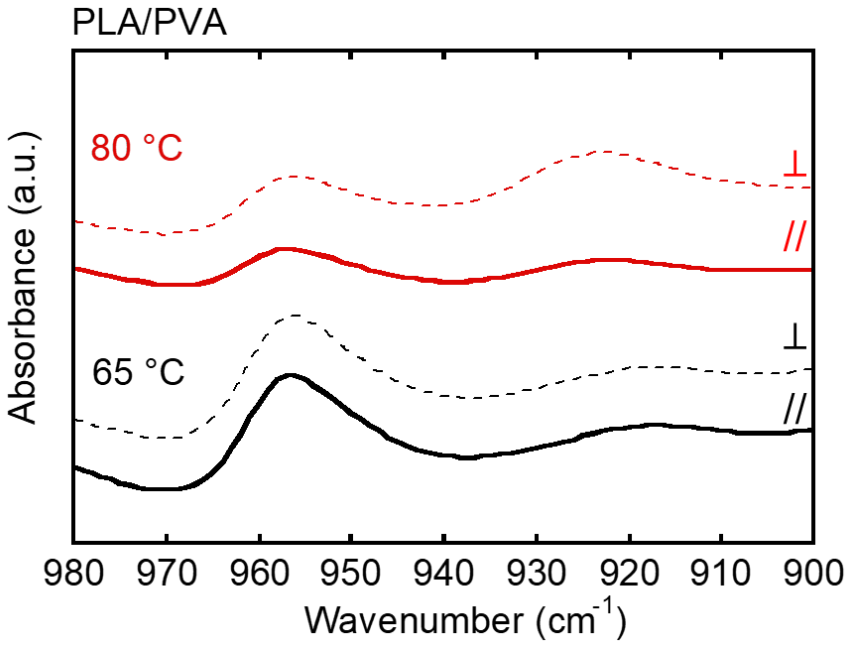

Figure 4.9. Polarized IR spectra of the injection-molded PLA/PVA (90/10) bars annealed at 65 °C (black) and 80 °C (red) for 3 h. The transition moment of IR beams perpendicular (dotted lines) and parallel (solid lines) in the flow direction.

The surfaces of injection-molded were analyzed by polarized FT-IR spectroscopy, as shown in **Figure 4.9**. The peak at 956 cm^{-1} was corresponded to the amorphous phase, whereas the peak at 921 cm^{-1} was attributed to the α′/α-form crystalline structure. Dichroic ratios for both peaks were determined using the following equation:

$$D = A_{\parallel}/A_{\perp}, \tag{4.1}$$

$$f_{IR} = \frac{\langle 3cos^2\theta - 1\rangle}{2} = \left(\frac{2}{(3cos^2\alpha - 1)}\right)\left(\frac{D-1}{D+2}\right) \tag{4.2}$$

where $A_{\parallel}$ and $A_{\perp}$ denote the absorbance intensities measured in the directions parallel and perpendicular to the flow direction, respectively. The θ represents the angle between the polymer chain axis and the flow direction, while α corresponds to the angle between the transition dipole moment and the molecular axis. Reported values of α are 4.27° for the amorphous band at 956 cm^{-1} and 90° for the crystalline band at 921 cm^{-1}, respectively [25,26]. The data from the Figure 4.9 are summarized in **Table 4.2**. Annealing at 65 °C did not change the dichroic ratio at 956 and 921 cm^{-1} due to no orientation and crystallization. However, the dichroic ratio at 921 cm^{-1}, corresponding to the parallel band, increased substantially after annealing at 80 °C for 3 h. It suggested that the molecular orientation developed greatly during annealing at this temperature. These findings correspond well with the 2D-WAXD profiles shown in Figure 4.7.

Table 4.2. Dichroic ratios and the Hermans orientation functions of PLA/PVA (90/10) injection-molded bars annealed at 65 and 80 °C for 3 h.

Annealing condition	D_{921}	D_{956}	f_{921}	f_{956}
Annealed at 65 °C	1.00	1.00	0.00	0.00
Annealed at 80 °C	0.37	1.26	0.53	0.08

As previously mentioned, the immiscible PVA droplets were phase-separated in PLA matrix, as shown in Figure 4.3. **Figure 4.10** shows the cut-surface images of a PLA/PVA (90/10) injection-molded bar after removal of PVA, captured in the MD-ND

plane at 1 mm below the surface. The orient-shaped voids were obviously observed, indicating that the PVA dispersion was deformed and oriented to the flow direction. Because PVA has a lower viscosity than PLA, the dispersed droplets tend to deform affinely without breaking during flow [27,28]. In fact, several studies have reported the formation of fibrous structures from low-viscosity dispersions using in-situ techniques [29–35].

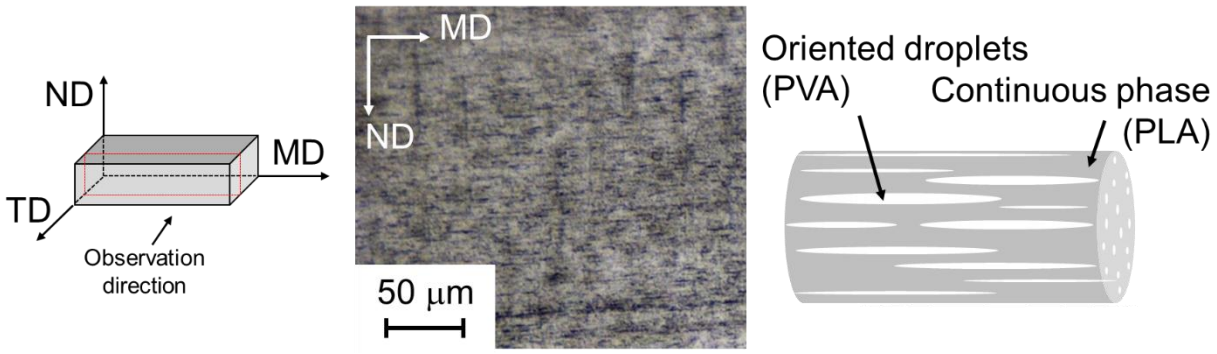

Figure 4.10. Digital microscopy image of a PLA/PVA (90/10) injection-molded bar obtained after the PVA removal in water at 80 °C.

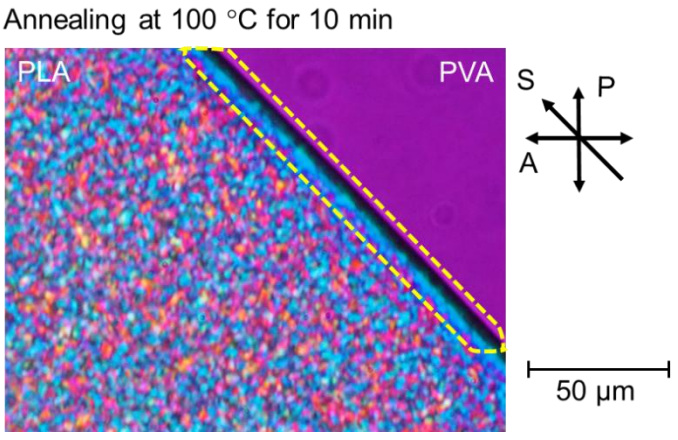

Figure 4.11. Polarized optical microscopy image of the jointed films of (left) PLA and (right) PVA after annealing at 100 °C for 10 min. The image was obtained using a full-wave plate (S is a slow axis) under crossed polarizers (A and P).

The transcrystallization induced by the fibrous PVA is required to achieve molecular orientation of PLA crystals in the MD. To investigate this, a quenched pure PLA film was attached at its edge to a pure PVA film. The assembled films were then annealed at 110 °C for 10 min on a hot stage. **Figure 4.11** shows a POM image obtained under crossed polarizers (A and P) with a full-wave plate after annealing. The image shows that PLA crystals adjacent to the PVA film appeared blue, indicating alignment in a single direction. Based on the slow axis of the full-wave plate (S), this morphology suggests that the PLA chains were oriented parallel to the boundary with the PVA film. In other words, the PLA lamellae in the vertical direction relative to the boundary. Using the Michel–Levy chart [36], the retardation was estimated to be approximately 150 nm. Far from the PVA boundary, the PLA displayed a typical spherulitic structure.

The flexural test of the injection-molded specimens before and after annealing at 100 °C for 3 h are summarized in **Table 4.3**. Prior to annealing, the blend samples exhibited a higher flexural modulus than pure PLA, attributable to the high modulus of the PVA dispersions [21,34,37], which contributed to the overall rigidity of the material. Structural changes, such as molecular orientation and crystallization, were found to significantly influence the mechanical performance. After annealing, both PLA and PLA/PVA injection-molded bars showed increased flexural modulus and strength, compared to before annealing. Molecular orientation, in particular, played a key role in enhancing the flexural modulus [38], with values of 3.84, 4.11, and 4.22 GPa for PLA, PLA/PVA (95/5), and PLA/PVA (90/10), respectively. However, the flexural strength of PLA/PVA was slightly

lower than that of pure PLA, likely due to thickness reduction associated with expansion along the flow direction.

Table 4.3. Flexural modulus and strength of the injection-molded sample before and after annealing

		Flexural modulus (GPa)	Flexural Strength (MPa)
PLA	Before annealing	3.39 ± 0.01	97.0 ± 1.0
	100 °C for 3h	3.84 ± 0.01	123.0 ± 2.0
PLA/PVA	Before annealing	3.51 ± 0.01	97.5 ± 0.5
(95/5)	100 °C for 3h	4.11 ± 0.02	123.0 ± 1.0
PLA/PVA	Before annealing	3.60 ± 0.02	99.5 ± 0.5
(90/10)	100 °C for 3h	4.22 ± 0.02	118.0 ± 2.0

4.5. Conclusion

In this study, the anomalous expansion during post-process annealing of a biodegradable binary blend composed of PLA and PVA was investigated. The PVA was immiscible with PLA, resulting in the phase-separated structure. The addition of PVA enhanced the cold crystallization during heating, which acted as nuclei for PLA crystallization. However, the nucleation ability of PVA was not good during cooling. The injected-molded samples showed no/less crystallinity during quench due to slow crystallization rate of PLA. Therefore, post-process annealing increased the crystallization of PLA, exhibiting the unique dimensional changes. This phenomenon can be attributed to the trancrystallization from the fibrous PVA dispersion, leading to increase in molecular orientation. It suggested that the highly-ordered structure was detected in the PLA/PVA injection-molded blends bar. This anomalous expansion can be used as the novel method to control precisely the dimensions of injection-molded products.

References

[1] K. Janchai, T. Kida, M. Yamaguchi, T. Sunagawa, T. Okura, Optimum processing conditions for the maximum crystallization rate of poly(3-hydroxybutyrate-co-3-hydroxyhexanoate), *Sci. Rep.* 13 (2023) 497.
https://doi.org/10.1038/s41598-023-27595-3

[2] T. Yokohara, M. Yamaguchi, Structure and properties for biomass-based polyester blends of PLA and PBS, *Eur. Polym. J.*, 44, (2008), 677–685.
https://doi.org/10.1016/j.eurpolymj.2008.01.008

[3] J. Wang, M. Xu, J. Yan, G. Guo, Y. Wang, J. Zhang, J. Wu, Biodegradable poly(butylene adipate-co-terephthalate) (PBAT) modified by 1,4 cyclohexanedimethanol, *Polymer*, 308, (2024), 127348.
https://doi.org/10.1016/j.polymer.2024.127348

[4] A. S. A. Hosni, J. K. Pittman, G. D. Robson, Microbial degradation of four biodegradable polymers in soil and compost demonstrating polycaprolactone as an ideal compostable plastic, *Waste Manag.*, 97, (2019), 105–114.
https://doi.org/10.1016/j.wasman.2019.07.042

[5] M. Yamaguchi, Manufacturing of High performance biomass-based polyesters by rheological approach, in: V. K. Thakur, M.K. Thakur and M. R. Kessler (Ed.), Handbook of Composites from Renewable Materials, John Wiley & Sons, 2017, 25–47.

[6] L. T. Sin, B. S. Tueen, Polylactic Acid - A Practical Guide for the Processing, Manufacturing, and Applications of PLA - 2nd Edition, Elsevier, Netherland, 2019.

[7] R. A. Auras, L. -T. Lim, S. E. M. Selke, H. Tsuji, Poly(lactic acid): Synthesis, Structures, Properties, Processing, Applications, and End of Life, 2nd Edition, Wiley, Hoboken, New Jersey, 2022.

[8] K. Saitou, M. Yamaguchi, Transparent poly(lactic acid) film crystallized by annealing beyond glass transition temperature, *J. Polym. Res.* 27, (2020), 104.
https://doi.org/10.1007/s10965-020-02071-y

[9] L. Yu, H. Liu, K. Dean, L. Chen, Cold crystallization and postmelting crystallization of PLA plasticized by compressed carbon dioxide, *J. Polym. Sci., Part B: Polym. Phys.*, 46, (2008), 2630–2636.
https://doi.org/10.1002/polb.21599

[10] H. Xiao, W. Lu, J. -T. Yeh, Effect of plasticizer on the crystallization behavior of poly(lactic acid), *J. Appl. Polym. Sci.,* 113, (2009), 112–121.
https://doi.org/10.1002/app.29955

[11] T. Huang, M. Miura, S. Nobukawa, M. Yamaguchi, Crystallization behavior and dynamic mechanical properties of poly(l-Lactic Acid) with poly(ethylene glycol) terminated by benzoate, *J. Polym. Environ.* 22 (2014) 183–189.
https://doi.org/10.1007/s10924-014-0638-y

[12] E. E. Mastalygina, K. V. Aleksanyan, Recent approaches to the plasticization of poly(lactic acid) (PLA) (a review), *Polymers* 16 (2024) 87.
https://doi.org/10.3390/polym16010087

[13] K. M. B. Jansen, D. J. Van Dijk, M. H. Husselman, Effect of processing conditions on shrinkage in injection molding, *Polym. Eng. Sci.*, 38, (1998), 838–846. https://doi.org/10.1002/pen.10249

[14] D. Annicchiarico, J. R. Alcock, Review of factors that affect shrinkage of molded part in injection molding, *Mater. Manuf. Process.*, 29, (2014), 662–682. https://doi.org/10.1080/10426914.2014.880467

[15] D. O. Kazmer, Injection Mold Design Engineering, in: Chen, S. C.; Turng, L. S.; Kamal, M. R. (Eds.), D. O. Kazmer (Ed.), Injection Mold Design Engineering (Second Edition), Hanser, 2016, I–XXIV.

[16] S. -C. Chen, Introduction to injection molding, in: S. -C. Chen, L. -S. Turng (Ed.), Advanced injection molding technologies, Hanser, Munich, Germany, 2019, 1-23.

[17] N. Zhao, J. Lian, P. Wang, Z. Xu, Recent progress in minimizing the warpage and shrinkage deformations by the optimization of process parameters in plastic injection molding: a review, *Int. J. Adv. Manuf. Technol.,* 120, (2022), 85–101. https://doi.org/10.1007/s00170-022-08859-0

[18] D. Bryce, Plastic Injection Molding: Manufacturing Process Fundamentals, SME, Southfield, MI, 2001.

[19] D. Huang, Z. -D. Hu, T. -Y. Liu, B. Lu, Z. -C. Zhen, G. -X. Wang, J. -H. Ji, Seawater degradation of PLA accelerated by water-soluble PVA, *E-Polymers*, 20, (2020), 759–772. https://doi.org/10.1515/epoly-2020-0071

[20] R. A. Saari, R. Maeno, R. Tsuyuguchi, W. Marujiwat, P. Phulkerd, M. Yamaguchi, Impact of lithium halides on rheological properties of aqueous solution of poly(vinyl alcohol), *J. Polym. Res.*, 27, (2020), 218.

https://doi.org/10.1007/s10965-020-02198-y

[21] R. Nishikawa, N. Aridome, N. Ojima, M. Yamaguchi, Structure and properties of fiber-reinforced polypropylene prepared by direct incorporation of aqueous solution of poly(vinyl alcohol), *Polymer*,199, (2020), 122566.

https://doi.org/10.1016/j.polymer.2020.122566.

[22] T. Sako, J. Date, M. Hagi, T. Hiraoka, S. Matsuoka, M. Yamaguchi, Anomalous viscosity decrease of polycarbonate by addition of polystyrene, *Polymer,* 170 (2019) 135–141.

https://doi.org/10.1016/j.polymer.2019.03.015.

[23] Y. Tanaka, T. Sako, T. Hiraoka, M. Yamaguchi, M. Yamaguchi, Effect of morphology on shear viscosity for binary blends of polycarbonate and polystyrene, *J. Appl. Polym. Sci.,* 137, (2020), 49516.

https://doi.org/10.1002/app.49516.

[24] N. Moonprasith, M. S. Nasri, R.A. Saari, P. Phulkerd, M. Yamaguchi, Viscosity decrease by interfacial slippage between immiscible polymers, *Polym. Eng. Sci.,* 61, (2021), 1096–1103.

https://doi.org/10.1002/pen.25642.

[25] D. Sawai, K. Takahashi, A. Sasashige, T. Kanamoto, S. -H. Hyon, Preparation of oriented β-form poly(l-lactic acid) by solid-state coextrusion: Effect of extrusion variables, *Macromolecules,* 36, (2003), 3601–3605.
https://doi.org/10.1021/ma030050z.

[26] J. Yan, Y. Zheng, Y. Zhou, Y. Liu, H. Tan, Q. Fu, M. Ding, Application of infrared spectroscopy in the multiscale structure characterization of poly(l-lactic acid), *Polymer*, 278, (2023), 125985.
https://doi.org/10.1016/j.polymer.2023.125985.

[27] J. J. Elmendorp, R. J. Maalcke, A study on polymer blending microrheology: Part 1, *Polym. Eng. Sci.*, 25, (1985), 1041–1047.
https://doi.org/10.1002/pen.760251608.

[28] H. E. H. Meijer, J. M. H. Janssen, P. D. Anderson, Mixing of immiscible liquids, in: I. M. Zloczower (Ed.), Mixing and compounding of polymers, Carl Hanser Verlag GmbH & Co. KG, 2009, 41–182.

[29] P. Cassagnau, A. Michel, New morphologies in immiscible polymer blends generated by a dynamic quenching process, *Polymer*, 42, (2001,) 3139–3152.
https://doi.org/10.1016/S0032-3861(00)00602-9.

[30] M. A. B. M. Ali, S. Nobukawa, M. Yamaguchi, Morphology development of polytetrafluoroethylene in a polypropylene melt (IUPAC Technical Report), *Pure Appl. Chem.,* 83, (2011), 1819–1830.
https://doi.org/10.1351/PAC-REP-11-01-10

[31] T. Yokohara, K. Okamoto, M. Yamaguchi, Effect of the shape of dispersed particles on the thermal and mechanical properties of biomass polymer blends composed of poly(L-lactide) and poly(butylene succinate), *J. Appl. Polym. Sci.,* 117, (2010), 2226–2232. https://doi.org/10.1002/app.31959

[32] T. Yokohara, S. Nobukawa, M. Yamaguchi, Rheological properties of polymer composites with flexible fine fibers, *J. Rheo.*, 55, (2011), 1205–1218. https://doi.org/10.1122/1.3626414

[33] H. You, Q. Zhao, T. Mei, X. Li, R. You, D. Wang, Facile fabrication of thermoplastic polymer nanoparticles by combining sea-island spinning and Rayleigh instability, *J. Appl. Polym. Sci.,* 139, (2022), e52728.

https://doi.org/10.1002/app.52728

[34] R. Nishikawa, A. Eno, K. Janchai, R. Han, T. Kida, T. Mori, N. Aridome, A. Miyamoto, M. Yamaguchi, Crystallinity enhancement of extruded polypropylene containing poly(vinyl alcohol) fibers prepared in situ, *Polymer*, 254, (2022), 125043. https://doi.org/10.1016/j.polymer.2022.125043

[35] Y. Kuroda, K. -I. Suzuki, G. Kikuchi, N. Moonprasith, T. Kida, M. Yamaguchi, Improvement in Processability for Injection Molding of Bisphenol-A Polycarbonate by addition of low-density polyethylene, *Materials* 16 (2023) 866.

https://doi.org/10.3390/ma16020866

[36] W. D. Nesse, Introduction to Optical Mineralogy, Oxford University Press, 2nd ed. Oxford University Press, Oxford, UK, 1991.

[37] M. Yamaguchi, Y. Irie, P. Phulkerd, H. Hagihara, S. Hirayama, S. Sasaki, Plywood-like structure of injection-moulded polypropylene, *Polymer*, 51, (2010), 5983–5989. https://doi.org/10.1016/j.polymer.2010.10.007

[38] R. Phillips, G. Herbert, J. News, M. Wolkowicz, High modulus polypropylene: Effect of polymer and processing variables on morphology and properties, *Polym. Eng. Sci.*, 34, (1994), 1731–1743. https://doi.org/10.1002/pen.760342304

Chapter 5. Exploration of the mechanism for dimensional change of the polymer containing flexible fiber under post-process annealing

5.1 Introduction

The commercially available PLA faces limitations in actual processing due to poor melt tension, i.e., melt strength. This is attributed to the absence of long-chain branching and a narrow molecular weight distribution, which prevents PLA from exhibiting strain-hardening behavior in transient uniaxial elongational viscosity. Strain-hardening during uniaxial elongation is known to be crucial for PLA processing, as it enhances the stability of tubular-blown film bubbles, minimizes neck-in and draw resonance during T-die extrusion, and reduces localized deformation in processes such as blow molding, foaming, or thermoforming [1]. Various strategies, often termed processing aids, have been developed to induce strain-hardening behavior, including introducing branched structures [2–4], adding flexible fibers [5–9] or weak gels [10,11], and blending with long-chain branched polymers, such as an ethylene-vinyl acetate copolymer [12–14]. Recently, incorporating flexible fibers such as polytetrafluoroethylene (PTFE) has emerged as an effective method [5–9]. A. Jalali et al. reported that PTFE formed nanofibrils around 150 nm in diameter, which was well-dispersed in PLA matrix and acted as nucleating agents, thereby enhancing crystallization kinetics. . In injection-molded samples, PTFE fibers align under high shear, forming a hybrid-shish structure at the skin layer [9]. However, as

previously mentioned, post-process annealing is often used in actual process because the crystallinity is still low during rapid quench. In chapter 4, an anomalous expansion to machine direction (MD) occurred during annealing. . In this study, commercially available acrylic-modified PTFE was used in place of EBHS fibrous nucleating agents or PVA to examine the dimensional changes of PLA/PTFE strands and films during annealing, and the mechanism behind the MD expansion was further clarified.

5.2 Experimental procedure

5.2.1 Materials

The polymers used in this study were a commercially available PLA (Ingeo 4032D; NatureWork, Minnetonka, MN, USA) and PTFE (METABLEN™ A3000; Mitsubishi Chemical, Tokyo, Japan). These materials were dried under vacuum at 80 °C to eliminate possible moisture prior to mixing.

5.2.2 Sample preparation

A PLA/PTFE blend was fabricated using a 30 cc internal mixer (Labo-plastomill, 10 M-100, Toyo Seiki Seisakusyo, Tokyo, Japan) at a temperature of 190 °C for 2 min with a screw speed of 50 rpm. The PTFE content was fixed at 1 wt.%. The pure PLA was prepared with the same processing history. Films with thicknesses of 200 μm and 900 μm were subsequently prepared by compression molding at 200 °C for 2 min, followed by quenching at 25 °C for 5 min. The film was cut into the strips with 5 mm wide and loaded into a capillary rheometer (140-SAS-2002; Yasuda Seiki Seisakusyo, Nishinomiya, Japan) at 200 °C for 5 min, as illustrated in **Figure 5.1**. Extrusion was carried out at 200 °C through a circular die (length of 40 mm and diameter of 1 mm) at a piston speed of 0.17 $mm \cdot s^{-1}$, corresponding to a wall shear rate of 124 s^{-1}. The extruded strand was then subjected to melt stretching using winding rollers of 30 mm diameter at a draw ratio of 1.6. Finally, the stretched strands were cut and stored in a freezer to minimize physical aging.

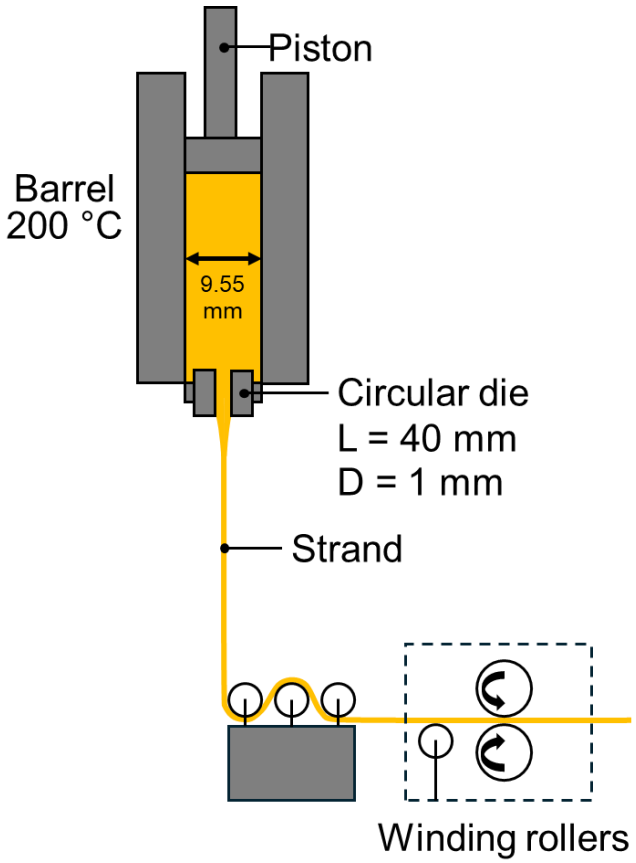

Figure 5.1. Schematic of experimental set-up for strand stretching after extrusion

To examine the dimensional change of the film before and after annealing, a sample piece was immobilized at the center of a 200 μm mold, as shown in **Figure 5.2**. It was then compressed at 200 °C for 2 min into a film using a compression-molding machine. The compressed film was sandwiched between the heat-resistance polyamide films for easy removal. Cooling process was carried out at 25 °C for 5 min, then a square film having 30 mm in length was cut from the corner of the prepared film.

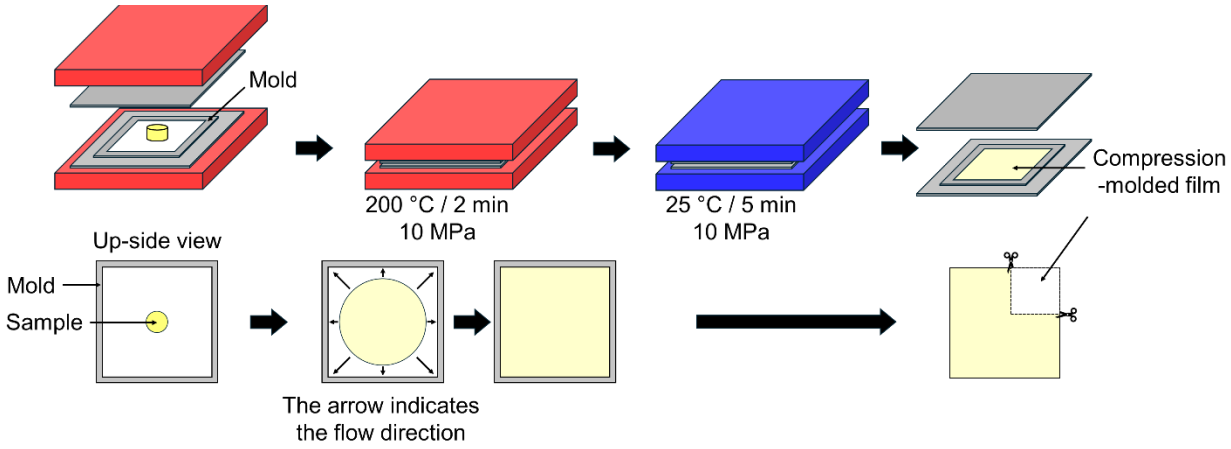

Figure 5.2. Preparation process of the film samples for dimensional change analysis

5.3 Characterization

The temperature dependence of the dynamic tensile moduli of the obtained compression-molded films were examined using a dynamical mechanical analyzer (Rheogel E-4000; UBM, Muko, Japan). The tests were carried out from 40 to 180 °C at a frequency of10 Hz under a heating rate of 2 °C min^{-1}.

The angular frequency dependencies of the oscillatory shear storage modulus G' and the loss modulus G'' of the molten PLA and PLA/PTFE were evaluated at various temperatures using a cone-and-plate rheometer (MCR301; Anton Paar, Austria) under a nitrogen. The cone had an angle of 2° and a 25 mm diameter.

Drawdown force measurements were performed using a capillary rheometer equipped with a tension detector (DT-413 G-04-3; Nidec Shimpo, Kyoto, Japan) and winding rollers with draw ratios of 1.6, 4.8, 6.4, 7.5, and 9.0.

The morphology of the PTFE was observed using a scanning electron microscope (SEM, TM3030Plus; Hitachi, Tokyo, Japan). Prior to the observation, PLA/PTFE strand was dissolved in chloroform for 2 h at 25 °C to remove the PLA parts. The remaining solid part was filtered, rinsed several times with chloroform, and dried in a vacuum. Then, the dried part was coated in platinum–palladium for SEM observation.

A 150-mm-long strand was employed to assess dimensional changes following post-process annealing. That strand was immersed in a temperature-controlled water bath at 65, 70, 75, and 80 °C for various periods. Molecular orientation after annealing was examined using a polarized optical microscope (POM; DMLP, Leica Microsystems, Wetzlar, Germany). A full-wave plate was used to determine the orientation direction, and a digital camera attached to one eyepiece captured images of the strand before and after annealing.

Two-dimensional wide-angle X-ray diffractometer (2D-WAXD; SmartLab; Rigaku, Akishima, Japan) was employed to investigate the crystalline structure of samples. The Cu-Kα radiation beam operated at 200 mA and 45 kV. Each sample was exposed to the X-ray beam for a duration of 15 min.

The polarized infrared spectra (IR) were conducted in both parallel and perpendicular to the flow direction of the films using the IR machine (Spectrum 100, Perkin Elmer, Shelton, CT, USA) equipped with a polarizer. The scanning was performed from 900 to 980 cm^{-1} at a resolution of 4 cm^{-1}, and the number of scans was 16.

The mechanical properties of the materials were evaluated through tensile tests at 25 °C and 80 °C using a universal tensile machine (Shimadzu Autograph AGS-X). For this analysis, PLA and PLA/PTFE films that had been annealed at 65 °C and 80 °C were first

dried for 24 h at 25 °C in a desiccator containing silica gel. The dried films were then cut into a dumbbell shape. During testing, the stretching direction was aligned with the flow direction. The tests were run with an initial clamp distance of 20 mm and a constant stretching speed of 20 mm min^{-1}.

5.4 Results and discussion

5.4.1 Effect of PTFE fiber on thermal and rheological properties of PLA

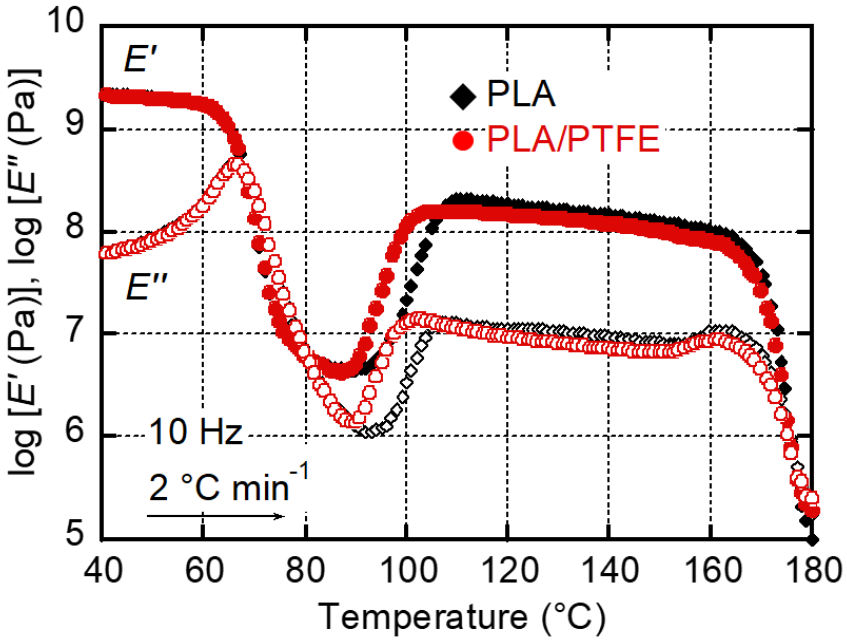

Figure 5.3. Temperature dependencies of the tensile storage modulus (E') (filled symbols) and the loss modulus (E'') (open symbols) at 10 Hz for compression-molded PLA (diamonds) and PLA/PTFE (circles).

Figure 5.3 shows the dynamical tensile test, of the compression-molded PLA and PLA/PTFE. The peak observed in E'' at approximately 66 °C corresponds to the T_g of PLA. For the PLA/PTFE, the cold-crystallization began at a lower temperature than it did for pure PLA. This suggests that the PTFE acted as nuclei sites, promoting the formation of PLA crystals during crystallization [9]. Beyond 165 °C, both samples began to melt, which is indicated by a sharp decrease in their respective E′ values..

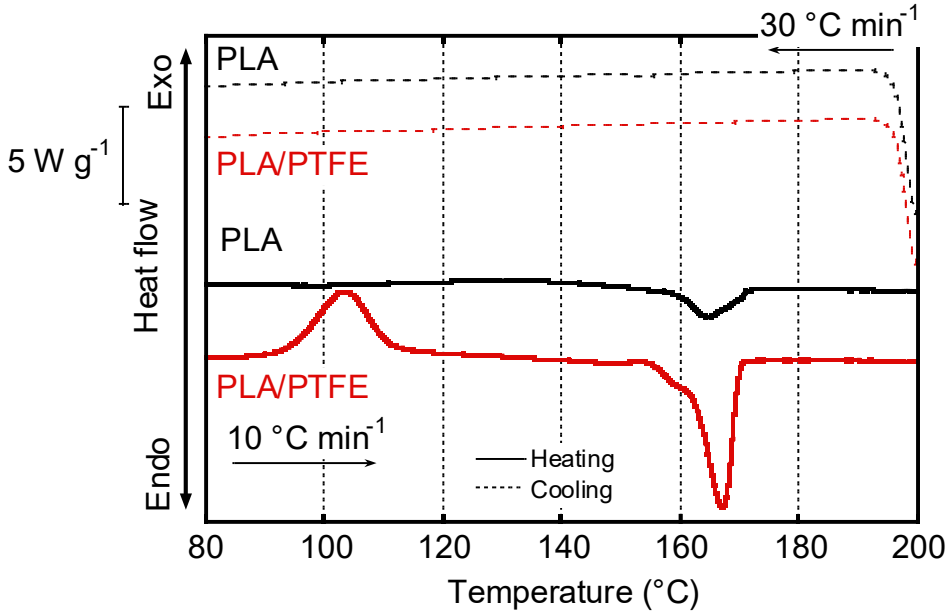

Figure 5.4. Differential scanning calorimetry cooling and second heating curves for the compression-molded PLA and PLA/PTFE films.

Figure 5.4 shows the DSC curves of the compression-molded films at cooling from the melt and second heating. The PLA crystallization was poor during cooling at a cooling rate of 30 C min^{-1}, even though the PTFE was added, resulting in poor nucleation activity of PTFE. In the second heating curves (heating rate of 10 °C·min^{-1}), a clear exothermal peak at 103 °C was found in the PLA/PTFE film. Prior to the melting of PLA/PTFE at 167 °C, a tiny exothermal peak was detected at approximately 155 °C, which must be ascribed to the crystal transformation from α′-to-α, as reported in Chapter 3.

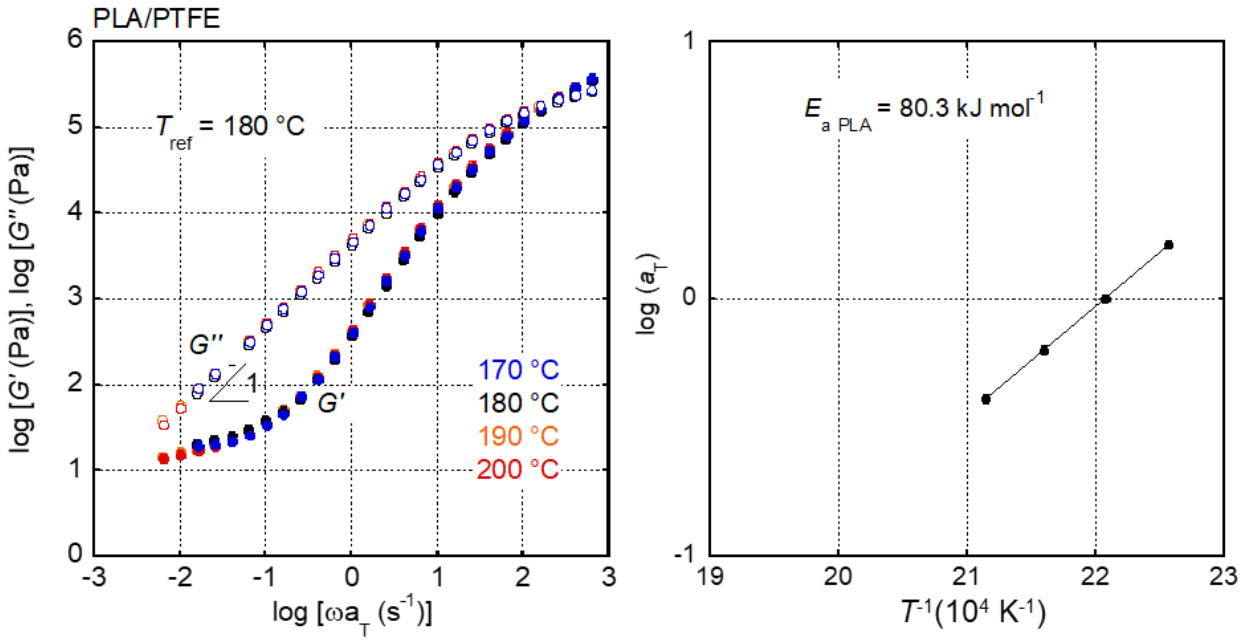

Figure 5.5. (Left) Master curves of the angular frequency dependencies of the shear storage modulus G' and the loss modulus G'' of PLA/PTFE at reference temperature, $T_{ref.}$ = 180 °C. (Right) Horizontal shift factor, a_T, versus T^{-1} (10^4 K^{-1}) of PLA/PTFE at T_{ref} of 180 °C.

Figure 5.5 shows the master curves of viscoelastic master curves for the PLA/PTFE at reference temperature of 180 °C. As reported in Chapter 2, G'' and G' of PLA was proportional to ω and ω^2, respectively, at the terminal region. In the case of PLA/PTFE, a plateau modulus appeared in the low angular frequency. It suggested that PTFE formed in the fibrils structure in the PLA continuous phase, as explained later. This phenomenon was similar to the formation of a network structure of 1,3:2,4-bis-o-(4-methylbenzylidene)-d-sorbitol in PP [15]. The flow-activation energy of PLA and PLA/PTFE was similar, around 80.2 kJ mol^{-1}, indicating that PTFE did not affect significantly to the flow-ability.

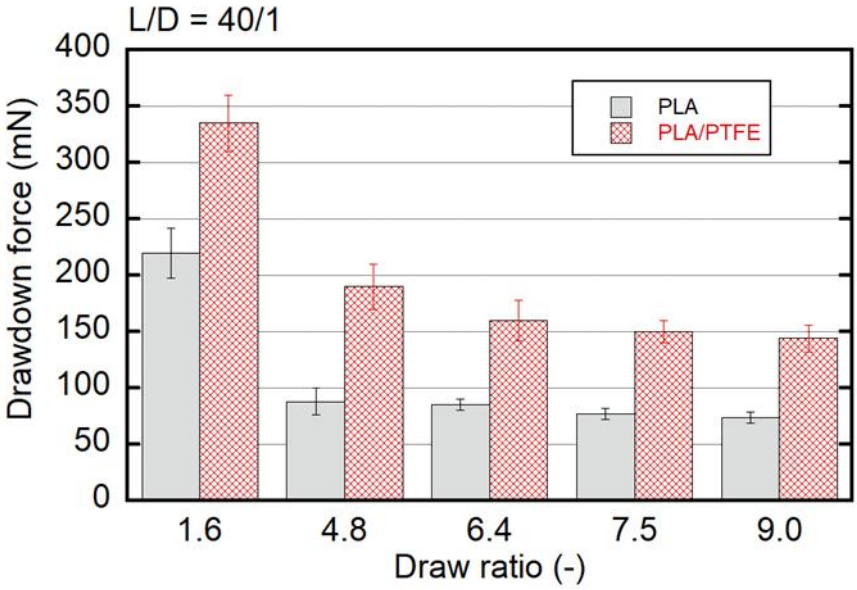

Figure 5.7. Drawdown force of PLA and PLA/PTFE at various draw ratios.

To examine the melt-tension, the drawdown force was evaluated using a capillary rheometer and a tension detector. The drawdown force values were recorded at various draw ratios, such as 1.6, 4.8, 6.4, 7.5, and 9.0, as shown in **Figure 5.7**. The drawdown force decreased as the draw ratio increased because of the reduction in the cross-section area of the strands [16–18]. Moreover, PLA/PTFE showed a higher the drawdown force value than PLA, indicating that PTFE improved the melt-tension for PLA. It was also reported that PTFE content in PLA enhanced the strain-hardening in transient elongational viscosity [8].

5.4.2 Structural growth and dimensional change of the extruded strand during annealing

The extruded strand was stretched at a draw ratio of 1.6. The strand had a smooth surface without melt-fracture, and the strands were approximately 720 ± 10 μm thick. **Figure 5.8** shows the SEM picture of the undissolved part of PLA strand containing 1 wt. % of PTFE. Since PLA is totally dissolved into chloroform, the undissolved part is PTFE. It was found that the PTFE was formed in fibrils with a diameter of 130 nm. Jalali et al. also reported the diameter of PTFE was 70 nm [9] in the injection-molded bar at the same PTFE concentration. Ali et al. reported that the primary particles of a PTFE was in ellipsoidal shape before melt-mixing [19], then it agglomerated together to generate the fibrous shape during melt-mixing, as reported elsewhere [5,6,19,20].

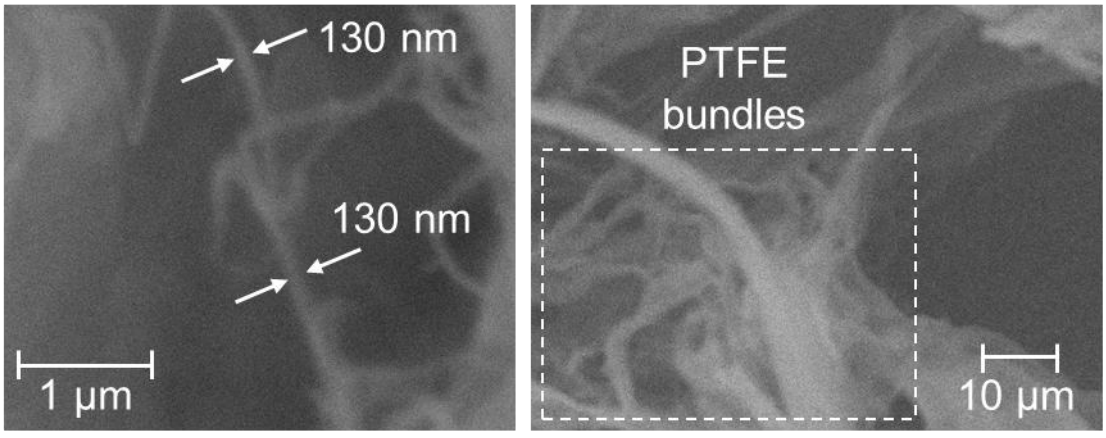

Figure 5.8. SEM image of PTFE fibrils after PLA removal using chloroform solution.

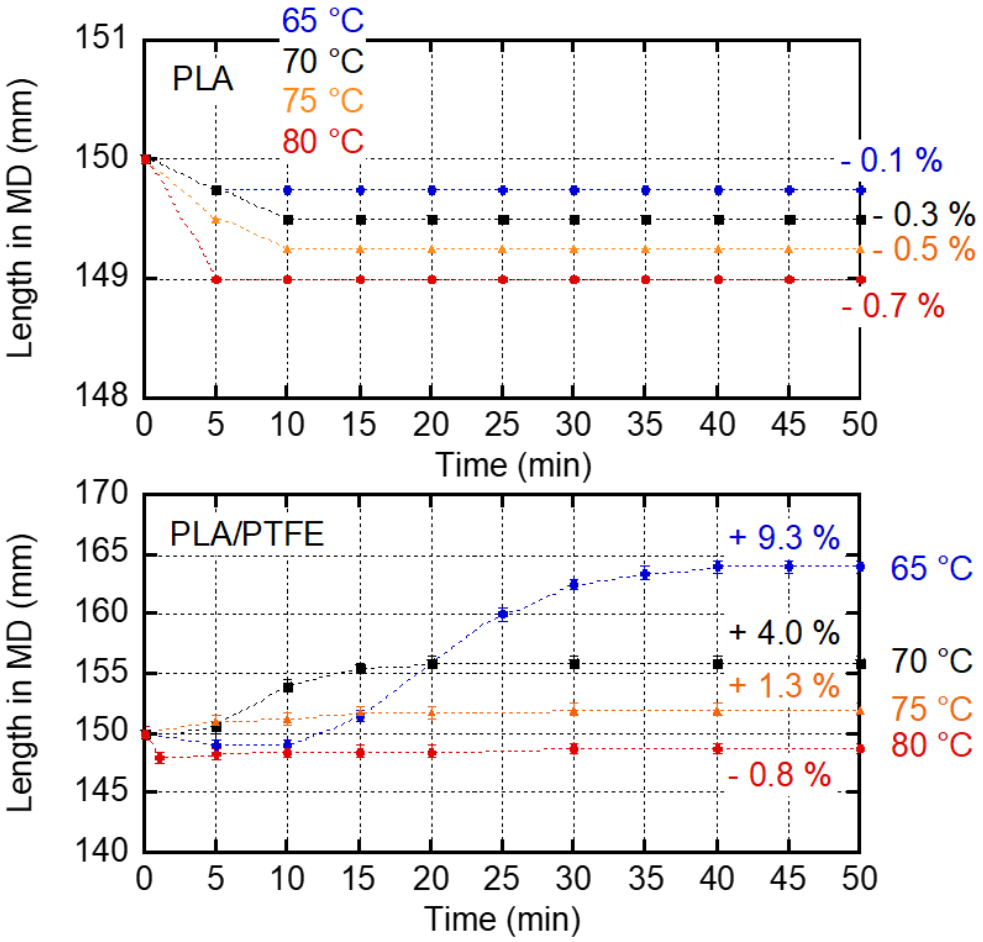

Figure 5.9. Dimensional changes in PLA (top) and PLA/PTFE (bottom) strands after post-process annealing at various temperatures and durations.

Figure 5.9 shows the dimensional change of the strand after annealed at various temperatures and periods. The PLA strand experienced a shrinkage of 0.1, 0.3, 0.5 and 0.7% of its length at 65, 70, 75, and 80 °C, respectively. In the case of PLA/PTFE, the strand gradually expanded its length to MD after annealing. This suggested that the structure growth must be affected on this anomalous expansion during annealing, such as isotropic and anisotropic structural development. Especially, the dramatical shrinkage then

expansion of the strand once annealed at 80 °C, as explained later. In the case of thickness, the thickness of the PLA/PTFE strand was decreased after annealing. This dimensional changes was similar to the Table 4.1, as reported in Chapter 4.

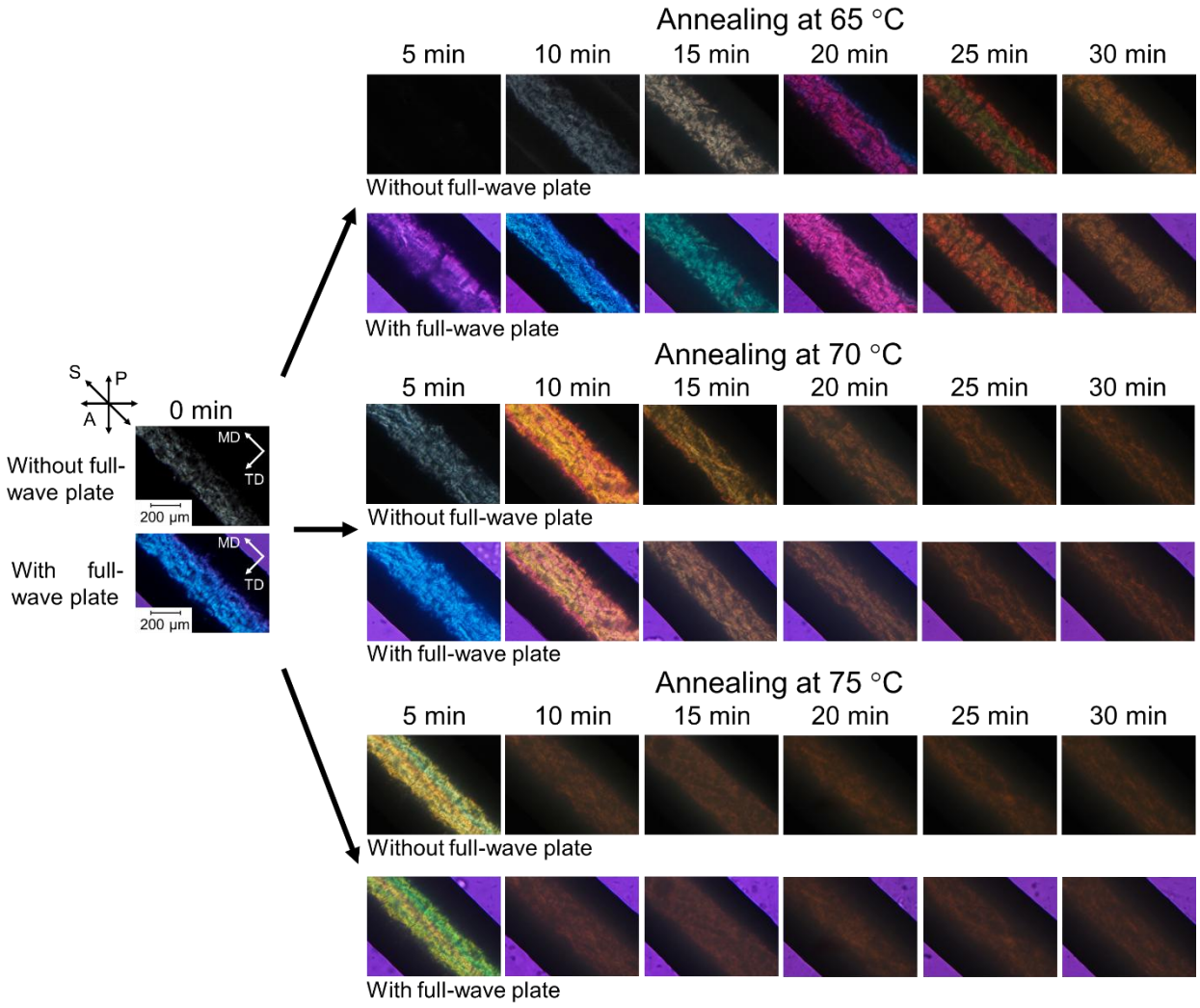

Figure 5.10. Polarized optical microscope images of PLA/PTFE strands obtained with or without a full-wave plate at various annealing histories.

Figure 5.10 illustrates the POM images of PLA/PTFE strand under cross-polarizers (A and P in the figure) with/without inserting a full-wave plate. Without inserting a full-

wave plate, the background was dark due to no orientation. It should be noted that a full-wave plate added 530 nm in the optical path-length to confirm the orientation direction, resulting in pink-purple color. The slow axis, noted as S, was indicated in the figure. **Table 5.1** summarizes the data of birefringence (Δn) and Hermans orientation function (F) of the center of a PLA/PTFE strand are summarized and calculated, as follows:

$$\Delta n = \frac{\Gamma}{d} \tag{5.1}$$

$$F = \frac{\Delta n}{\Delta n^0} \tag{5.2}$$

where Γ and d are the retardation, intrinsic birefringence (0.03) for PLA [21], and thickness of the strand (720 μm), respectively. The retardation of the extruded strand after winding, as a strand before annealing, under POM was white-grey, indicating a slight orientation to MD. Upon heating for 5 min at 65 °C, the birefringence disappeared due to orientation relaxation, i.e., losing its orientation. This orientation relaxation must induce the anisotropic shrinkage during annealing. Although the orientation relaxation did not record at 5 min for the annealing temperature of 70, 75, and 80 °C, it must appear in any materials having an orientation after rapid quenching. Then, the orientation development gradually corresponded to the expansion to MD over the annealing period, as shown in Figure 5.9.

Table 5.1. Birefringence Δn and Hermans orientation function F of PLA/PTFE strands annealed at various temperatures and periods.

Annealing period	65 °C		70 °C		75 °C	
	Δn ($\times 10^{-5}$)	F	Δn ($\times 10^{-5}$)	F	Δn ($\times 10^{-5}$)	F
0 min	5.8 ± 0.1	0.002	5.8 ± 0.1	0.002	5.8 ± 0.1	0.002
5 min	0.0	0.000	16.2 ± 0.2	0.006	186.8 ± 2.0	0.062
10 min	5.4 ± 0.1	0.002	57.4 ± 0.3	0.020	nd	nd
15 min	19.2 ± 0.1	0.006	nd	nd	nd	nd
20 min	78.3 ± 0.4	0.026	nd	nd	nd	nd
25 min	249.0 ± 2.0	0.083	nd	nd	nd	nd
30 min	nd	nd	nd	nd	nd	nd

nd: not detected

Figure 5.11 shows the 2D-WAXD images with 2θ profiles, and azimuthal angle distribution of the (200)/(110) plane (2θ = 16.3°) of PLA/PTFE strands annealed at 65, 80 °C for various periods. Prior to annealing, the PLA/PTFE exhibited an amorphous structure, as indicated by a halo in Figure 5.11a. The intensity of the peak at 16.3° gradually increased after annealing for more than 10 minutes, demonstrating crystal formation. To evaluate the molecular orientation of crystals, the azimuthal angle distribution of the (200)/(110) planes was measured from 0° to 360°. It should be noted that peak intensities at 90° and 270° increased progressively with annealing beyond 10 minutes, indicating that

crystal growth was aligned along MD. This orientation corresponds well with the POM observations shown in Figure 5.9. During extrusion, the PTFE fibrils oriented to flow direction, i.e., MD, during extrusion, then acted as a pseudo-shish structure [9,15,22–25]. Consequently, PLA crystals nucleated and grew along the oriented PTFE fibers during annealing, forming the characteristic kebab-like structures.

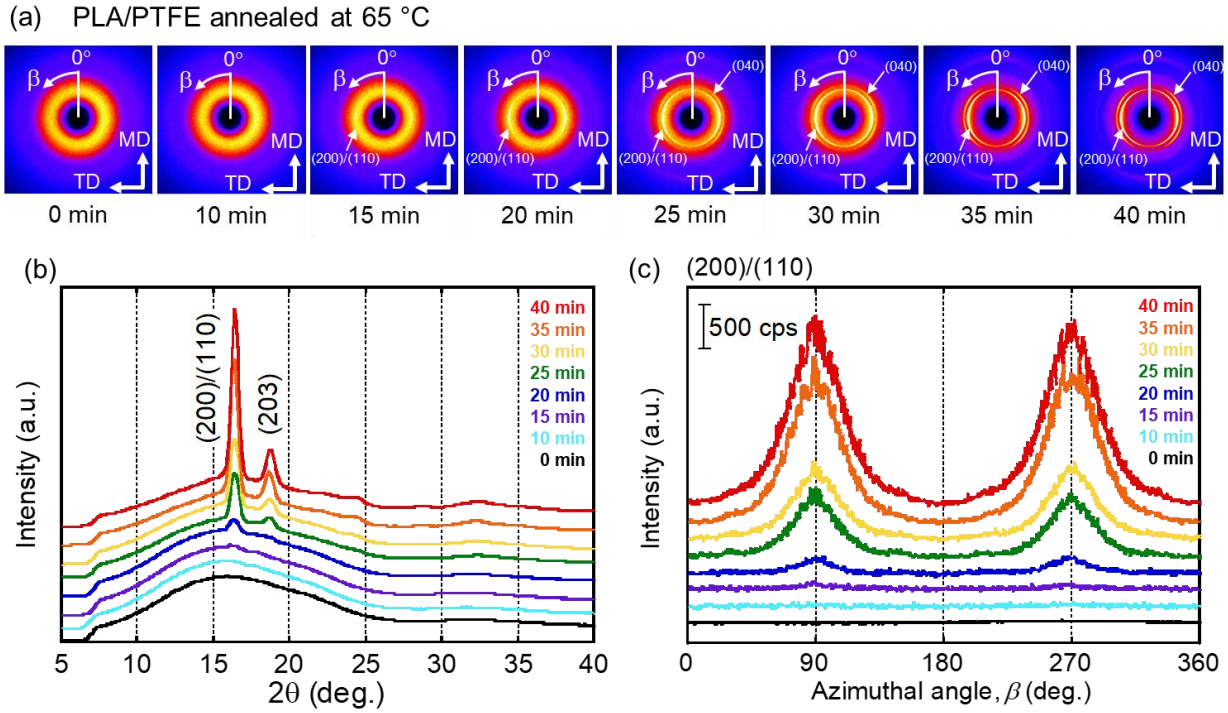

Figure 5.11. (a) 2D-WAXD images, (b) 2θ profiles, and (c) azimuthal angle distributions of the (200)/(110) planes of PLA/PTFE strands after annealing at 65 °C for various periods.

The further quantitative evaluation was conducted using the peak intensity on the equator, i.e., 90°, from the azimuthal angle distribution, as shown in **Figure 5.12**. It indicated that the increase in crystallinity was well corresponded to the increase in

molecular orientation. In other words, the majority of kebab structures developed from the oriented PTFE fibers, inducing the anomalous expansion.

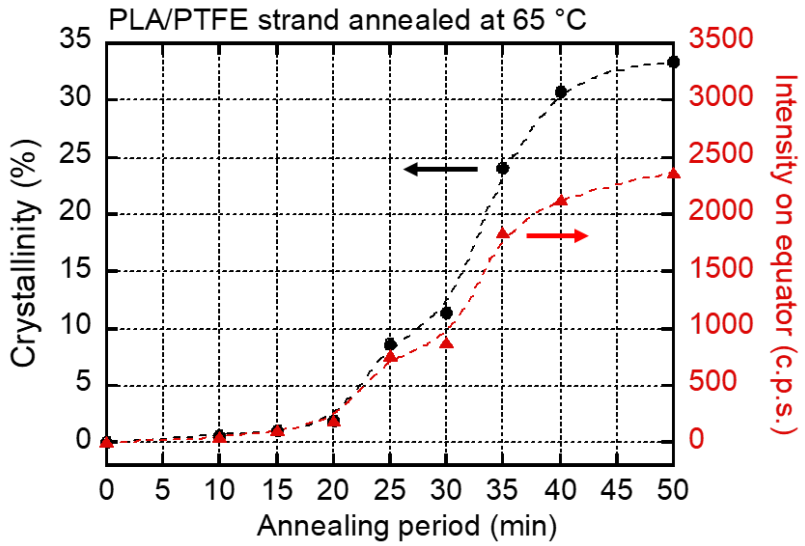

Figure 5.12. Growth curves of the crystallinity and the peak intensity on equator at 90° obtained from the azimuthal angle distribution of the (200)/(110) planes for the PLA/PTFE strand during annealing at 65 °C.

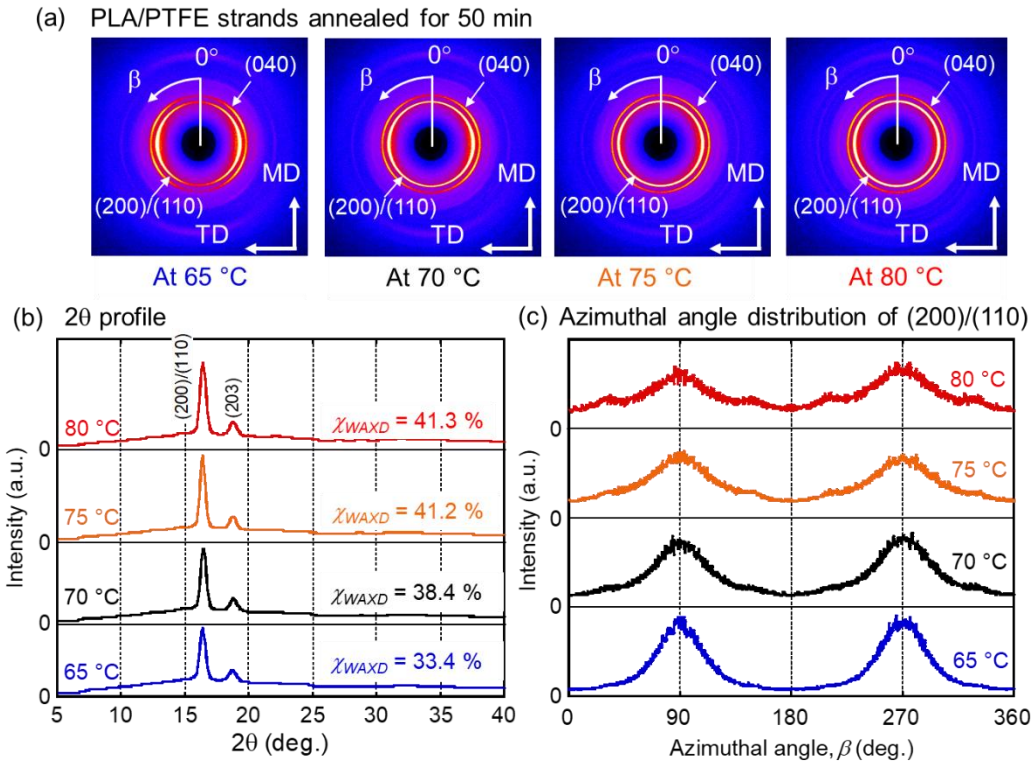

Figure 5.13. (a) 2D-WAXD images, (b) 2θ profiles, and (c) azimuthal angle distributions of the (200)/(110) planes of PLA/PTFE strands after annealing at 65, 70, 75, and 80 °C for 50 min.

Figure 5.13 shows the 2D-WAXD images, 2θ profiles, and azimuthal angle distribution of the PLA/PTFE strands annealed at various temperatures for 50 min. The 2D-WAXD images clearly displayed crystalline rings, and the corresponding crystallinity values from 2θ profiles were calculated to be 33.4%, 38.4%, 41.2%, and 41.3% for annealing at 65, 70, 75, and 80 °C, respectively. In Figure 5.12(c), the reduction in peak intensity at 90° accompanied by an increase at 30° and 150° suggests that some crystals were misaligned along the MD. In addition, higher annealing temperatures led to the

appearance of rings corresponding to the (200)/(110) planes, indicating three-dimensional bulk crystallization, characteristic of spherulitic growth, i.e., spherulitic crystal growth. It suggested that the spherulites and kebab structure developed at the same time once annealed at a high temperature, i.e., 80 °C.

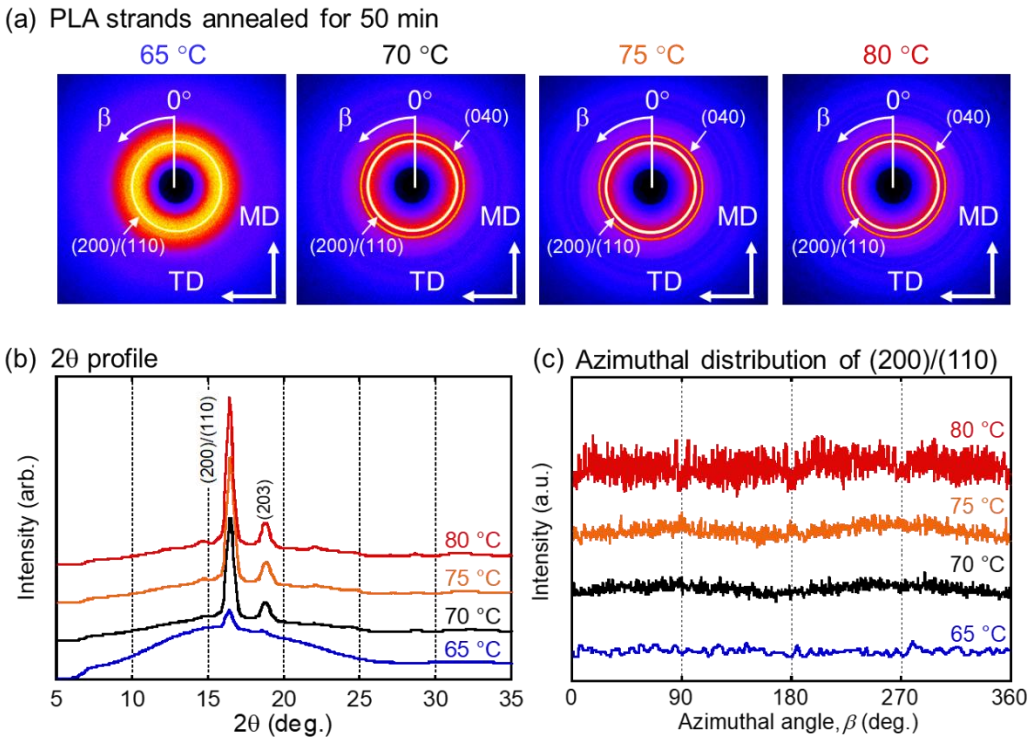

Figure 5.14. (a) 2D-WAXD images, (b) 2θ profiles, and (c) the azimuthal angle distribution of (200)/(110) plane for PLA strand after annealing at 65, 70, 75, and 80 °C for 50 min.

The structure and orientation of PLA strand annealed at various temperatures were shown in **Figure 5.14**. Due to slow crystallization, PLA showed a low crystallinity without orientation once annealed at 65 °C. However, the orientation was weak, as supposed to no

orientation, upon annealed above 70 °C. Therefore, in this study, both orientation relaxation and bulk crystallization led to the volume reduction, resulting in shrinkage.

5.4.3 Effect of molecular orientation on the dimensional change and mechanical properties

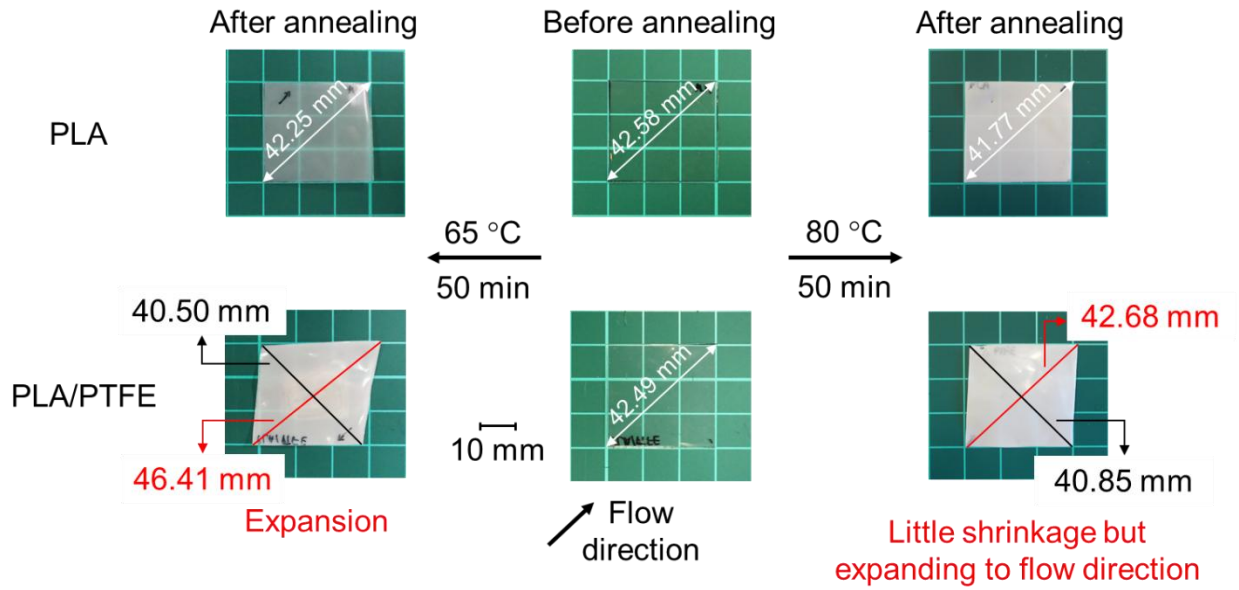

Figure 5.15. Dimensional change of the compression-molded films before and after annealing in the temperature-controlled water bath at 65 °C (left) and 80 °C (right) for 50 min. A square film, approximately 30 mm in length, was cut from the corner of the compression-molded film.

To confirm the effect of orientation on the anomalous expansion after annealing, the dimensional change of compression-molded films having a flow-field was further

examined, as shown in **Figure 5.15**. The square films measured 30.00 mm on each side, giving a diagonal of 42.42 mm. When annealed at 65 and 80 °C for 50 minutes, the PLA films exhibited shrinkage, with reductions observed in their diagonal, width, and length. In contrast, the PLA/PTFE films showed expansion along the flow direction, resulting in an increase in the diagonal length (highlighted in red).

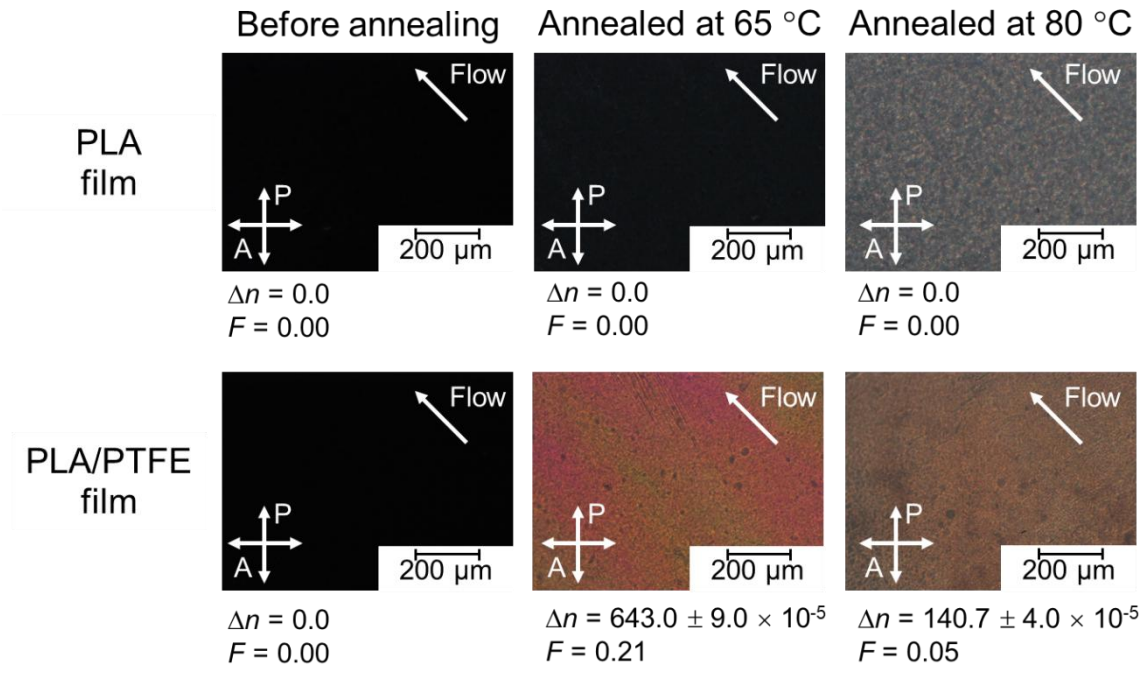

Figure 5.16. POM images under crossed polarizers of PLA and PLA/PTFE films before annealing (left), and after annealing at 65 °C (center) and 80 °C (right) for 50 min.

The molecular orientation was assessed by measuring birefringence using POM, as shown in **Figure 5.16**. The microscope was focused on the center of the films. Before annealing, both PLA and PLA/PTFE films showed a dark background, indicating an

absence of molecular orientation. After annealing at 65 and 80 °C, retardation appeared in the PLA/PTFE films. In comparison, the PLA film annealed at 80 °C exhibited the formation of small spherulites.

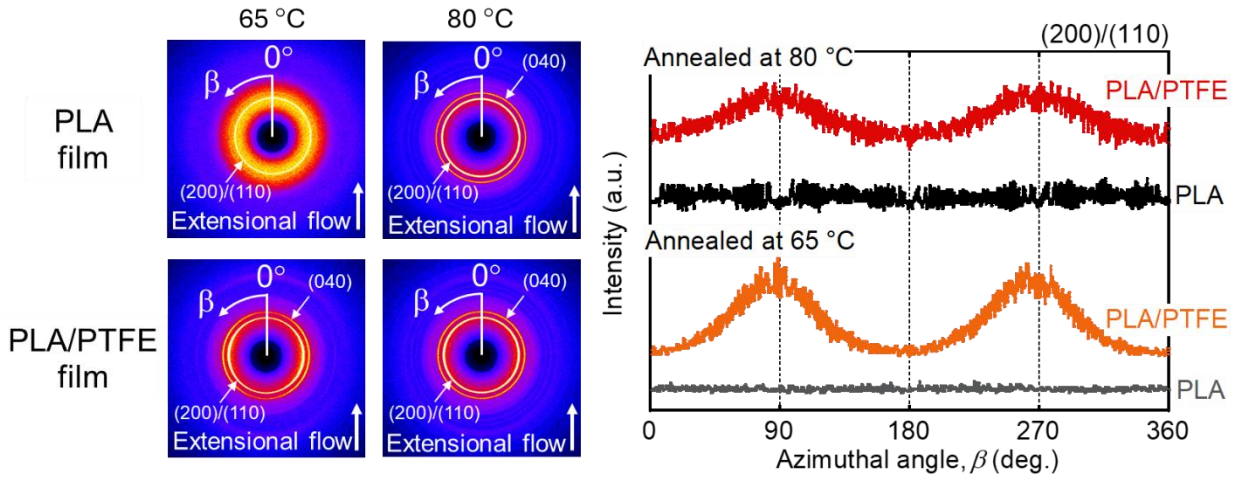

Figure 5.17. 2D-WAXD images and azimuthal angle distributions of the (200)/(110) planes of the PLA and PLA/PTFE films annealed at 65 and 80 °C for 50 min.

The crystalline structure and molecular orientation of PLA and PLA/PTFE films annealed at 65 and 80 °C were analyzed using 2D-WAXD, as shown in **Figure 5.17**. The PLA films showed no molecular orientation at either annealing temperature. This was accompanied by an increase in crystallinity (ring of (200)/(110) and (040) planes) without molecular orientation induced shrinkage in the PLA film, as demonstrated in Figure 5.15. In contrast, incorporating PTFE promoted significant chain orientation originating from the aligned crystals after annealing. In other words, the expansion of the PLA/PTFE film in the flow direction may be due to an internal stretching force for aligning the PLA chains, i.e., PLA lamellae, along the PTFE fibers during annealing.

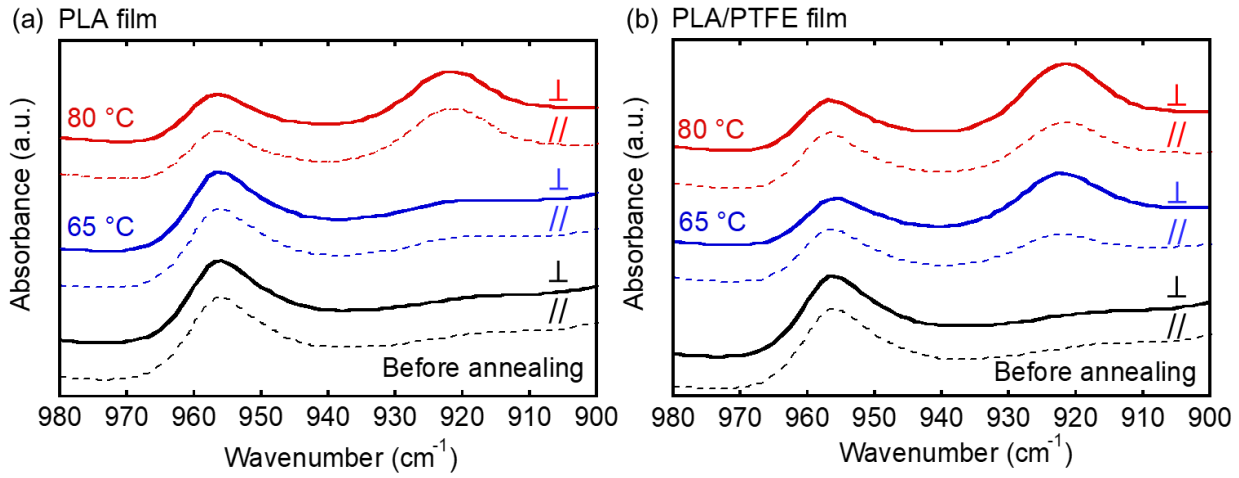

Figure 5.18. Polarized FTIR spectra of PLA (a) and PLA/PTFE (b) films before and after annealed at 65 and 80 °C for 50 min. The transition moment of IR beams perpendicular (solid lines) and parallel (dotted lines) to the extensional flow direction.

The IR spectra of the PLA and PLA/PTFE films were obtained using a polarizer, as shown in **Figure 5.18**. The dichroic ratio, D, and Hermans orientation function, , were obtained using the equations (4.1) and (4.2). D and f_{IR} values of the PLA/PTFE film before and after annealing are summarized in **Table 5.2**. Prior to annealing, neither samples exhibited molecular orientation or crystallization. After annealing at 65 °C, however, the PLA/PTFE film exhibited significant orientation, with f_{921} (oriented crystals) and f_{956} (oriented amorphous polymer chains) values around 0.4 and 0.05, respectively. These observations are consistent with the POM images in Figure 5.16 and the azimuthal angle distributions shown in Figure 5.17.

Table 5.2. Dichroic ratios and the Hermans orientation functions of a compression-molded PLA and PLA/PTFE film before and after annealing for 50 min.

	PLA			PLA/PTFE		
	Before annealing	Annealing at 65 °C	Annealing at 80 °C	Before annealing	Annealing at 65 °C	Annealing at 80 °C
f_{921}	0.00	0.00	0.00	0.00	0.40	0.26
f_{956}	0.00	0.00	0.00	0.00	0.05	0.00

Figure 5.19 shows the stress-strain behavior of the films at 23 and 80 °C, with all samples annealed at 65 and 80 °C. The results clearly indicate that molecular orientation strongly affects mechanical properties. As shown in Figure 5.19(a), the PLA film exhibited a brittle fracture behavior, whereas a PLA/PTFE film displayed the ductile deformation accompanied by strain-hardening. Although the exact mechanism remains unclear, it is noteworthy that the oriented structure may influence the failure mechanism. Annealing-induced structural changes significantly enhanced tensile properties, surpassing those reported in previous studies with the same composition [24,26]. Previous research demonstrated that incorporating a small amount of metal-organic frameworks [27] or melanin-like nanoparticles [28] enhanced the compatibility of immiscible PLA/poly(butylene succinate) (PBS) blends, providing ductile nature to PLA/PBS. At 80 °C, i.e., above T_g, PLA demonstrated a rubber-like behavior due to its low crystallinity, as shown in Figure 5.19(b). The strain-hardening began at a strain of approximately 0.07

and increased sharply beyond a strain of 1.5. A small crystalline fraction is likely to act as crosslink points. In the PLA/PTFE film, a highly-oriented shish-kebab structure resulted in a significant increase in tensile modulus while maintaining ductile behavior. This structural evolution via post-annealing provides valuable guidance for designing PLA materials with mechanical properties comparable to conventional plastics like polyethylene and polypropylene.

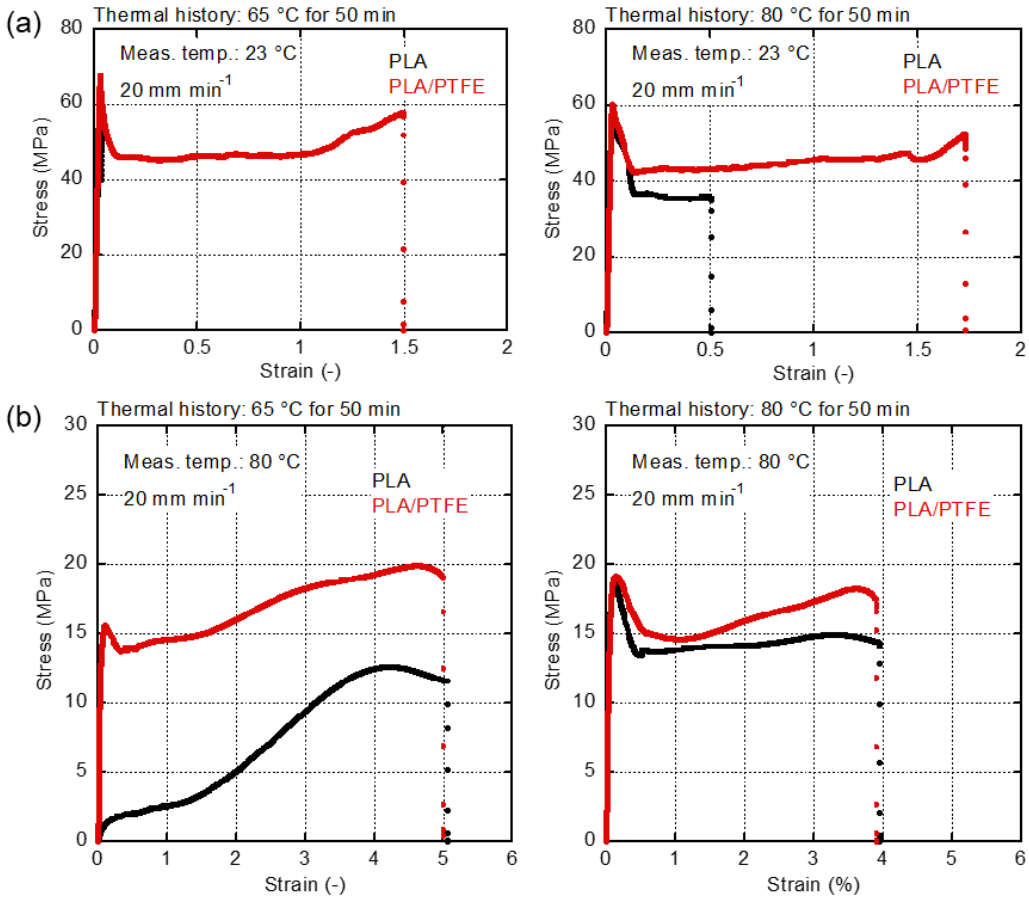

Figure 5.19. Stress-strain curves of PLA (black) and PLA/PTFE (red) films with various annealing histories, e.g., 65 °C and 80 °C. The measurements were performed at (a) 23 °C and (b) 80 °C.

Table 5.3. Dimensional change in the machine direction of PLA samples reported in various studies.

	Samples		**Dimensional change in MD**
Y. H. Seo et al. [29]	PLA yarn		- 7.90 %
J. Butt et al. [30]	Injection-molded PLA bar		- 5.6 %
	Cu/PLA composite 80/20 bar		- 1.3 %
H.-G. D. Vo et al. [25]	PLA strand		- 2.04 ± 0.27 %
(Chapter 3)	PLA/EBHS strand		- 0.80 ± 0.19 %
Yamaguchi et al. [31]	Injection-molded PLA bar		- 1.82 %
(Chapter 4)	Injection-molded PLA/PVA bar		+ 2.8 %
This chapter [32]	PLA strand	(65 °C)	- 0.1 %
	PLA strand	(70 °C)	- 0.3 %
	PLA strand	(75 °C)	- 0.5 %
	PLA strand	(80 °C)	- 0.7 %
	PLA/PTFE strand	(65 °C)	+ 9.3 % ± 0.33%
	PLA/PTFE strand	(70 °C)	+ 4.0 % ± 0.33%
	PLA/PTFE strand	(75 °C)	+ 1.3 % ± 0.33%
	PLA/PTFE strand	(80 °C)	- 0.8 % ± 0.33%

(PLA = poly(lactic acid); EBHS = N,N′-ethylenebis(12-hydroxystearamide); PVA = poly(vinyl alcohol); PTFE = poly(tetrafluoroethylene))

Table 5.3 summarizes the dimensional change of the various samples, such as strand, injection-molded bar, during annealing. Excerpting our studies, most of studied reported that PLA products showed a shrinkage after annealing, e.g., below 0% of its dimensional change in MD. In chapter 3, the anisotropic shrinkage to flow direction has been limited, that is, the dimensional change in MD was detected at only 0.8 %. However, the orientation was still low. In chapter 5, it was found that the dimensional change was well correlated to the amount of molecular orientation and crystallization. Therefore, these studies proposed a novel method to control the anisotropic shrinkage during annealing using molecular orientation enhancement from the oriented crystals.

5.5 Conclusion

The structure and properties of PLA containing 1 wt.% of PTFE were investigated. In the molten state, a plateau in the modulus at low angular frequencies indicated that PTFE fibers had formed a network structure. The addition of PTFE significantly increased the drawdown force. During melt-stretching, the PTFE fibers aligned along the flow direction. Although the PTFE fibers did not significantly promote nucleation of PLA during cooling, they accelerated the cold crystallization of PLA. As a result, PLA crystals developed around the fiber surfaces during post-processing annealing. This crystal growth enhanced molecular orientation in the PLA, promoting expansion in the MD. In contrast, PLA strands without PTFE exhibited minimal molecular orientation, even after annealing. An anomalous MD expansion was also exhibited in compression-molded PLA/PTFE films, which deformed along the flow direction after annealing. This behavior could be useful for controlling dimensional stability and structural features of PLA-based products through post-process annealing.

References

[1] B. Mallet, K. Lamnawar, A. Maazouz, Improvement of blown film extrusion of poly(lactic acid): Structure–processing–properties relationships, *Polym. Eng. Sci.*, 54, (2014), 840-857.

https://doi.org/10.1002/pen.23610

[2] A. Jalali, M. A. Huneault, M. Nofar, P. C. Lee, C. B. Park, Effect of branching on flow-induced crystallization of poly (lactic acid), *Eur. Polym. J.,* 119, (2019), 410–420.

https://doi.org/10.1016/j.eurpolymj.2019.07.045

[3] L. Gu, Y. Xu, G.W. Fahnhorst, C. W. Macosko, Star vs long chain branching of poly(lactic acid) with multifunctional aziridine, *J. Rheol.,* 61, (2017), 785–796.

https://doi.org/10.1122/1.4985344

[4] P. Li, W. Zhang, M. Kong, Y. Lv, Y. Huang, Q. Yang, G. Li, Ultrahigh performance polylactide achieved by the design of molecular structure, *Mater. Des.,* 206, (2021), 109779.

https://doi.org/10.1016/j.matdes.2021.109779

[5] M. A. B. M. Ali, K. Okamoto, M. Yamaguchi, T. Kasai, A. Koshirai, Rheological properties for polypropylene modified by polytetrafluoroethylene, *J. Polym. Sci., Part B: Polym. Phys.,* 47, (2009), 2008–2014.

https://doi.org/10.1002/polb.21799

[6] M. Yamaguchi, K. Fukuda, T. Yokohara, M. A. B. M. Ali, S. Nobukawa, Modification of rheological properties under elongational flow by addition of polymeric fine fibers, *Macromol. Mater. Eng.*, 297, (2012), 654–658.

https://doi.org/10.1002/mame.201100270

[7] T. Yokohara, S. Nobukawa, M. Yamaguchi, Rheological properties of polymer composites with flexible fine fibers, *J. Rheol.,* 55, (2011), 1205–1218.

https://doi.org/10.1122/1.3626414

[8] M. Yamaguchi, T. Yokohara, M. A. B. M. Ali, Effect of flexible fibers on rheological properties of poly(lactic acid) composites under elongational flow, *Nihon Reoroji Gakkaishi,* 41, (2013), 129–135.

https://doi.org/10.1678/rheology.41.129

[9] A. Jalali, J. -H. Kim, A. M. Zolali, I. Soltani, M. Nofar, E. Behzadfar, C. B. Park, Peculiar crystallization and viscoelastic properties of polylactide/polytetrafluoroethylene composites induced by in-situ formed 3D nanofiber network, *Compos. Part B Eng.,* 200 (2020), 108361.

https://doi.org/10.1016/j.compositesb.2020.108361

[10] M. Yamaguchi, H. Miyata, Strain hardening behavior in elongational viscosity for binary blends of linear polymer and crosslinked polymer, *Polym. J.,* 32 (2000) 164–170.

https://doi.org/10.1295/polymj.32.164

[11] M. Yamaguchi, K. -I. Suzuki, Rheological properties and foam processability for blends of linear and crosslinked polyethylenes, *J. Polym. Sci., Part B: Polym. Phys.,* 39 (2001) 2159–2167.

https://doi.org/10.1002/polb.1189

[12] D. Kugimoto, S. Kouda, M. Yamaguchi, 2019. Improvement of mechanical toughness of poly(lactic acid) by addition of ethylene-vinyl acetate copolymer, *Polym. Test.,* 80, 106021.

https://doi.org/10.1016/j.polymertesting.2019.106021.

[13] D. Kugimoto, S. Kouda, M. Yamaguchi, Modification of poly(lactic acid) rheological properties using ethylene–vinyl acetate copolymer, *J. Polym. Environ.* 29 (2021) 121–129.

https://doi.org/10.1007/s10924-020-01856-y.

[14] R. Feng, D. Kugimoto, M. Yamaguchi, 2024. Modification of processability and shear-induced crystallization of poly(lactic acid), *Polymers* 16, 3487.

https://doi.org/10.3390/polym16243487.

[15] K. Janchai, T. Kida, T. Inoue, S. Iwasaki, M. Yamaguchi, Crystallization behavior of isotactic polypropylene containing a fibrous nucleating agent in a flow field, *Polym. J.*, 54, (2022), 367–375.

https://doi.org/10.1038/s41428-021-00596-7.

[16] M. H. Wagner, H. Bastian, A. Bernnat, S. Kurzbeck, C. K. Chai, Determination of elongational viscosity of polymer melts by RME and rheotens experiments, *Rheol. Acta.*, 41, (2002), 316–325.

https://doi.org/10.1007/s00397-002-0228-0.

[17] J. Seemork, M. Siriprumpoonthum, Y. Lee, S. Nobukawa, M. Yamaguchi, Effect of die geometry on drawdown force of polypropylene at capillary extrusion, *Adv. Polym. Tech.*, 34, (2015).

https://doi.org/10.1002/adv.21477.

[18] P. Phulkerd, T. Nakabayashi, S. Iwasaki, M. Yamaguchi, Enhancement of drawdown force in polypropylene containing nucleating agent, *J. Appl. Polym. Sci.*, 136, (2019), 47295.

https://doi.org/10.1002/app.47295.

[19] M. A. B. M. Ali, S. Nobukawa, M. Yamaguchi, Morphology development of polytetrafluoroethylene in a polypropylene melt (IUPAC Technical Report), *Pure Appl. Chem.,* 83, (2011), 1819–1830.

https://doi.org/10.1351/PAC-REP-11-01-10.

[20] S. G. Hatzikiriakos, A. B. Ariawan, S. Ebnesajjad, Paste extrusion of polytetrafluoroethylene (PTFE) fine powder resins, *J. Chem. Eng.,* 80, (2002), 1153–1165.

https://doi.org/10.1002/cjce.5450800617.

[21] Y. Furuhashi, Y. Kimura, H. Yamane, Higher order structural analysis of stereocomplex-type poly(lactic acid) melt-spun fibers, *J. Polym. Sci., Part B:Polym. Phys.*, 45, (2007), 218–228.

https://doi.org/10.1002/polb.21035.

[22] R. Nishikawa, N. Aridome, N. Ojima, M. Yamaguchi, Structure and properties of fiber-reinforced polypropylene prepared by direct incorporation of aqueous solution of poly(vinyl alcohol), *Polymer*, 199, (2020), 122566.

https://doi.org/10.1016/j.polymer.2020.122566.

[23] S. Iwasaki, M. Inoue, Y. Takei, R. Nishikawa, M. Yamaguchi, Modulus enhancement of polypropylene by sorbitol nucleating agent in flow field, *Polym. Cryst.,* 4, (2021), e10170.

https://doi.org/10.1002/pcr2.10170.

[24] T. Kuang, M. Zhang, X. Lian, J. Zhang, T. Liu, S. Zhang, X. Peng, 2022. External flow-induced highly oriented and dense nanohybrid shish-kebabs: a strategy for achieving high performance in poly (lactic acid) composites. Compos. Commun. 29, 101042. https://doi.org/10.1016/j.coco.2021.101042.

[25] H. -G. D. Vo, M. Yamaguchi, Growth of molecular orientation during post-process annealing of poly(lactic acid) containing a fibrous nucleating agent, *J. Appl. Polym. Sci.,* 141, (2024), e55714. https://doi.org/10.1002/app.55714

[26] J. Chai, G. Wang, A. Zhang, S. Li, J. Zhao, G. Zhao, C.B. Park, Ultra-ductile and strong in-situ fibrillated PLA/PTFE nanocomposites with outstanding heat resistance derived by CO2 treatment, *Compos. - A: Appl. Sci. Manuf.,* 155, (2022), 106849. https://doi.org/10.1016/j.compositesa.2022.106849

[27] T. Kuang, H. Guo, W. Guo, W. Liu, W. Li, M.R. Saeb, M. Vatankhah-Varnosfaderani, S.S. Sheiko, Boosting the strength and toughness of polymer blends via ligand-modulated MOFs, *Adv. Sci.,* 11, (2024), 2407593. https://doi.org/10.1002/advs.202407593

[28] C. Pei, H. Zhang, Y. Li, Z. Gu, X. Chen, T. Kuang, Robust and durable biodegradable polymer-based triboelectric nanogenerators enabled by trace amounts of melanin-like nanoparticles, *Nano Energy,* 135, (2025), 110643. https://doi.org/10.1016/j.nanoen.2025.110643

[29] Y. H. Seo, S.S. Han, T. H. Oh, M. S. Khil, Annealing effects on structural changes and thermal shrinkage of poly(lactic acid) draw-textured filaments, *J. Text. Inst*., 105, (2014), 553–558.

https://doi.org/10.1080/00405000.2013.827390

[30] J. Butt, R. Bhaskar, Investigating the effects of annealing on the mechanical properties of FFF-printed thermoplastics, *J. Manuf. Mater. Process.*, 4, (2020), 38.

https://doi.org/10.3390/jmmp4020038

[31] M. Yamaguchi, W. Shu, T. Kimura, H.-G.D. Vo, T. Kida, T. Mori, M. Kitani, N. Aridome, A. Miyamoto, Anomalous postprocessing dimensional change of injection-molded products composed of poly(lactic acid) and poly(vinyl alcohol), *ACS Appl. Polym. Mater.,* 5, (2023), 2136–2143.

https://doi.org/10.1021/acsapm.2c02155

[32] H. -G. D. Vo, M. Yamaguchi, Elucidating the effect of chain orientation on the dimensional change of a poly(lactic acid) composite containing a flexible fiber, *Polymer*, 333, (2025), 128589.

https://doi.org/10.1016/j.polymer.2025.128589

Chapter 6. General conclusion

In this study, my research focused on a method to improve the crystallinity, as well as the molecular orientation of semi-crystalline polymers using a shear flow. Moreover, the effect of molecular orientation on the anomalous expansion to flow direction was also investigated, as follows:

Chapter 2: Effect of shear history on the structure development during annealing

Basically, the polymer molecule undergoes the Brownian motion, leading to the relaxation above glass-transition temperature during heat-treatment. As a result, the spherulites, i.e., isotropic structure, developed during annealing. In chapter 2, the polymer having ordered structures with the orientation to flow direction was designed. This ordered structure can be employed to counter the natural shrinkage of the relaxation and crystallization.

Chapter 3: Structure development of polymer containing fibrous nucleating agent under post-process annealing

The addition of nucleating agent has been known as an appropriate method to increase the crystallization of semi-crystalline polymer. In chapter 3, the strategy was to enhance the molecular orientation using the fibrous nucleating agent. It has been found that

the fibrous nucleating agent oriented easily under the shear flow, then rapidly formed the network structure during quench. During annealing, the homogeneously-oriented structures were developed with high crystallinity. Notably, the shrinkage was limited in the sample having a high orientation, i.e., PLA/EBHS strand, compared to that having a low orientation (PLA strand). From this result, the increase in molecular orientation can be employed to prevent the anisotropic shrinkage during annealing.

Chapter 4: Anomalous post-processing dimensional change of immiscible blend

In the chapter 4, a low molecular-weight immiscible polymer was introduced to fabricate the binary polymer blend. Due to PVA having a low-viscosity and phase-separation with PLA, the dispersion of PVA droplets deformed to the oriented fibrils to the flow direction in the continuous PLA matrix. This oriented dispersions, which acted as fibrils structure, and promoted the transcrystallization during post-process annealing. Moreover, the anomalous expansion to flow direction during annealing, owing to the greatly increasing molecular orientation after annealing. As a result, the mechanical properties, such as flexural modulus, were greatly enhanced.

Chapter 5: Exploration of the mechanism for dimensional change of the polymer containing flexible fiber under post-process annealing

In chapter 5, the rheological properties of PLA, such as melt-strength, was improved by the addition of a small amount of commercially available PTFE. The fibrils formed in the continuous PLA matrix, which enhanced the processability of PLA, such as melt-tension. Moreover, it also acted as nucleus and accelerated the crystallization. During applying a shear flow, the PTFE fibrils oriented to flow direction, which induced a high orientation of PLA during crystallization, leading to expansion to flow direction. This study elucidated the effect of PTFE fibrils on the dimensional change of PLA, resulting in the information for controlling the natural shrinkage of PLA products during annealing.

Future Scope

Post-process annealing is an appropriate method to improve the crystallization of the semi-polymers having low crystallization rate. Moreover, it can reduce the cycle time in the production, such as quenching. Based on the research on the flow-induced crystallization, the crystallization and molecular orientation can be promoted. The results obtained from this thesis will be helpful for the high-performance biodegradable polymer. The fibrous nucleating agent significantly enhanced the crystallization, as well as the molecular orientation after post-process annealing. Moreover, the addition of immiscible low-molecular-weight polymer in the blend induced the fibrils structure after injection-molding, leading to high orientation and anomalous expansion during post-process annealing. The anomalous expansion was explained by the orientation enhancement, suggesting that this phenomenon can be applicable for other semi-crystalline polymers, such as poly(3-hydroxulbutyrate-co-3-hydroxylhexanoate) (PHBH) or polypropylene. I believe this enhancement of molecular orientation could be employed industrially to compensate for the orientation relaxation during annealing, thereby reducing shrinkage and warpage in plastics products. Additionally, incorporating nucleating agents with various shapes, such as zero-dimensional (dots, nanoparticles), one-dimensional (tubes, rods, fibers), and two-dimensional (sheets, layers) materials, might provide synergistic effects to further enhance dimensional stability.

Achievements

Publications

[1] **H. -G. D. Vo**, T. Kida, M. Yamaguchi, Role of Shear Flow on Structure Development during Post-Processing Annealing for Poly(lactic acid), *Polymers, 15*, 693, **2023**.

[2] M. Yamaguchi, W. Shu, T. Kimura, **H. -G. D. Vo**, T. Kida, T. Mori, M. Kitani, N. Aridome, A. Miyamoto, Anomalous Post-processing Dimensional Change of Injection-molded Products Composed of Poly(lactic acid) and Poly(vinyl alcohol), *ACS Appl. Polym. Mater.*, *5*, 2136-2143, **2023.**

[3] **H. -G. D. Vo**, M. Yamaguchi, Growth of Molecular Orientation during Post-process Annealing of Poly(lactic acid) Containing a Fibrous Nucleating Agent, *J. Appl. Polym. Sci.*, *141*, e55714, **2024**.

[4] **H. -G. D. Vo**, M. Yamaguchi, Anomalous Expansion of Poly(lactic acid) with Fibrils under Post-Process Annealing, *Novel Trends in Rheology X, AIP Conference Proceeding,* 3400, 040003, **2025**.

[5] **H. -G. D. Vo**, M. Yamaguchi, Elucidating the Effect of Chain Orientation on Dimensional Change of Poly(lactic acid) Composite Containing Flexible Fiber, *Polymer*, 333, 128589, **2025**.

Other publications

[1] Y. H. Chen, M. Yamaguchi, P. H. Tsai, **H. -G. D. Vo**, J. L. Chang, J. Ruan, Simultaneously Enhanced Alginate-based Hydrogel Self-recovery and Mechanical

Strength upon Intramolecular Nodes and Nanoparticulate Joints, *Int. J. Biol. Macromol.*, *307*, 142056, **2025.**

[2] Y. Fujii, **H. -G. D. Vo**, T. Kida, M. Yamaguchi, T. Okumura, Effect of low-density polyethylene on the processability of a tubular-blown polypropylene film*, Polym. Eng. Sci.,* 1-9, **2025**.

International and domestic conferences

Oral Presentations:

[1] *Controlling dimensional change of poly(lactic acid) during post-process annealing via molecular orientation enhancement*, Materials Processing section, the 9th Asia-Pacific Rim Conference on Rheology (A-PRCR2025), July 20-25th, 2025.

Hoang-Giang Dai Vo, Masayuki Yamaguchi

[2] *Role of fibrous nucleating agent on controlling isotropic shrinkage of poly(lactic acid)*, 74th SPSJ Annual meeting, May 19-23rd, 2025.

Hoang-Giang Dai Vo, *Masayuki Yamaguchi*

[3] *Growth of chain orientation during post-processing annealing of poly(lactic acid) and its blend with poly(vinyl alcohol)*, Biopolymers section, ANTEC® 2024, St. Louis, USA, March 4-7th, 2024.

Hoang-Giang Dai Vo, Masayuki Yamaguchi

[4] *Modification of dimensional changes for poly(lactic acid) by addition of polytetrafluoroethylene*, Asian Workshop on Polymer Processing 2025, Kanazawa, Japan, December 1-4th, 2025.

Hoang-Giang Dai Vo, Masayuki Yamaguchi

Poster Presentations:

[5] *Anomalous expansion during annealing of poly(lactic acid) containing poly(tetrafluoroethylene) fibers,* 74th Symposium on Macromolecules, September 16-18th, 2025.

Hoang-Giang Dai Vo, *Masayuki Yamaguchi*

[6] *Structural Growth of Poly(lactic acid) Blends during Post-process Annealing,* Materials Processing section, the 9th Asia-Pacific Rim Conference on Rheology (A-PRCR2025), July 20-25th, 2025.

Hoang-Giang Dai Vo, Masayuki Yamaguchi

[7] *Anomalous expansion of poly(lactic acid) with fibrils under post-process annealing, Novel trends in rheology X, Zlín, Czech Republic, July 30-31st, 2025.*

Hoang-Giang Dai Vo, *Masayuki Yamaguchi*

[8] *Structure development during post-process annealing of poly(lactic acid) containing fibrous nucleating agent, International Conference in Advanced Material Technology, Hanoi University of Science and Technology, Hanoi, Vietnam, October 9-12th, 2024.*

Hoang-Giang Dai Vo, *Masayuki Yamaguchi*

[9] *Crystallization behavior of poly(lactic acid) containing nucleating agent under flow field*, 72nd Symposium on Macromolecules, Kagawa University, Japan, September 26-28th, 2023.

Hoang-Giang Dai Vo, Takumitsu Kida, Masayuki Yamaguchi

[10] *Effect of annealing on molecular orientation for pre-sheared poly(lactic acid)*, 72nd SPSJ Annual meeting, Gunma, Japan, May 24-26th, 2023.

Hoang-Giang Dai Vo, Takumitsu Kida, Masayuki Yamaguchi

[11] *Effect of shear flow on crystallization behavior of poly(lactic acid)*, ANTEC® 2023, Denver, Colorado, USA, March 27-30th, 2023.

Hoang-Giang Dai Vo, Takumitsu Kida, Masayuki Yamaguchi.

[12] *Crystallization behavior of poly(lactic acid) under shear flow*, 71st Symposium on Macromolecules, Hokkaido University, Japan, September 5-7th, 2022.

Hoang-Giang Dai Vo, Khunanya Janchai, Takumitsu Kida, Masayuki Yamaguchi.

[13] *Evaluation of flow-induced crystallization for poly(lactic acid)*, The International Chemistry Conference (CHEMEET 2022), June 27-29th, 2022.

Hoang-Giang Dai Vo, Khunanya Janchai, Takumitsu Kida, Masayuki Yamaguchi.

Awards

Best Poster Award, International Chemistry Conference Online, June 2022.

Mitani Scholarship Foundation for doctoral course, April 2023 to October 2025.